Ion Temperature Measurements in STOR-M Boundary Plasmas Using a Retarding Field Energy Analyzer

A Thesis Submitted to the
College of Graduate Studies and Research
in Partial Fulfillment of the Requirements
for the degree of Master of Science
in the Plasma Physics Laboratory,
Department of Physics and Engineering Physics
University of Saskatchewan
Saskatoon

By
Damian Rohraff

Permission to Use

In presenting this thesis in partial fulfilment of the requirements for a Postgraduate degree from the University of Saskatchewan, I agree that the Libraries of this University may make it freely available for inspection. I further agree that permission for copying of this thesis in any manner, in whole or in part, for scholarly purposes may be granted by the professor or professors who supervised my thesis work or, in their absence, by the Head of the Department or the Dean of the College in which my thesis work was done. It is understood that any copying or publication or use of this thesis or parts thereof for financial gain shall not be allowed without my written permission. It is also understood that due recognition shall be given to me and to the University of Saskatchewan in any scholarly use which may be made of any material in my thesis.

Requests for permission to copy or to make other use of material in this thesis in whole or part should be addressed to:

Head of the Department of Physics and Engineering Physics
116 Science Place
University of Saskatchewan
Saskatoon, Saskatchewan
Canada
S7N 5E2

Abstract

The Retarding Field Energy Analyzer (RFEA, RFA) is a simple and reliable diagnostic technique to measure the ion temperature in the Scrape-Off Layer (SOL) and edge of magnetic fusion devices. Design and operation features of a single-sided (facing the ion down stream side) RFEA for ion temperature measurements in the STOR-M tokamak are described. Its compact size ($21 \times 15 \times 20$ mm^3) allows RFEA measurements without perturbing plasma significantly. Both ion and electron temperature have been measured by RFEA in the STOR-M tokamak. A method is proposed to correct the effects of ion flow on the ion temperature using the simultaneously measured Mach number. The measured electron temperature is consistent with the previously reported Langmuir probe data. Abnormal behavior of the RFEA has been observed in both ion and electron modes when RFEA is inserted deep into the plasma.

Acknowledgements

I would like to thank Dr. Akira Hirose for serving as supervisor and chief motivator during this project. Dr. Hirose's guidance has been instrumental in developing research and scientific skills throughout this project. His demand for excellence has fostered in me a drive and motivation that I hope will bring great success in the future. It has truly been a privilege to work with Dr. Hirose. Dr. Chijin Xiao is owed a debt of gratitude for his guidance, and feel I have gained tremendously from his wisdom and experience. Thanks go to Dave McColl for his discussions, instruction, technical experience, and general friendship. I would also like to thank Dr. Mykola Dreval who has been an excellent colleague. As well, my fellow graduate students, the machine shop crew, and many people around campus have all contribute to my experience here.

This work is dedicated to my family

Contents

List of Tables

List of Figures

List of Abbreviations

ADP	Asymmetric Double Probe
AU	Arbitrary Units
CASTOR	Experimental fusion reactor of the IPP Prague, Academy of Sciences of the Czech Republic
CT	Compact Toroid
DAQ	Data Acquisition System
ECRH	Electron Cyclotron Resonance Heating
FZJ	Forschungszentrum Jülich
GP	Gundestrup Probe
ICRH	Ion Cyclotron Resonance Heating
ID	Inner Diameter
ITER	International Thermonuclear Experimental Reactor
JET	Joint European Torus
JT-60U	Japan Tokamak-60 Upgrade
LCFS	Last Closed Flux Surface (Separatrix)
LHH	Lower Hybrid Heating
LP	Langmuir Probe
MHD	Magneto-Hydrodynamic
NBI	Neutral Beam Injection
OD	Outer Diameter
OFE	Oxygen Free Electronics Copper
OH	Ohmic Heating
PIC	Particle-in-Cell simulation
RP	Rake Probe
RFA	Retarding Field Energy Analyzer
RFEA	Retarding Field Energy Analyzer
SDP	Symmetric *(Cylindrical)* Double *(Rotating)* Probe
SOL	Scrape-Off Layer
STOR-M	Saskatchewan Torus Modified
STP	Segmented Tunnel Probe
SXR	Soft X-Ray
TEXTOR	Fusion reactor situated in Forschungszentrum Jülich, Germany
TH	Turbulent Heating
Tore Supra	Fusion reactor situated at the nuclear research center of Cadarache, Bouches–du–Rhône, France
USCTI	University of Saskatchewan Compact Toroid Injector
XOOPIC	Object Oriented Particle-in-Cell simulation (for X-windows)

List of Symbols

a	Minor Radius
B_ϕ, B_T	Toroidal Magnetic Field
B_θ	Poloidal Magnetic Field
c_s	Ion Sound Speed
e	Elementary Charge
E_r	Radial Electric Field
I_p	Plasma Current
$I_{\mathrm{sat,e}}$	Electron Saturation Current
$I_{\mathrm{sat,i}}$	Ion Saturation Current
$J_{i,e}$	Ion and Electron Saturation Current Density
$m_{i,e}$	Ion and Electron Mass
$M_{\|\|}$	Mach Number of the Plasma Flow Parallel to the Total Magnetic Field
$M_\perp$	Mach Number of the Plasma Flow Perpendicular to the Total Magnetic Field
$n_{i,e}$	Plasma Density of Ions and Electrons
p	Pressure
q	Safety Factor
R	Major Radius
$r_{\mathrm{L,e}}$	Electron Larmor Radius
$r_{\mathrm{L,i}}$	Ion Larmor Radius
$T_{i,e}$	Ion and Electron Temperature
$T_{+,-}$	Downstream and Upstream Ion Temperature (with Respect to Plasma Current)
V_{fl}	Floating Potential
V_{lp}	Plasma Loop Voltage
V_{p}	Plasma Potential
Z	Atomic Number
$\mathrm{v}_\perp$	Perpendicular Velocity
ε_0	Permittivity of Free Space
λ^e_{mfp}	Electron Mean Free Path
λ^i_{mfp}	Ion Mean Free Path
μ_0	Permeability of Free Space
$\omega_{\mathrm{c,e}}$	Electron Cyclotron Frequency
$\omega_{\mathrm{c,i}}$	Ion Cyclotron Frequency

Chapter 1

Introduction

1.1 Motivation

Currently, as shown in Table 1.1, about 85% of produced energy comes from burning fossil fuels [1–3]. The demand for new energy source has reached a critical point as

Energy source	Contribution to primary energy production
Fossil Fuels (Oil, Coal, Gas)	85 %
Fission	7 %
Hydro-electricity	7 %
Solar, wind, wood, waste	1 %

Table 1.1: Contribution of different energy sources to world's energy production.

the increasing energy consumption will soon lead to the depletion of fossil resources. The depletion of natural resources forces us to find alternative energy sources and fusion is preferred mainly for three reasons: the abundance of fuel in nature that can be used to produce energy, the negligible impact of the energy generation on the environment and safety [4, 5]. Fusion does not emit large quantities of pollution when compared with burning fossil fuels and does not produce highly radioactive waste in contrast to fission (Sec. 1.2).

Leading candidates for fusion reactors that use magnetic plasma confinement are tokamaks [6, 7] and stellarators [8, 9].

Tokamaks are the most advanced present-day fusion machines. Process of develop-

ment of a tokamak that would fullfil working condition

$$Q = \frac{P_F}{P_H} \gg 1, \tag{1.1}$$

where P_F is the produced fusion power and P_H is the external heating power ($Q = 1$ is called breakeven), has been slow, yet significant progress toward the final fusion reactor has been made. The several tokamaks have been able to approach or even pass the breakeven limit: in 1997, JET achieved $Q = 0.6$ and in 1998, JT-60U achieved an equivalent of $Q = 1.25$ [10, 11]. The goal of the next tokamak, ITER, is to achieve $Q = 5 - 10$. ITER, the International Thermonuclear Experimental Reactor [12], is an international project that involves collaboration of countries: EU, Japan, USA, Russia, China, India and Korea. ITER is being built in Cadarache, France and is expected to start operation in 2015. The approach to the final design of the fusion reactor is based on building larger tokamaks and using knowledge from the previous smaller tokamaks. ITER, the "proof of principle" tokamak, is expected to be the bridge between present-day tokamaks and electricity-generating power plants. Its main purpose is to demonstrate that fusion can be maintained for a long time (modern tokamaks can operate up to a few minutes) and to determine how materials used for its construction will respond in a long time scale to factors such as high heat loads or radioactive activation.

1.2 Fusion Power

1.2.1 Deuterium–Tritium Reaction

In fusion reaction the reacting nuclei have positive electric charges and their natural electrostatic repulsion (Coulomb repulsion) must be overcome before they can fuse. In laboratory experiments magnetic forces are used to confine plasma with high densities and temperatures to allow fusion reaction to occur. There are different types of reactions for controlled fusion [15]. One of them is a reaction between hydrogen isotopes Deuterium (D) and Tritium (T)

$$\mathrm{D} + \mathrm{T} \rightarrow {}^{4}_{2}\mathrm{He} + {}^{1}_{0}\mathrm{n} + 17.59\ \mathrm{MeV}. \tag{1.2}$$

This reaction was chosen over others, i.e. $\mathrm{D}-\mathrm{D}$ or $\mathrm{D}-{}^{3}_{2}\mathrm{He}$, mainly because it is the least demanding in terms of critical ignition temperature T_{ignition}, ion density n_i and confinement time τ [16,17]. Thermonuclear fusion requires high temperatures so the plasma particles can overcome the Coulomb repulsion. Such high temperature, called the critical ignition temperature T_{ignition}, needs to be maintained for the minimum length of time, called the confinement time τ, and with the adequate ion density n_i. The minumum value of the ion density and confinement time required for a fusion reaction is given by the Lawson's criterion [18] (Table 1.2).

	$\mathrm{D}-\mathrm{T}$ fusion	$\mathrm{D}-\mathrm{D}$ fusion
Lawson's criterion	$n_i\tau \geq 10^{14}$ s/cm^3	$n_i\tau \geq 10^{16}$ s/cm^3
Critical ignition temperature	$T_{\text{ignition}} \geq 4.5 \cdot 10^{7}$ K	$T_{\text{ignition}} \geq 4 \cdot 10^{8}$ K

Table 1.2: Comparison of required conditions for Deuterium–Tritium ($\mathrm{D}-\mathrm{T}$) and Deuterium–Deuterium ($\mathrm{D}-\mathrm{D}$) fusion.

Reaction 1.2 has the largest cross-section (Fig. 1.1) due to an extra neutrons in nucleus, one in Deuterium and two in Tritium. Additionally hydrogen and its isotopes are single charged, so the electrical repulsion is correspondingly small. Finally the $\mathrm{D}-\mathrm{T}$ reaction has relatively high energy output (17.59 MeV). For comparison energy outputs of $\mathrm{D}-\mathrm{D}$ fusion are 3.27 MeV and 4.03 MeV (Eq. 1.3)

$$\mathrm{D}+\mathrm{D} \rightarrow {}^{3}_{2}\mathrm{He} + {}^{1}_{0}\mathrm{n} + 3.27 \text{ MeV}, \tag{1.3a}$$

$$\mathrm{D}+\mathrm{D} \rightarrow {}^{3}_{1}\mathrm{He} + {}^{1}_{1}\mathrm{H} + 4.03 \text{ MeV}. \tag{1.3b}$$

The $\mathrm{D}-\mathrm{T}$ reaction results in the production of α-particles (He nuclei) and energetic neutrons. Their kinetic energies are 3.56 MeV and 14.03 MeV, respectively. Since α-particles are charged, they are confined by the magnetic field and transfer their energy to the plasma. In a burning plasma, plasma heating by α-particles is sufficient to maintain fusion reactions. One of the objectives of ITER will be to demonstrate this basic principle of magnetic fusion [12]. On the other hand, neutrons can freely leave the magnetic confinement and its energy converted into heat for electricity generation.

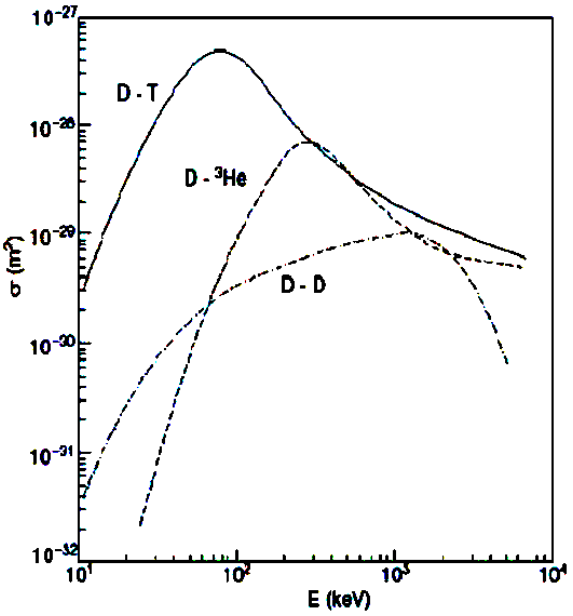

Figure 1.1: Comparison of the cross-sections of D − T, D − D and D − $^3_2$He reactions as a function of energy E [13, 14].

Deuterium can be segregated from sea water which contains heavy water (D_2O) at an abundance of approximately 1 Deuterium atom in every 10000 hydrogen atoms [21]. Tritium cannot be found in nature due to its short half life ($\sim$ 12.3 years) and hence it has to be produced through nuclear reactions. Fusion reactors can breed T through [22, 23]

$$^6_3\text{Li} + \ ^1_0\text{n} \rightarrow \ ^4_2\text{He} + \text{T} + 4.8 \text{ MeV}, \tag{1.4a}$$

$$^7_3\text{Li} + \ ^1_0\text{n(fast)} \rightarrow \ ^4_2\text{He} + \ \text{T} + \ ^1_0\text{n(slow)} - 2.47 \text{ MeV}. \tag{1.4b}$$

By combining equations 1.2 and 1.4a, it is seen that the Deuterium–Tritium reaction is the effect of the Deuterium–lithium reaction

$$\text{D} + \ ^6_3\text{Li} \rightarrow 2 \ ^4_2\text{He} + 22.4 \text{ MeV}. \tag{1.5}$$

Process of lithium production described by Eq. 1.5 requires complete utilization of the neutrons produced during the reaction given by Eq. 1.2 for a sustainable fusion process, else additional Tritium must be provided.

1.2.2 Basic Parameters of Plasma

Plasma (the Greek word for "moldable substance" or "jelly") is often called the fourth state of matter [24, 25]. When materials are heated to a temperature of 10^4 K or higher, electrons are separated from nuclei (ionization) and plasma is formed. Plasma is a mixture of electrons and ions with gross charge mutually separated.

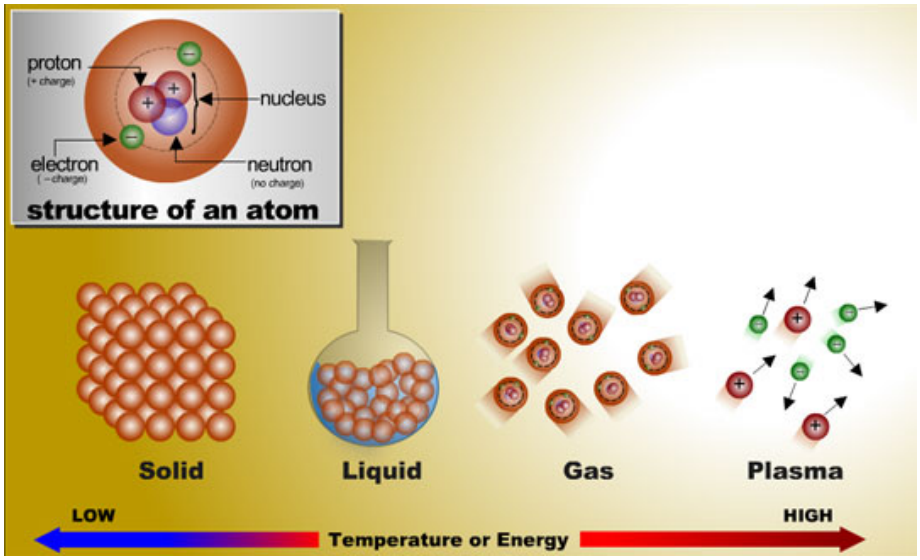

Figure 1.2: A cartoon of the four states of matter as the temperature increases: solid, liquid, gas, and plasma [26].

Terrestrial plasmas can be found in natural phenomena such as lighting or the Aurora Borealis or in artificial environments such as laboratories, fluorescent lamps or plasma TVs. The degree of ionization of a gas in equilibrium is expressed by the Saha equation

$$\frac{n_i}{n_n} \sim 2.4 \cdot 10^{21} \frac{T^{3/2}}{n_i} \mathrm{e}^{-U_i/kT}, \tag{1.6}$$

where n_i and n_n are the number densities (per m^3) of the ion and neutral species, T is the gas temperature (in K), k is the Boltzmann's constant and U_i is the ionization energy of the gas [27, 28].

Most basic plasma parameters are: plasma frequency ω_p, Debye length λ_D and plasma parameter Λ [28]. The plasma frequency, a fundamental time-scale quan-

tity used to describe plasma, is defined as

$$\omega_p = \sqrt{\frac{ne^2}{\varepsilon_0 m}} = \frac{2\pi}{\tau_p}, \tag{1.7}$$

where n is the density, e is the electric charge, m is the mass, ε_0 is the permittivity of free space and τ_p is the plasma oscillation period.

The charged particles present in an ionized gas participate in the screening effect, which can be simply described as a positive particle surrounded by negative particles. The distance of screening, or the distance at which the nonuniformity in the electric field distribution is felt, is called the Debye length (λ_D) and is defined as:

$$\lambda_D = \sqrt{\frac{\varepsilon_0 k T_e}{n_e e^2}} \tag{1.8}$$

The shielding mainly occurs by electrons, since they are lighter than ions and quickly position themselves to balance the deficit or excess of negative charge. For such collective behavior, it is required that the plasma satisfies the condition $\lambda_D \ll L$, where L describes dimensions of the plasma system.

The number of particles present in the sphere of radius equal to the Debye length is given by

$$\Lambda = 4\pi\lambda_D^3 n \tag{1.9}$$

and is called the plasma parameter [29]. Equation 1.9 can be also rewritten in the form

$$\Lambda = \frac{1}{\sqrt{4\pi}} \left(\frac{r_d}{r_c}\right)^{3/2} = 4\pi \frac{(\varepsilon_0 kT)^{3/2}}{e^3 n^{1/2}}, \tag{1.10}$$

combining two essential values: average distance between particles $r_d = n^{-1/3}$ and the distance of closest approach $r_c = e^2/4\pi\varepsilon_0 kT$.

The $\ln\Lambda$ is called the Coulomb logarithm, because it is equal to the natural logarithm of the ratio of the maximum $d_{max} \sim r_d$ to minimum $d_{min} \sim r_c$ impact parameters for Coulomb collisions.

In conclusion, the characteristic collective plasma behavior is only observed on time-scales longer than the plasma period ($\tau_p = 1/\omega_p$), and on length-scales larger than the Debye length ($\lambda_D \ll L$).

	n [m^{-3}]	T [K]	ω_p [s^{-1}]	λ_D [m]	Λ	$\ln \Lambda$
Glow discharge	10^{19}	$3 \cdot 10^3$	$2 \cdot 10^{11}$	10^{-6}	$3 \cdot 10^2$	5.7
Chromosphere	10^{18}	$6 \cdot 10^3$	$6 \cdot 10^{10}$	5^{-6}	$2 \cdot 10^3$	7.6
Interstellar medium	$2 \cdot 10^4$	10^4	10^4	50	$4 \cdot 10^4$	10.6
Magnetic fusion	10^{20}	10^8	$6 \cdot 10^{11}$	$7 \cdot 10^{-5}$	$5 \cdot 10^8$	20

Table 1.3: Key parameters for some typical plasmas [29].

1.2.3 Concept of Tokamak

The idea of a tokamak, a thermonuclear reactor which magnetically confines a high temperature fusion plasma, was proposed by Igor Tamm and Andrei Sakharov in 1950' [6]. The term tokamak is a Russian acronym for Toroidal'naya Kamera s Magnitnymi Katushkami, which means Toroidal Chamber with Magnetic Coils. The

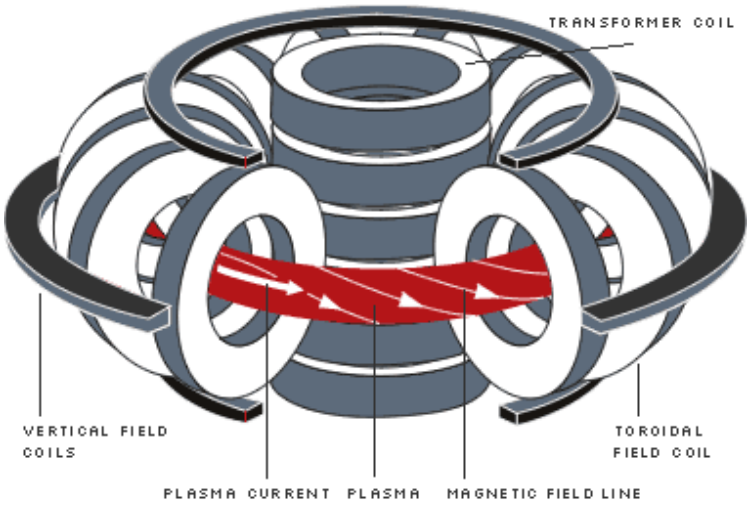

Figure 1.3: Schematic diagram of a tokamak [30].

original concept was to achieve an ohmically ignited fusion reactor, because plasma is an electrical conductor, and can be heated by passing a current through it. This method is called Ohmic (or resistive) heating (OH).

The schematic diagram of a tokamak is shown in Figure 1.3. The main components of a tokamak are a vacuum chamber, a set of toroidal coils, a set of primary Ohmic heating coils to drive a toroidal plasma current, and a set of vertical coils to control

the plasma position. The purpose of toroidal field is to provide main confinement by keeping the Larmor radii of the plasma particles sufficiently small. The toroidal magnetic field alone does not form closed magnetic surfaces, and hence is unable to confine the plasma. It is required to use additional, poloidal magnetic field produced by the toroidal current, which is usually driven by a transformer. Combination of both magnetic fields results in a helical magnetic field with closed, nested magnetic surfaces. The produced helical field can be described in terms of the degree of twisting, or helicity through the safety factor q:

$$q(a) = \frac{aB_\phi}{RB_\theta(a)} \tag{1.11}$$

where B_θ is the poloidal magnetic field, B_ϕ is the toroidal magnetic field and a and R are the minor and major radii, respectively. In tokamaks q is nonuniform, starting at slightly less than unity at the magnetic axis (at the core), and increasing toward the periphery. The safety factor $q(a)$ in STOR-M in the edge plasma or in the Scrape–Off Layer (SOL) is usually about 4.

In addition to the toroidal field, and the poloidal field produced by the plasma current, the tokamak requires a vertical magnetic field to counter the radial expansion force of the plasma [20].

To achieve D−T fusion, plasma must be heated to the temperature more than 10 keV. The primary source of heating is ohmic heating (OH), but this method has very limited range, since the resistivity of the plasma decreases as the temperature increases. This limits OH to about 1 keV. One of the method for further plasma heating is by using electromagnetic waves, such as Lower Hybrid Heating (LHH), Electron Cyclotron Resonance Heating (ECRH) and Ion Cyclotron Resonance Heating (ICRH). Another method is to inject into tokamak plasma a beam of fast neutral particles. Energetic neutral particles become ionized and travel around tokamak many times and by colliding with plasma particles, transfer energy to the plasma. This heating method is called Neutral Beam Injection (NBI).

In a simplified picture, in tokamak plasmas, two regions can be distinguished: core plasma and the Scrape–Off Layer (SOL) plasma, separated by the Last Closed Flux

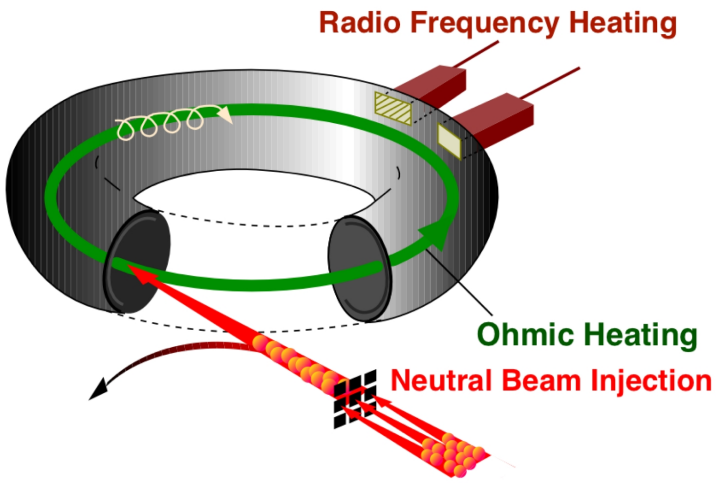

Figure 1.4: Schematic diagram of methods used to heat the tokamak plasma [31].

Surface (LCFS) or Separatrix. Core plasmas are "closed" in the sense that the magnetic field lines do not contact material walls. The plasma in SOL interacts with the limiter or divertor. In SOL closed magnetic field lines are interrupted by a limiter (or a divertor), which scrapes off plasma from the core [7]. Limiter, usually made from the material that can handle high power fluxes, is in contact with plasma and its design helps distribute locally high power loads and localizes the plasma surface interactions. A divertor allows more efficient particle transport and its main objectives are minimizing the presence of impurities by moving the plasma surface interactions outside from the confined plasma and managing the alpha particles. The management of α-particles includes heat transfer later used in generating electrical power and removing the helium ash, the result of the fusion reaction [32].

1.2.4 Scrape–Off Layer and Edge Plasma of a Tokamak

Recent experiments have shown clear correlation between the global plasma performance and the edge plasma layer [34]. This means that by controlling the edge plasma and SOL, one can influence core temperature profiles and the global energy

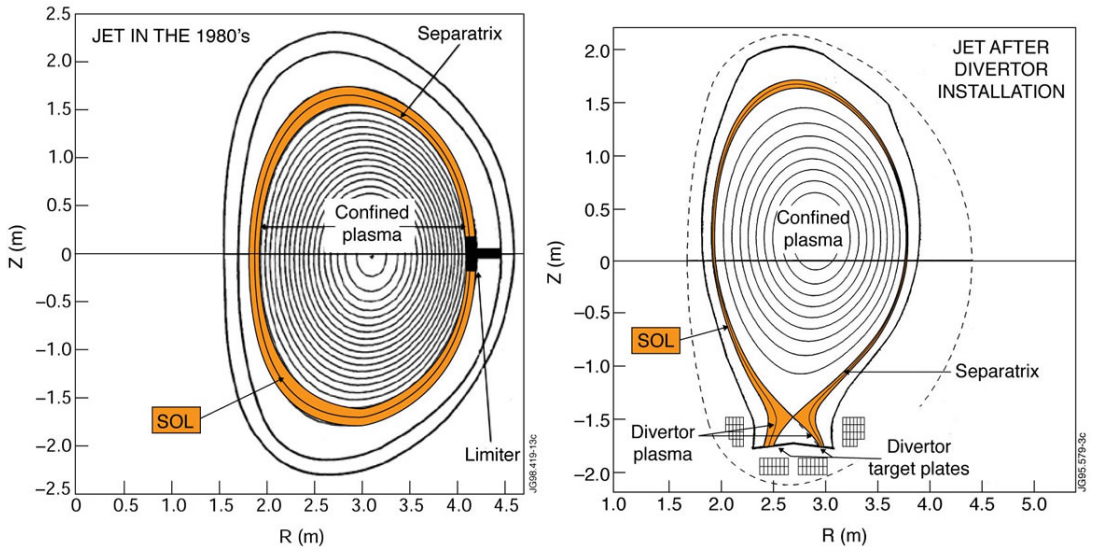

Figure 1.5: A vertical cross section of the tokamak torus of the limiter and the divertor configurations [33].

confinement. To control it we need to understand such phenomena as the recycling flux, the plasma flow or the radial transport [7, 35, 36].

The Radial Force Balance Equation

Let's consider the fluid equation of motion for ions

$$mn\left[\frac{\partial \mathbf{v}}{\partial t} + (\mathbf{v}\cdot\nabla)\,\mathbf{v}\right] = qn\left[\mathbf{E} + \mathbf{v}\times\mathbf{B}\right] - \nabla p, \tag{1.12}$$

where m is the ion mass, n - ion density, v - single fluid plasma velocity, q - ion charge, p - ion pressure, E and B - electric and magnetic fields, respectively. When a time frame is large as it is for slow drifts compared with the ion cyclotron frequency $\omega_{\mathrm{c,i}}$, time derivative of velocity, $\partial\mathbf{v}/\partial t$, can be neglected. The convection term $(\mathbf{v}\cdot\nabla)\,\mathbf{v}$ for the case when $\mathbf{E}$ and ∇p are in the same direction, can be omitted. Then the equation of motion can be written as

$$qn\left[\mathbf{E} + \mathbf{v}\times\mathbf{B}\right] - \nabla p = 0 \tag{1.13}$$

and can be used to derive the radial force balance equation for a tokamak plasma

$$E_r = \frac{1}{nq}\frac{\partial p}{\partial r} - \left[v\times B\right]_r = \frac{1}{nq}\frac{\partial p}{\partial r} + v_\phi B_\theta - v_\theta B_\phi, \tag{1.14}$$

where the subscripts r, ϕ and θ indicate, the radial, toroidal and poloidal directions, respectively. Equation 1.14 indicates that there is a connection between the radial electric field E_r, the radial pressure gradient $\partial p/\partial r$, the toroidal flow velocity v_ϕ and the poloidal flow velocity v_θ [38]. To measure different terms of the radial force balance equation several probes must be employed. Radial electric field and ion density can be obtained from a Rake probe. The ion pressure gradient can be acquired from the ion sensitive probe that measures T_i and relation between pressure and temperature: $p = nkT$. Analysis of the data from the Gundestrup probe can provide perpendicular and parallel flow velocities and the magnetic field can be obtained from magnetic probes.

Ion Impurities

Ion temperature is a very important parameter in SOL and edge plasma studies. During tokamak operation, high heat ion flux present in the boundary plasma interacts with the inner wall of the chamber. The impact energy of the ion increases with the ion temperature and momentum transfer between the plasma ions and wall atoms results in sputtering. Sputtering is one of the fundamental mechanism of impurity production and the rate of sputtering increases with the ion energy [39]. The sputtered atoms from the wall are initially neutral and get ionized while entering plasma. Impurity ions trapped by magnetic field can travel to the plasma core. The distribution of the impurities within the plasma depends on many factors such as impurity charge state Z_{imp}, background ion charge state Z_{bg}, impurity ion temperature T_{imp} and background ion temperature T_{bg} [40–42].

Impurities have been studied in many tokamaks using ion mass spectrometry which is very helpful in diagnosing the conditions of the edge plasma. Matthews noted in [40] that *"an elegant solution to the problem of impurity effects* [in determining the ion temperature] *would be to incorporate retarding grids into mass spectrometer so that an analysis of individual state distributions would be possible"*. By combining a gridded energy analyzer with an ion mass spectrometer, it would be possible to measure the temperature of each species separately. Combination of RFEA with an

ion mass spectrometer (omegatron probe) was done in Alcator C-Mod tokamak [42].

1.3 Thesis Outline

Chapter One has provided the basic background for the work to come in this thesis.
Chapter Two deals with ion temperature measurements. A brief review of ion temperature measurement techniques is given.
Chapter Three details the STOR-M machine and existing diagnostics used in this work. Magnetic coils, Langmuir probe (Rake probe), Mach probe (Gundestrup probe) and Soft X-Ray are discussed.
Chapter Four describes the design and construction of the Retarding Field Energy Analyzer (RFEA) and the specific requirements of STOR-M are detailed.
Chapter Five reports on the experimental results obtained.
Chapter Six contains the conclusion and a discussion of future work.

Chapter 2

Ion Temperature Measurements in Tokamaks

2.1 Introduction

The application of electric probes to study plasmas started with the pioneering work of Langmuir and collaborators [43–45]. The operating principle of Langmuir probe is as follows. A conducting wire (electrode), inserted into a plasma, is biased with a voltage ramp relative to the vessel. The current is then recorded as a function of the bias voltage. In a typical $I-V$ characteristic, three regions can be distinguished (Fig. 2.1). When a high enough negative voltage ($V < V_a$) is applied to the probe tip, the probe collects mainly positive ions. This current is called ion saturation current $I_i^{\rm sat}$. If the applied voltage is in the range $V_a < V < V_b$, the probe collects both ions and electrons, with the transition point $V = V_{\rm fl}$, when the ion current and the electron current are equal. $V_{\rm fl}$ is called the floating potential. In the region $V_{\rm fl} < V < V_p$, the current is dominated by the electron current

$$I(V) = I_e^{\rm sat} \exp\left(\frac{e(V_p - V)}{kT_e}\right), \qquad V < V_p. \tag{2.1}$$

The electron temperature T_e can be determined from the $I-V$ characteristic in this region.

Such an $I - V$ characteristic contains basic information about plasma parameters such as temperature (energy) of the ions and electrons and their densities. With some modifications of the shape to the Langmuir probe, the plasma flow velocity can be measured [47, 48].

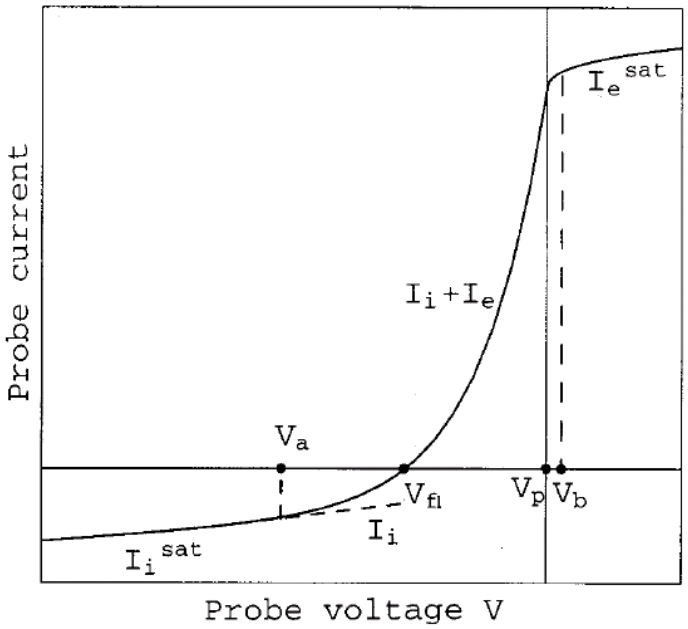

Figure 2.1: General form of the Langmuir probe characteristic: V_{fl} is the floating probe potential, V_p is the plasma potential, I_e, I_e^{sat}, I_i and I_i^{sat} are the electron, electron saturation, ion and ion saturation currents, respectively. For $V < V_a$ the probe collects the ion saturation current and for $V > V_b$ it collects the electron saturation current [46].

The ion temperature cannot be obtained with Langmuir probe. This is because even in the ion saturation current regime, the ion current is controlled by the electron temperature due to sheath formation ($I_i^{\text{sat}} = 0.6An_e e\sqrt{kT_e/m_i}$, where A is the area of the probe, n_e and T_e are the electron density and temperature, e is the electric charge, k is the Boltzmann constant and m_i is the ion mass.). Due to the large difference between masses of the electron and the ion the ion current collected by the Langmuir probe is much smaller than the electron current. This means that to be able to measure the ion current, the electron current must be removed or at least reduced to a level comparable to the ion current because the exponential drop of the ion current, which delivers the ion temperature, is buried in the electron retarding field region. This turns the probe into an "ion sensitive" probe and can be achieved, for example, by adjusting the electric field, modifying the shape of the collecting areas (and using the differences in gyroradii between ions and electrons) and/or by proper alignment of the probe to the magnetic field.

There is no "general" ion sensitive probe valid for all plasmas. In designing such a probe, many conditions should be considered, such as the presence of the magnetic field, energy of the electrons and the ions, the discharge time (or the time of measurement), plasma density, to name a few. Since this research was devoted to the study of the ion temperature in the boundary plasma of a tokamak, only the case of strong magnetized plasma with ion energies in the range between 10 and 100 eV will be discussed.

2.2 Review of Ion Sensitive Probes Used in Fusion Devices with Application to STOR-M

2.2.1 Katsumata Probe

The ion sensitive probe developed by Katsumata [49] uses the difference in the Larmor radii between the ions and electrons $r_{\mathrm{L,i}} \gg r_{\mathrm{L,e}}$ (Table 4.1). The head of the probe is aligned perpendicularly to the magnetic field and consists of a cavity with an ion collector hidden within it (Fig. 2.2), which acts as a recessed Langmuir probe. Electrons cannot reach the collecting surface of the probe, due to their small Larmor radius and the collected ion current obeys the field retardation form $I \sim \exp(-eV/kT_i)$, from which T_i can be estimated.

The advantages of this probe are high spatial and temporal resolutions. The main disadvantage of the Katsumata probe is the complicated geometry in the magnetic field, which requires considerable theoretical and numerical efforts to describe sheaths and current collection [50]. A reliable calibration of the Katsumata probe requires 3D, self-consistent particle-in-cell (PIC) simulations because the magnetic field is perpendicular to the cylindrical axis of the probe, which complicates the ion trajectories and can give rise to an electron current to the collector due to an $\mathbf{E} \times \mathbf{B}$ drift. It has been shown that the value of the collected current depends on the distance h between the top surface of the ion collector and the upper end of the guarding electrode as well as on the size of the collector and applied bias [50, 51].

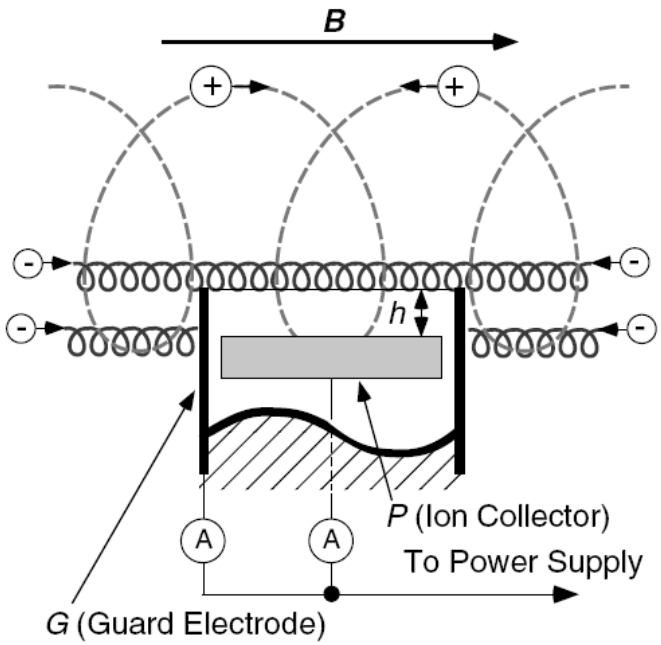

Figure 2.2: Schematic of ion collection on a Katsumata probe in a magnetic field. T_i is estimated by the analysis of the probe current–voltage characteristic of the ion collecting electrode (P–electrode) [50].

The detailed mechanism of the separation of ions and electrons on the collecting electrode in such geometry is not fully understood and the motion of plasma particles around the Katsumata probe is not yet understood in detail [41, 50].

2.2.2 Asymmetric Double Probe

Amemiya [52] invented an asymmetric double probe (ADP) to determine the ion temperature from the difference between the probe currents to two cylindrical electrodes with different lengths whose axes are parallel to the magnetic field (Fig. 2.3). The ADP theory is based on the difference between the mean Larmor radii of electrons and ions and the assumption that the temperature of the ions is comparable to the temperature of the electrons (or higher) in the tokamak's Scrape–Off Layer (SOL) so that no presheath is formed. It is also assumed that the ion velocity distribution is Maxwellian.

The ADP used in the JFT-2M tokamak has two pins with identical cross-section diameters (4 mm) but different lengths (6 mm and 14 mm) and the distance between

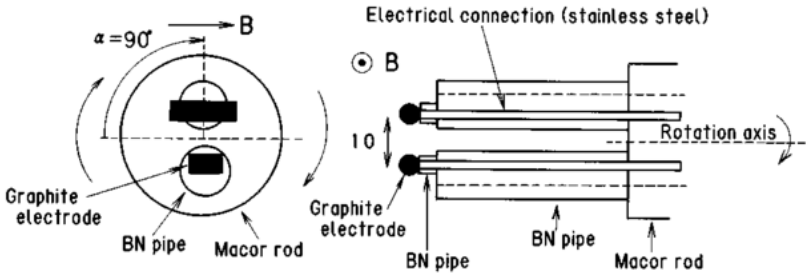

Figure 2.3: Details of the asymmetric double probe. Top and side views. The curved arrows indicate the rotation direction of the probe [53].

pins is 10 mm. The head of the probe can be rotated with respect to the magnetic field **B** and at certain angle pins begin to shadow each other [53]. To obtain the ion temperature, it is not necessary for the asymmetric probe to rotate contrary to the symmetric double probe described in Sec. 2.2.3. By rotating the ADP about an axis perpendicular to the magnetic field (Fig. 2.3), it is possible to find the best alignment of the probe with respect to the magnetic field, since the ion saturation current decreases as the electrodes become parallel to the magnetic field lines. Still, the ion current of one electrode is larger than that of the other electrode since the longer electrode can collect a larger current as the ion temperature increases. Perpendicular ion temperature can be estimated by measuring the ratio R_{ADP} of the ion saturation currents flowing into two electrodes when the probe train begins to be parallel to the magnetic field lines since the value of R_{ADP} is a function of T_i [52,53].

The current collected by the probe can be expressed in an integral form which can be analytically calculated in some cases. Application of the ADP is restricted to tokamaks with strong and stable magnetic fields (> 1 T) and high ion temperatures (~ 100 eV). These restrictions are due to geometrical factors of the probe because for smaller magnetic fields and less energetic particles the dimensions of collecting electrodes decrease and so does the magnitude of the collected currents. In such cases, the probe must be perfectly aligned with the magnetic field, which was done in JFT–2M tokamak by rotating the probe during the discharge [53]. Discharge time in the STOR–M tokamak (~ 40 ms) is not sufficient for such operation and

also decay of the toroidal field during a discharge ($\sim 10 - 20\%$) would affect the measurements.

2.2.3 Symmetric Double Probe

The symmetric double probe (SDP) was invented by the group from Forschungszentrum Jülich and tested on the TEXTOR tokamak. The probe consists of two symmetric electrodes placed perpendicularly to the magnetic field (Fig. 2.4). The probe pins are made of carbon (graphite), 5 mm in diameter and 75 mm in length with the length exposed to plasma equal 4 mm. The distance between pins is 10 mm. Insulation for the graphite rods was made of boron nitride and the pin tubes were fixed in a MACOR rod for electrical insulation [53].

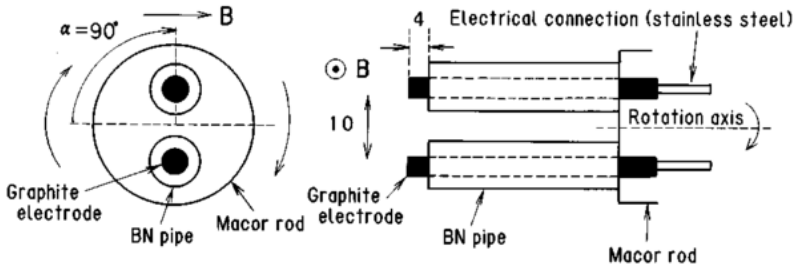

Figure 2.4: Details of the symmetric cylindrical double probe. Top and side views. The curved arrows indicate the rotation direction of the probe [53].

Electrodes rotate (up to 8.2 Hz) during the discharge about an axis perpendicular to the magnetic field and the collected current depends on the rotation angle of the probe (electrodes begin to shadow each other when the angle of rotation reaches 60° from original configuration). If the angle between electrodes and the magnetic field is zero, the region between the two electrodes is in shadow and only ions with a specific velocity can enter this shadow region. When angle diverts from zero, the shadow region reduces so the ions from a wider region of space velocity can reach the collectors. If $T_i = 0$, when the shadow region is formed, the ion saturation current decreases by the amount of the decrease of the effective collecting area, since no ions can enter the shadow region. However, ions with a finite temperature can enter the

shadow region and the envelope of the ion saturation current against the rotation angle reflects the ion temperature as calculated by the Monte Carlo method [53, 54]. To investigate the screening effect, Höthker *et al.* [54] performed Monte Carlo calculations based on the assumption that the velocity distribution of the ions is Maxwellian. By fitting a calculated profile of the flux of the collected particles to the measured ion saturation current profile the ion temperature was determined.

In collaboration with the group from the JFT–2M tokamak, joint experiments were carried out with the aim of the application of the symmetric and asymmetric double probes for the ion diagnostics in the JFT–2M boundary plasma. The experimental setup is well described in [53]. Both probes gave comparable results for ion temperature, confirming that the ion temperature is larger than the electron temperature in the boundary plasma of the noncircular tokamak JFT–2M. Similar results ($T_i > T_e$) were also reported for the TEXTOR tokamak [55].

2.2.4 Tunnel probes

The Tore Supra/CASTOR tokamak group used the Segmented Tunnel Probe for ion temperature measurements. This method was successfully tested on the CASTOR tokamak [56, 57].

The idea of the tunnel probe originated from work done on Tore Supra. A prototype of a tunnel probe was a probe with a head containing 6 graphite pins with a cylindrical carbon fiber composite shield with 6 holes that were aligned with the magnetic field direction. In this setup, three pins collected charges from the upstream side and three from the downstream side. The effective collecting area of the pins was reduced to a fraction of the the cross-sectional area of the holes because some fraction of the ions, as they passed through the CFC shield, were neutralized on the interior sides of the holes. From the $I - V$ characteristic of such a probe, the electron temperature T_e, parallel ion current density $J_{||}$ and the "unperturbed floating potential" $V_{\text{fl},}$ were obtained. Simulations run for this modified probe showed that the radial electric field gradient was steep enough to break the adiabatic ion orbits so that, in addition to the azimuthal vertical $\mathbf{E} \times \mathbf{B}$ motion, there is a strong radial flow

of ions away from their initial guiding center trajectories to the wall. This brought attention to another modification of this Langmuir probe. The idea was to replace the probe's head with the orifice with one conducting tunnel aligned parallelly to the magnetic field and closed from one side by an electrically isolated conducting back plate (Fig. 2.5). The tunnel and the back plate were biased negatively to collect ions

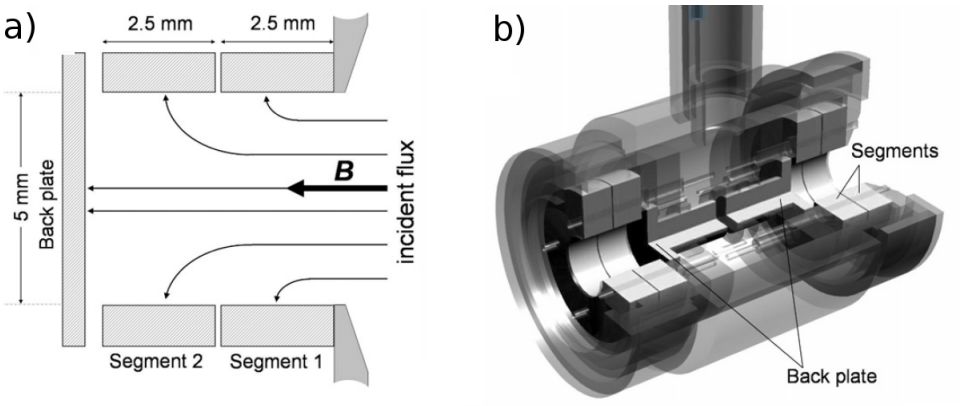

Figure 2.5: (a) Scheme of the STP tunnel. The ion trajectories are shown by black arrows [58]. (b) Schematic drawing of the probe head. Two segmented tunnels are mounted back-to-back in a Mach probe arrangement [58].

and repel electrons. In this setup, plasma flowed through the orifice and the ions were distributed between the tunnel and the back plate. It was assumed that only ions with guiding center trajectories that intersect the tunnel's orifice were collected because the dimensions of the probe are larger than the ion gyroradius or the sheath thickness. Ion current from other directions was neglected.

Experimental values directly give current the ratio of the ion saturation current collected by the tunnel I_{tun} to the ion saturation current collected by the back plate I_{bp}

$$R_{\mathrm{c,e}} = \frac{I_{\mathrm{tun}}}{I_{\mathrm{bp}}}, \tag{2.2}$$

and also the incident parallel ion current density which is the sum of currents collected by the tunnel I_{tun} and the back plate I_{bp} divided by the cross section of the orifice

$$J_{||} = \frac{I_{\mathrm{tun}} + I_{\mathrm{bp}}}{\pi r^2}, \tag{2.3}$$

where $r = 2.5$ mm is the radius of the orifice. The ratio $R_{\mathrm{c,e}}$ is determined by the magnetic sheath thickness at the concave surface of the tunnel, which makes $R_{\mathrm{c,e}}$ a function of electron temperature [59].

To describe the ion collecting mechanism of the tunnel probe and its derivatives, it is necessary to include many factors such as the presence of the magnetic field, sheath and presheath as the cause of the self–consistent electric field, and assuming a Maxwellian distribution of ions and electrons entering the probe. It is also important to consider the effect of the angular misalignment between $\mathbf{B}$ and the probe axis. Probe dimensions and geometry are also relevant as they explicitly influence ratio $R_{\mathrm{c,e}}$. Due to the need to take into account all these conditions and assumptions, solving the problem in analytical way would be very difficult, if possible at all. To obtain the analytical expression for T_e and later for T_i, the Tore Supra/CASTOR team used instead the self-consistent, two–dimensional kinetic code XOOPIC – Object Oriented Particle-in-Cell simulation for X-windows [61]. XOOPIC was developed at the University of California, Berkeley and originates from a kinetic model called PIC (Particle in Cell). The main advantage of the PIC codes is the ability to reproduce with high accuracy experimental measurements of the electron and the ion energy distributions in the plasma. Individual particle trajectories are being followed in a simulation area divided into grids, which makes PIC codes computationally intensive and complex.

2.2.5 Retarding Field Energy Analyzer

The application of a Retarding Field Energy Analyzer (RFEA, RFA) as a probe that can measure both electron and ion energy distribution functions dates from the 1960's and was originally used on beam-type devices [62]. To study edge plasma in tokamaks, RFEAs have been in use since the 1980's and they are used to measure the ion energy distribution parallel to the magnetic field. The probe consists of several biasable grids and a current collector (Fig. 2.6). The RFEA can operate in two modes: ion mode and electron mode, for measuring the ion and electron velocity distributions, respectively. Since the electron velocity distribution can be measured

by the Langmuir probe, the main objective of energy analyzers is to measure the ion velocity distribution.

In the case of a three-grid RFEA, the first grid is usually biased negatively to repel electrons and the second grid is swept from zero to large positive voltage to obtain the $I - V$ characteristic. The purpose of the third grid is to block secondary electrons from reaching the collecting electrode which is placed behind the grid. The whole probe (orifice plate, grids and collector) is oriented perpendicular to the magnetic field so the ion temperature, which corresponds to the ion motion parallel to the magnetic field can be measured. Investigation of the effect of disturbance of the retarding field ion energy analyzer on the plasma (and thus ion temperature measurements) was studied in [63].

Simplicity of operation (in principle) and an inexpensive design makes the Retarding Field Energy Analyzer a favorite probe for ion temperature measurements in small tokamaks [64]. In designing RFEAs certain constraints and effects must be considered. More detailed descriptions of the RFEA and its design, construction and preparation for measurements on the STOR–M tokamak can be found in Chapter 4.

Principles of RFEA operation

Figure 2.6 shows the basic operating principle of an RFEA probe. It consists of an electrode with an orifice, two or three grids and a collector plate. All conducting elements (orifice, grids and collector) are electrically isolated and can be biased independently. As this work is devoted to measuring ion temperature, the focus will be on "ion analysis mode" only.

The entrance orifice (# 0) is usually biased negatively to repel all electrons except the ones with the highest energy. The size of the aperture must be wide enough to let sufficient plasma flux enter the probe, but small enough so the electrostatic sheath can be established and the orifice can be sealed. Despite the fact that the sheath extends over a distance of a few Debye lengths λ_D, the potential significantly drops over the first Debye length, which makes a reasonable condition for a slit width ($\sim 2\lambda_D$). This condition was verified experimentally on the DITE tokamak.

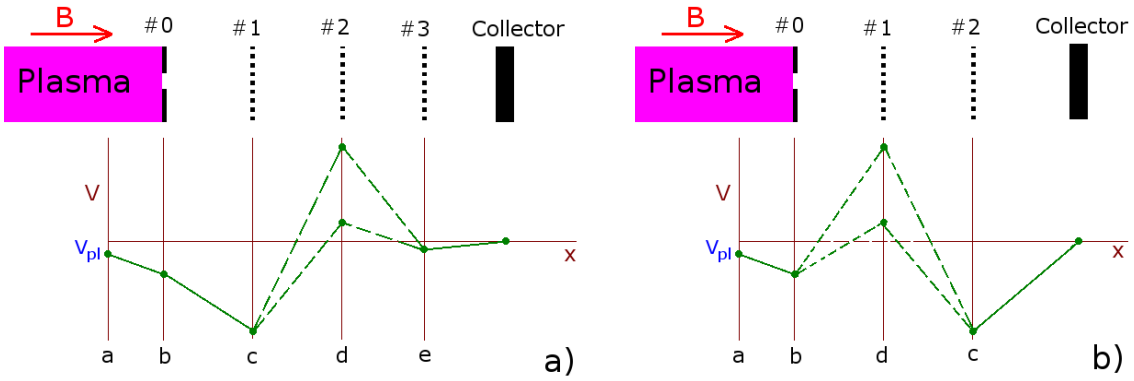

Figure 2.6: Principle and bias potential for a RFEA operating in the ion mode. Additional bias is applied to the electrode with the orifice to repel electrons. (a) 3 grid scheme used in ISTTOK. (b) 2 grid scheme used in JET.

The small slit shows that sheath was established and Maxwellian decay of the ion distribution was very clear whereas the large slit shows neither of these features [41, 65]. Ions and highly energetic electrons that enter the device are subject to the negative bias applied to grid 1 (in the 3-grid RFEA case). This grid is biased to sheath potential $V_{\text{sheath}} = 3T_e/e$ to repel any remaining electrons. Grid 2 is swept from zero to large positive values allowing the ion energy distribution to be obtained. Secondary electrons produced by impact of ions on the first two grids are repelled by grid 3 (Fig. 2.6a). The collected current depends mainly on two factors: the size of the orifice and the transparency of the grids, and is on the order of μA. All potentials are with respect to tokamak ground.

In ion mode (3-grid RFEA), grid 2 is swept from zero to large positive voltage (denoted as retarding potential V_r) and ion current collected by the collector I_i gives the current-voltage characteristic. The $I-V$ characteristic describes the integral ion parallel velocity distribution

$$I_i = Aq_i\Xi \int_{V_r}^{\infty} v_{||} f\left(v_{||}\right) dv_{||} \tag{2.4}$$

where A is the total area of the orifice, q_i is the ion charge, V_r is the biasing potential of the primary retarding electrode and Ξ is the total transmission coefficient, which is calculated in Section 4.2.2 [66]. Due to the presence of noise in the edge plasma and the small-scale signal, numerical differentiation of the characteristic given by Eq. 2.4

is impractical. Experiments showed that velocity distribution can be approximated as Maxwellian [67,68], so the collected current I_i as a function of retarding potential V_r is given by

$$I_i(V_r) = I_{i,0}, \qquad V_r \leq V_{\text{shift}} \tag{2.5a}$$

$$I_i(V_r) = I_{i,0} \exp\left(\frac{-q_i(V_r - V_{\text{shift}})}{kT_i}\right), \qquad V_r \geq V_{\text{shift}} \tag{2.5b}$$

where $I_{i,0}$ is the current collected when none of the ions are repelled by the retarding potential and V_{shift} is the potential difference between the plasma potential and the probe ground.

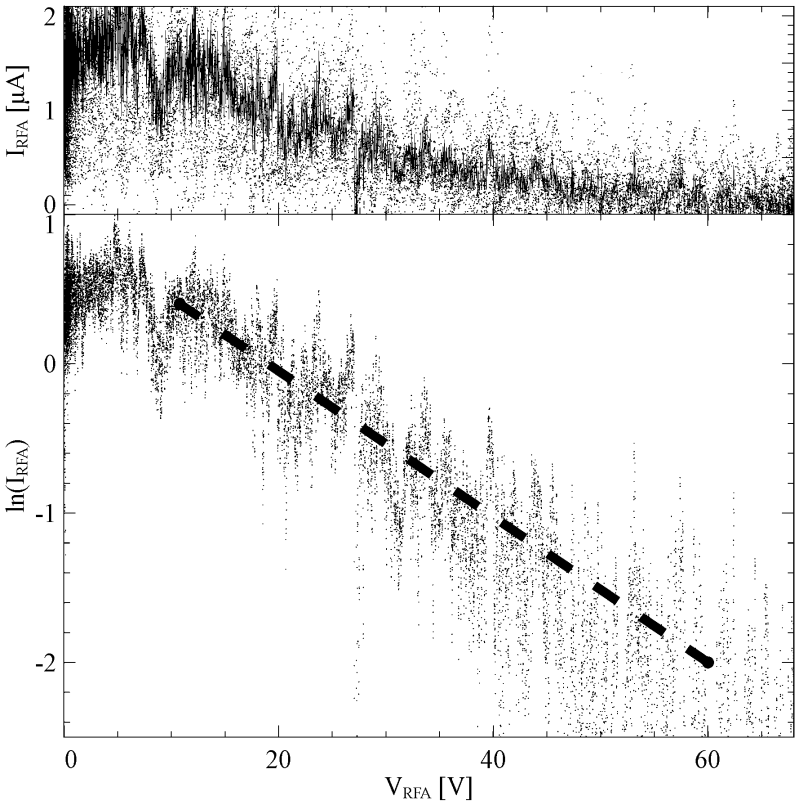

Figure 2.7: Example of RFEA $I - V$ characteristic in ion mode and fitting line in logarithmic scale.

A typical $I(V)$ characteristic from the STOR-M RFEA and fitting line on a logarithmic scale is shown in Figure 2.7.

As mentioned, the RFEA is generally used for measuring the ion temperature. However, by reversing the polarity of the grids and by measuring the electron distribution

function, T_e can be obtained. The results are comparable to those obtained using the Langmuir probe in previous experimental campaigns.

Retarding Field Energy Analyzers in Other Tokamaks

The RFEA is widely used for ion temperature measurements. In several tokamaks, RFEAs and their derivatives were used to study edge/SOL plasma.

Alcator C

In Alcator C, a standard Retarding Field Energy Analyzer was combined with a Langmuir probe and a calorimeter. The whole probe, called a Janus probe, was bi-directional and aligned in such a way as to allow simultaneous measurements from ion downstream and upstream sides. Janus was able to provide the following information:

- *Langmuir probe*: electron temperature, plasma density, ion saturation current and floating potential
- *RFEA*: electron temperature (independently from the Langmuir probe) and ion temperature
- *Calorimeter:* parallel plasma heat flux (incident on an electrically floating plate).

Due to large probe dimensions, Janus must be treated as "large" or perturbing probe [66]. The influence of a perturbing probe on a measured plasma parameters has been addressed in [69].

Alcator C-Mod

In the Alcator C-Mod tokamak, combining an energy analyzer with an ion mass spectrometer was the main objective in the design of the omegatron probe. This allowed the temperature of each species to be measured separately. Observations and experimental results (such as the presence of isotopes of boron, carbon and oxygen in the scrape-off layer plasma) are summarized in [42] with suggestions for further applications of the probe.

JET

In the JET tokamak, a two-gridded RFEA was used for ion and electron temperature measurements [67]. In ion analysis mode, ions were sampled by sweeping the first grid from zero to large positive values of voltage. The second grid was biased negatively to repel all electrons, with the collector held at such potential that secondary electrons caused by ion impacts were returned to its surface and therefore made no contribution to the total collected current. The two-grid analyzer was chosen mainly because of tight space restrictions and observations that ion-induced secondary electron emission from the grids was negligible when compared to that occurring at the collector surface itself. Due to high power fluxes in JET, the probe was deployed on a reciprocating drive, which can drive the probe head into the plasma. Similarly to the Janus probe, the RFEA was bi-directional.

ISTTOK

An energy analyzer built for the ISTTOK tokamak uses a more refined approach to ion mode analysis than the RFEA employed in JET [64]. It consists of three grids and its operation is similar to the energy analyzer built for STOR-M tokamak. During measurements, Nedzelskiy *et al.* observed "abnormal" behavior which might indicate space-charge accumulation inside the analyzer [64]. In principle such a situation might occur in the electron free space between the collector and grid 1. The positive space charge of the ions develops an electric field sufficient to repel ions with a given energy. "Abnormal" behavior was not observed in lower density plasmas which supports the above conclusion. With appropriate modifications, the RFEA will be used for boundary plasma characterization on the TJ-II stellarator.

Tore Supra

The Retarding Field Energy Analyzer used in Tore Supra is similar to design of the RFEA used in JET [67, 71]. The energy analyzer is located in a top port and, since the discharge time in Tore Supra can last around 1 minute [72], such long exposure of the probe would damage it. The RFEA was mounted on a fast reciprocating drive which allows several insertions into the edge plasma during a single discharge. Protecting housing of RFEA with outer diameter of 40 mm and thickness of 3.5 mm

was made from carbon fiber composite (CFC).

A thin nickel foil was used as a slit plate, which was pressed between two Inconel protective plates. A slit with a rectangular shape 5 mm$\times$30 μm was laser cut into the foil. Additionally, during experimental campaigns, nickel foils with three different thicknesses were used ($s = 250, 150$ and 100 μm) to examine ion transmission through the slit plate.

Nickel was also used as the material for grids with wire width $2r_{\mathrm{gr}} = 63$ μm and hole width $D = 0.4$ mm, giving a geometrical grid transmission of $\Xi \sim 0.71$. Additionally to grids 1 and 2, another grid was attached to the rear Inconel protective plate of the slit plate in order to render the electric field behind the Inconel plate as planar as possible. The grids and collector (made of copper) were separated by 2 mm which is the distance given by spatial restrictions [71, 73].

Chapter 3

Machine Description

3.1 Introduction

This chapter briefly describes the STOR-M tokamak (Section 3.2) which is equipped with a standard set of diagnostics used for monitoring plasma and its parameters during operation. The main diagnostics includes magnetic coils, a Rake probe, a Gundestrup Probe and Soft X-Ray detectors.

To understand processes that take place in tokamak plasma, it is necessary to employ proper diagnostics capable of monitoring plasma parameters. Diagnostic equipment can be divided into invasive and non-invasive. The former is mainly restricted to edge plasma and SOL regions due to high heat loads. The latter has no or limited physical contact with the plasma and can provide information about the plasma core [40, 41]. An excellent review on probes used in tokamak plasmas was given in [41].

When an invasive diagnostic is in use, beside the requirement for the high temperature tolerance, it should not perturb plasma parameters. The level of the perturbation depends on many factors, one of which is the probe dimension. The size of the probe must be as small as possible, so the level of the perturbation introduced to plasma can be neglected. This is one of the reasons why it is impossible to build an ideal probe, which would be able to measure all required parameters at one point. A brief discussion on how the size of the probe affects plasma perturbation, including an analysis of the influence of the Retarding Field Energy Analyzer on STOR-M plasma, is given in Section 3.1.1.

The detailed design of RFEA is discussed in Chapter 4.

3.1.1 Overall Experimental Setup and Considerations

1. Probes must be small enough to be considered as nonperturbing. Probes are classified as "nonperturbing" when the natural ambipolar collection length $L_{\text{col}}^{\text{amb}}$ is smaller than the magnetic connection length L_{con}, as explained in Section 3.1.2.

2. The probe should be able to withstand high power fluxes (up to a few MW/m^2) during discharge (up to 50 ms in duration). In the case of the RFEA, the size of the orifice must allow for a high enough current to measure ion velocity distribution, but small enough so the electrostatic sheath can be established and the orifice can be sealed. In this case grids will not melt and space charge accumulation will not occur. The distance between grids should be optimized for prevention of breakdown.

3. The probe axis must be aligned to the magnetic field within a few degrees.

3.1.2 Plasma perturbation caused by RFEA in STOR-M

When a probe is inserted into plasma it may perturb plasma parameters, so the parameters measured at the probe surface may be different from the unperturbed parameters (i.e. without the presence of the probe). The level of perturbation, which corresponds to the ambipolar collection length $L_{\text{col}}^{\text{amb}}$, is determined by the dimensions of the inserted probe. The $L_{\text{col}}^{\text{amb}}$ describes the required parallel length such that the parallel flux lost to the solid can be balanced exactly by the perpendicular flux entering the collecting flux tube, which is defined by extending the field lines intersecting the solid inserted into plasma. The concept of the parallel flow to an object immersed in a magnetized plasma is shown in Fig. 3.1. A probe may be defined as "small" or nonperturbing if

$$L_{\text{col}}^{\text{amb}} < L_{\text{con}}, \tag{3.1}$$

where $L_{\text{col}}^{\text{amb}}$ is the ambipolar collection length and L_{con} is the connection length. If condition 3.1 is satisfied, the probe may act as a limiter and will establish a

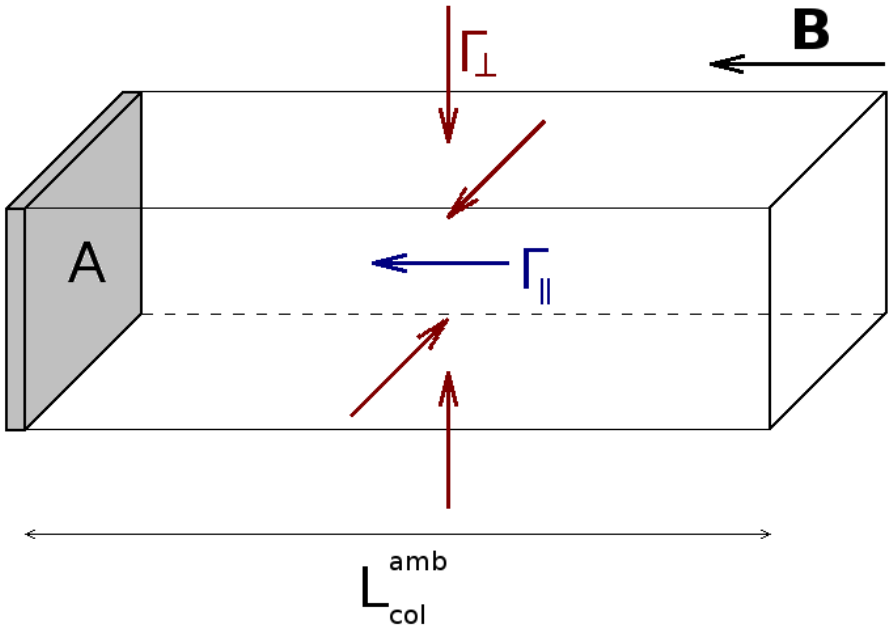

Figure 3.1: Balance of parallel ($\Gamma_{||}$) and perpendicular ($\Gamma_{\perp}$) fluxes entering a flux tube defined by the area (A) of the probe facing plasma [66].

new parallel connection length between itself and the "real" limiter intercepting the probe flux tube and create its own Scrape–Off Layer. Therefore plasma parameters measured in a newly formed SOL would be different from the natural, unperturbed plasma parameters.

The ambipolar collection length is given by

$$L_{\mathrm{col}}^{\mathrm{amb}} \sim \frac{c_s A}{16 D_{\perp}^{\mathrm{amb}}}, \tag{3.2}$$

where $c_s^2 = k\left(T_e + T_i\right)/m_i$ is the ion speed of sound, A is the area of the probe perpendicular to the plasma ($A = 0.00029$ m^2 for the STOR-M RFEA) and $D_{\perp}^{\mathrm{amb}}$ is the cross-field diffusion coefficient, which for the SOL of STOR-M size tokamak is ~ 1 m^{2}s^{-1} [64, 69]. In the STOR-M SOL, the ambipolar collection length for the RFEA is $L_{\mathrm{col}}^{\mathrm{amb}} \sim 1$ m ($T_i \sim 20$ eV, $T_e \sim 20$ eV, $n_e \sim 0.1 - 0.5 \cdot 10^{18}\mathrm{m}^{-3}$).

In the shadow of the poloidal limiter the connection length L_{con}, which describes the parallel connection length along the flux tube to the solid surface, is limited to one toroidal turn

$$L_{\mathrm{con}} \sim 2\pi R, \tag{3.3}$$

which for STOR-M gives $L_{\text{con}} \sim 2.9$ m.

The results show that the degree of disturbance caused by the probe insertion is relatively small, and the plasma parameters are not expected to be significantly perturbed.

3.2 STOR-M Tokamak

Figure 3.2 presents top view of the STOR-M tokamak and shows the main diagnostics locations. The STOR-M is a small tokamak with a major radius $R = 46$ cm and minor radius $a = 12$ cm [37, 38]. The minor radius is determined by the radius of the limiter, which by utilizing a combination of circular and horizontal rail limiters, allows for a horizontal displacement of up to 1 cm without additional scrape off.

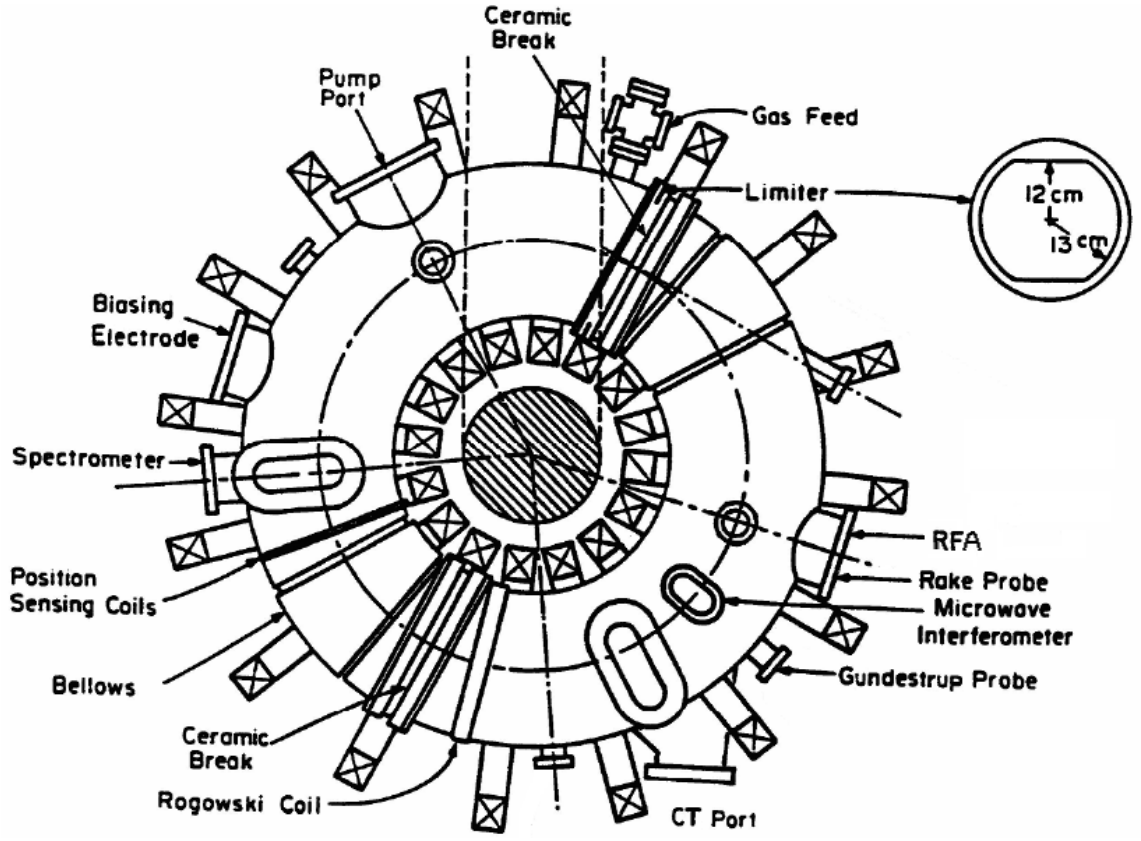

Figure 3.2: Top view of STOR-M showing the access ports with diagnostic locations and limiter geometry. The limiter (3 mm thick) is made of stainless steel and its shape allows horizontal plasma displacement up to ± 1 cm without being scraped off.

The STOR-M chamber is made from 304L stainless steel and consists of two halves. Such a design reduces the amount of mechanical stress on the chamber during tokamak operation. Both halves are separated by two alumina breaks. This isolation prevents current induction in the chamber by the Ohmic coils.

STOR-M has 23 ports available (11 vertical, 10 horizontal and 2 tangential), which are mainly used for diagnostics and tokamak operation such as pumping and gas feeding.

The main STOR-M parameters are listed in Table 3.1.

Major radius	R	46 cm
Minor radius (limiter)	a	12 cm
Toroidal magnetic field	B_φ	1 T
Plasma current	I_p	30-50 kA
Average electron density	n_e	$0.5 - 3 \cdot 10^{13}$ cm^{-3}
Electron temperature	T_e	220 eV
Ion temperature	T_i	50-100 eV
Discharge duration	t_d	50 ms
Energy confinement time	τ_E	1-3 ms

Table 3.1: STOR-M parameters [37, 38].

3.3 Magnetic Coils

3.3.1 Rogowski Coils

The Rogowski coil is a single layered N-turn winding which is wound on a rigid toroidal non-magnetic dielectric core. When windings encircle a current-carrying conductor completely, the Rogowski coil produces a voltage V_{RC} proportional to the coil's mutual inductance M. The time rate of the change of current I in the

conductor is given by

$$V_{\mathrm{RC}} = M\frac{\mathrm{d}I(t)}{\mathrm{d}t}. \tag{3.4}$$

By integrating Eq. 3.4, the current can be obtained. Integration can be done either using hardware such as an electronic integrator or numerically.

3.3.2 Mirnov Coils

A Mirnov coil is a modified Rogowski coil with a specific winding density. In the STOR-M tokamak Mirnov coils are used to measure different modes of fluctuation in the poloidal magnetic field B_θ, which can be Fourier expanded as follows:

$$B_\theta(\theta) = B_{\theta,0} + \sum_{m=1} \left[C_m \cos(m\theta) + D_m \sin(m\theta)\right], \tag{3.5}$$

where $B_{\theta,0}$ is the unperturbed poloidal magnetic field.

In the STOR-M Mirnov coils for $m = 2$ and $m = 3$ are employed and the variable winding density is accomplished using a step function approximation. An additional Mirnov coil with 12 independent outputs magnetic coils has been installed. Such a setup allows the output signals of the coils to be numerically combined for the modes $m = 2$, $m = 3$ and $m = 6$.

3.3.3 Plasma Loop Voltage

Plasma loop voltage V_{lp} is monitored using a toroidal loop of wire parallel to the plasma. This along with the plasma current I_{pl} are the main parameters characterizing plasma discharge. The plasma loop voltage is given by

$$V_{\mathrm{lp}} = R_{\mathrm{pl}} I_{\mathrm{pl}} + \frac{\mathrm{d}}{\mathrm{dt}}\left(L_{\mathrm{pl}} I_{\mathrm{pl}}\right) \tag{3.6}$$

where I_{pl} is the plasma current, R_{pl} and L_{pl} are plasma resistance and inductance respectively. The plasma resistance can be obtained from above equation or it can be expressed using the average plasma resistivity $\eta_{||}$:

$$R_{\mathrm{pl}} = \frac{2\pi R}{\pi a^2}\eta_{||} \tag{3.7}$$

where R is the plasma major radius and a is the minor radius of the tokamak. The plasma inductance is given by

$$L_{\rm pl} = \mu_0 R \left(\ln \left(\frac{8R}{a} \right) + \frac{l_i}{2} - 2 \right) \tag{3.8}$$

where l_i is the plasma internal inductance parameter [32, 75] which is given by

$$l_i = \frac{\bar{B_\theta^2}}{B_\theta^2(a)} = \frac{2\int_0^a B_\theta^2(r) r {\rm d}r}{a^2 B_\theta^2(a)}, \tag{3.9}$$

where $B_\theta(r)$ is the poloidal magnetic field at a distance r from the axis of the plasma column and $B_\theta(a)$ is the poloidal magnetic field at the edge of the plasma column. From the measurements of the plasma current and the loop voltage, the plasma resistivity can be estimated, which in equilibrium is roughly $R_{\rm pl} \sim V_{\rm lp}/I_{\rm pl}$.
From the neoclassical resistivity η_{nc}

$$\eta_{nc} = \frac{\eta_S}{1 - 1.95\sqrt{\varepsilon} + 0.95\varepsilon} \tag{3.10}$$

the average electron temperature can be obtained [32]. In Eq. 3.10 η_S describes the Spitzer resistivity

$$\eta_S = 1.65 \cdot 10^{-9} \frac{Z_{\rm eff} \ln \Lambda}{T_e^{1.5}}, \tag{3.11}$$

where $\varepsilon = a/R$ is the inverse aspect ratio of the tokamak, $Z_{\rm eff}$ is the effective ion charge number, T_e is the electron temperature (given in keV) and $\ln \Lambda$ is the Coulomb logarithm. The Coulomb logarithm is the natural logarithm of the ratio of the maximum (Debye length $d_{\rm max} \sim \lambda_D = \sqrt{\epsilon_0 T_e / n e^2}$) to minimum (distance of the closest approach $d_{\rm min} \sim r_c = e^2/4\pi\epsilon_0 T_e$) impact parameters for Coulomb collisions and is essentially the number of electrons in a Debye sphere. For STOR-M plasma, $\ln \Lambda \sim 17$.
From the measured resistivity, the electron temperature can be estimated as follows

$$T_e \sim \left[\frac{2.6 \cdot 10^{-4}}{(1 - 1.95\sqrt{\varepsilon} + 0.95\varepsilon)} \frac{2 Z_{\rm eff} I_{\rm pl} R \ln \Lambda}{V_{\rm lp} a^2} \right]^{\frac{2}{3}} \sim \left[\frac{0.01326}{(1 - 1.95\sqrt{\varepsilon} + 0.95\varepsilon)} \frac{I_{\rm pl} R}{V_{\rm lp} a^2} \right]^{\frac{2}{3}}, \tag{3.12}$$

where R and a are the tokamak major and minor radii respectively. For a typical ohmic STOR-M discharge the average electron temperature is about 220 eV.

3.3.4 Position Sensing Coils

The quality of the discharge depends on many factors, and one of these factors is the position of the plasma column. To achieve good quality of discharge, six magnetic probes, four for the poloidal field B_θ and two for the radial component of the magnetic field B_r, are mounted around the outside of the vacuum chamber at a minor radius of 170 mm to monitor the plasma position. The orientation of the coils is shown in Figure 3.3. The coils are wound on a cylindrical former made

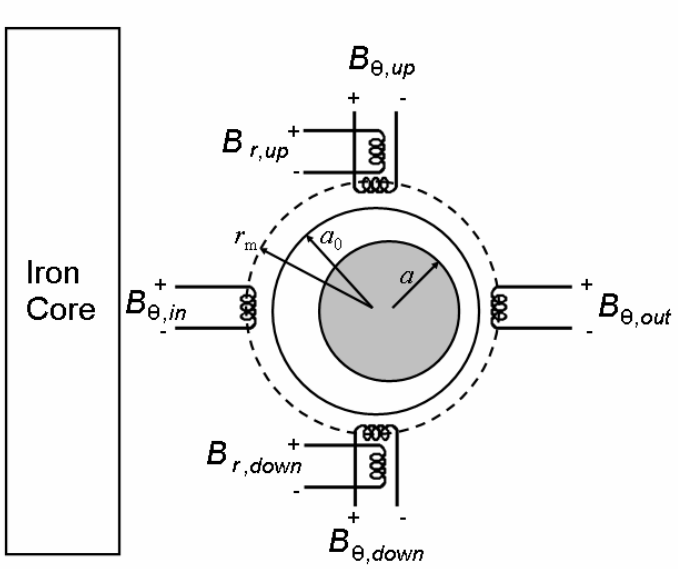

Figure 3.3: The plasma position sensing coils.

of Teflon with an average radius of 3.5 mm. On each coil 460 turns of 34 AWG enameled wire are wound. An unwanted "pick up" signal from coil misalignment and imperfection is accounted for by a compensation circuit, which by employing Rogowski coil determines the unwanted magnetic fields.

3.4 Rake probe

A Rake probe used in STOR-M tokamak is an array of 16 Langmuir tips made of tungsten, which are inserted into a plasma and biased relative to the vacuum chamber. The probe is mounted on a Huntington® Mechanical Laboratories LR-

2200-2 linear and rotary feedthrough which allows for measurements of electron temperature T_e, density n_e and the plasma potential V_p in Scrape–Off Layer and edge plasma of STOR-M (between minor radii of 15 cm and 10 cm), where plasma is not seriously perturbed and the probe will not be damaged.

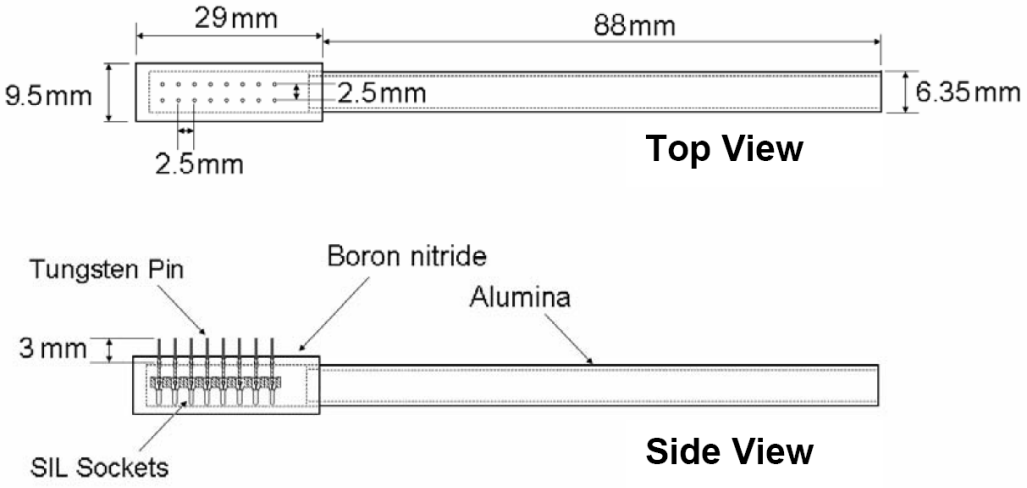

Figure 3.4: Schematic of the STOR-M rake probe.

The rake probe head has a diameter of 9.5 mm and length of 29 mm and is made of Boron Nitride (AX05 Combat®). Langmuir tips, arranged in two rows with spatial separation 2.5 mm, are made of 0.5 mm diameter tungsten wire. The tungsten wires are 8 mm long and are inserted into sockets, which leave a 3 mm exposed tip. These pins are pressure fit in the socket, which make it possible to repair if they are damaged by the plasma.

The head of the rake probe is attached to a 93 mm long alumina rod with 6.35 mm and 5 mm outer and inner diameters respectively. This supporting rod is attached to a stainless steel mount which is screwed to the feedthrough. The other end of the alumina rod is inserted 5 mm into the boron nitride probe head. The leads from the sockets are fed through this supporting rod to the feedthrough. The whole assembly is secured with Torr Seal epoxy.

3.5 Gundestrup Probe

To measure plasma flow, two alike electrodes are placed back to back with an insulation between them. A single electrode can receive an ion flux from one direction only and the whole configuration is called a Mach probe. The ratio of the ion fluxes is used to determine the Mach number. To distinguish perpendicular and parallel flows, it is necessary to perform measurements at more than one angle θ relative to the magnetic field. This can be achieved by rotating a planar Mach probe or by redesigning a Mach probe into a probe with a multiple current collectors placed at certain angles [78] as shown in Fig. 3.5.

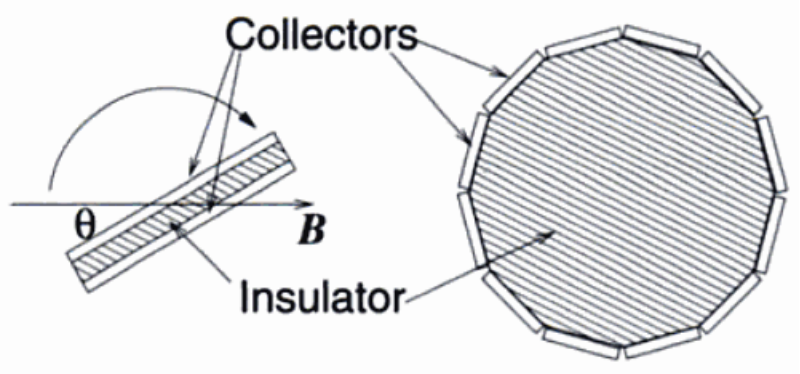

Figure 3.5: Probe configurations for perpendicular and parallel velocity measurements. Either a rotatable probe (left) or multiple collector "Gundestrup" probe (right) are required to give multiple angles (θ) of collection [79]

For plasma flow measurements in the STOR-M tokamak, a system of 8-collector probe arrays, called a Gundestrup probe (GP, G-probe), is used. The advantage of Gundestrup-type probes is the possibility to measure simultaneously (with respect to the magnetic field) parallel and perpendicular plasma flow velocity components. This ability makes a Gundestrup probe a main tool in flow measurements used in many tokamaks.

The Gundestrup probe used in STOR-M tokamak is mounted on linear shift mechanism built by UHV Design, which allows 10 cm of travel to study plasma flow in SOL and the plasma edge. The main G-probe components are the insulating housing

which forms the basic structure of the probe, the insulating cap and between them the eight collectors biased negatively enough with sufficient negative bias to measure the ion saturation current. By collecting $I^{\mathrm{i}}_{\mathrm{sat}}$ from all eight collectors the polar distribution of ion saturation current can be obtained. The collectors form a cylinder with radius of 11.4 mm and have an exposed length of 4.5 mm. Theoretical models used to interpret data from Gundestrup probe assume the probe is in magnetized regime, which means that the size of collectors has to be larger than the ion Larmor radius. Also the shape of the collectors must be considered in data analysis. Each collector spans approximately 44° around the circumference of the probe head and the centers of adjacent collectors are separated by 45° with a 0.2 mm gap between each collector. Boron Nitride was used to manufacture the insulating housing and cap. This material was used due to its high heat tolerance, excellent electrical insulation and machinability. It does not outgas in an ultra-high vacuum, which makes it a desirable material for probe construction.

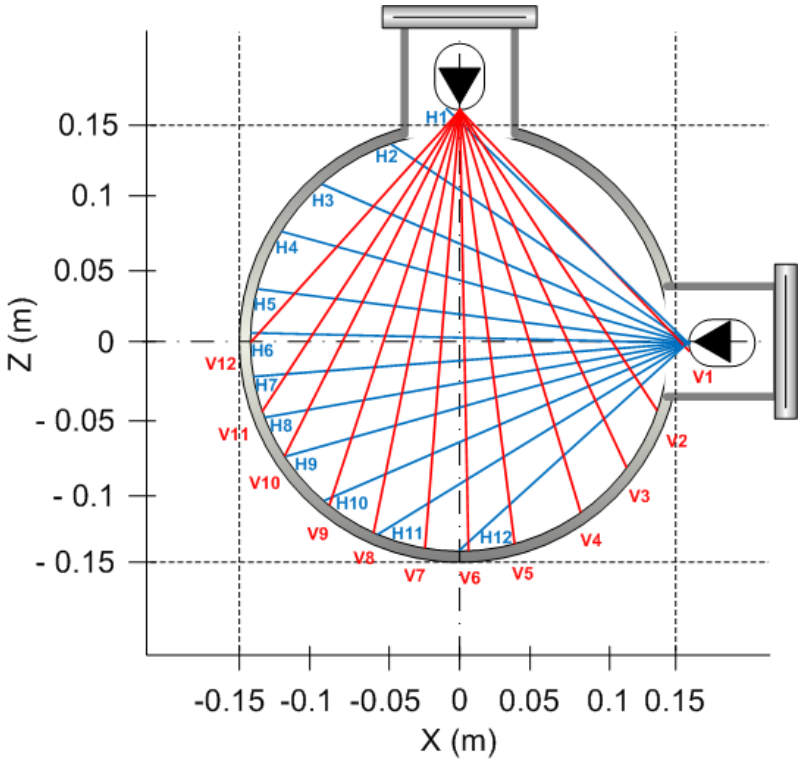

Figure 3.6: Schematic of SXR camera fitted on vertical and horizontal ports of the STOR-M tokamak [80].

3.6 Soft X-Ray Detectors

The Soft X-Ray camera (SXR) is a system that consists of two miniature arrays that are installed through a 4.8 cm port of STOR-M (Fig. 3.6). Each array is a 20 channel photodiode linear array (IRD AXUV-20EL) and a 1×4 mm^2 pinhole, which is located 1 cm away from the array. The size of the pinhole and its location relative to the diode array is optimized to cover the whole poloidal cross section and to achieve good spatial resolution with minimum overlap with nearby channels [80]. The diode current is amplified by IRD AMP16 preamplifiers, with fixed gains of 10^5. The preamplifiers are placed near the diode assembly, minimizing the coaxial cable length to approximately 1 m. The preamplified signals are connected to custom built amplifiers with variable gains through long coaxial cables. National Instruments digitizer cards (NI 6133) with 14 bit resolution and 3 MS/s sampling rate are used for data acquisition [80].

The typical time resolution of a SXR camera is on the order of a few μs, which makes it a desired diagnostic for studies of MHD plasma perturbations [81, 82].

Chapter 4

Probe Modelling and Instrumentation

4.1 Introduction

The ability to measure the desired parameters of the SOL lies in the proper design of the probe as well as in the proper data analysis. To design and build a sophisticated probe like Retarding Field Energy Analyzer (Fig. 4.1 and Fig. 4.2), certain scenarios must be considered such as thorough analysis of the probe influence on plasma or the probe operation under different conditions. Proper electronics and connection to DAQ are also very important. Whole process of the RFEA design is presented in this chapter.

4.2 Probe Design

4.2.1 Orifice Plate

One of the most crucial components of RFEA is the orifice plate which acts as a barrier that separates the more delicate grids from the plasma. The aperture must be large enough to let sufficient current into the probe, but small enough so that electrostatic sheath can be established. To maintain continuity of the sheath potential across the orifice, its radius (or half width in the case of a slit) should be comparable to (or less than) the Debye length. This assures us that the charged particle distribution will not be perturbed by an uneven distribution of the sheath potential so the particles that pass through the slit will be representative of those arriving anywhere at the probe's surface. To fulfil these requirements, the radius of

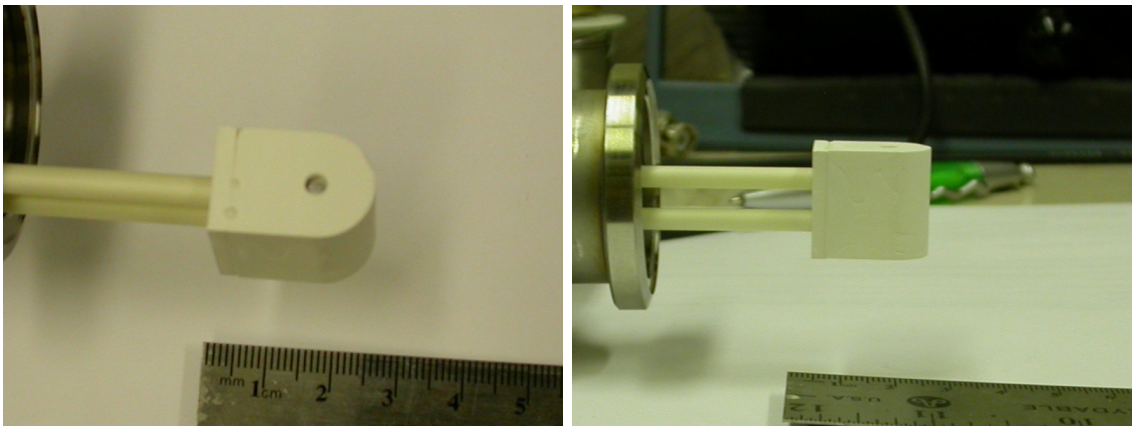

Figure 4.1: Retarding Field Energy Analyzer before preliminary, "proof of the principle" tests . Photos present the front and the side of the probe.

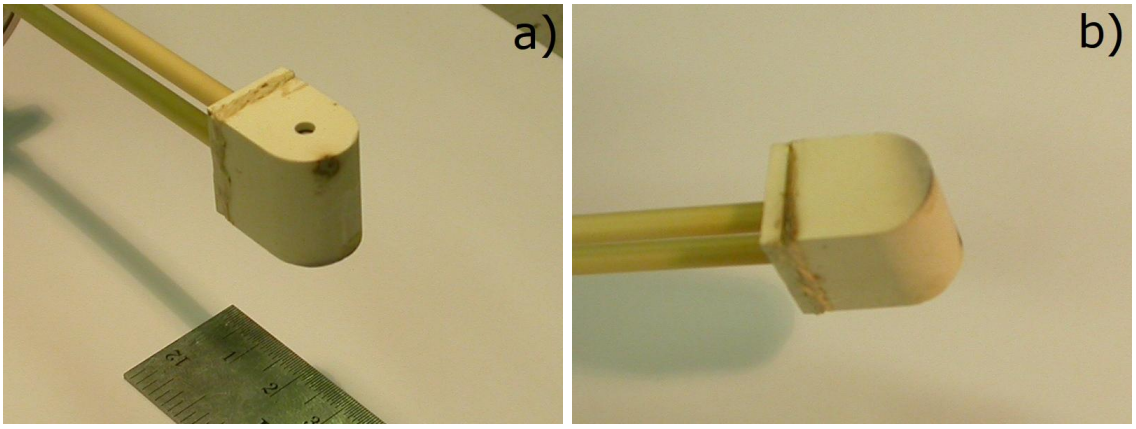

Figure 4.2: The photos of the front and the back of RFEA after about 300 discharges. The probe was facing ion downstream side and measurements were performed in SOL and edge plasma. The edges of the probe's housing are slightly burned, yet internal components were not damaged.

the orifice of the STOR-M's RFEA is 75 μm, which is comparable with the Debye length ($\lambda_D \sim 50 - 100$ μm) in the SOL (Table 4.1).

Parameter	**Magnitude** [μm]
Ion Larmor radius [$r_{L,i}$]	~ 1500
Electron Larmor radius [$r_{L,e}$]	~ 25
Debye length [λ_D]	$\sim 50 - 100$

Table 4.1: Typical parameters of the SOL of STOR–M.

Because the orifice plate must withstand extremely high heat fluxes and be biasable, the applicable materials are very limited. Stainless steel (SAE grade 316) was chosen due to its overall thermal properties, high melting point (> 1200 ^{o}C), machinability and compatibility with silver solder [83]. The plate was carved out of the stainless steel and the orifice was produced using laser cutting (Razortip Industries Inc.). In designing the orifice, the thickness of the plate must be considered. Because in magnetized plasmas ions and electrons gyrate about magnetic field lines with a Larmor radius r_L (see Table 4.1), a large fraction of the ions with gyroradii larger than the orifice will be scraped off as they pass through it. To minimize the perturbations to the ion transmission characteristics we can reduce the thickness of the orifice plate or design the orifice like a knife-edge [66, 84], with the angle $\theta = 45^{\circ}$ or larger. In this way, as soon as an ion enters the orifice the overall aperture for transmission is enlarged (Fig. 4.3). In such setup the high perpendicular components are cut off, but the perturbation to the parallel component of ion velocity is small, so the performance of RFEA is not compromised [42, 71].

The electron transmission characteristic is not affected by the orifice because the electron Larmor radius is much smaller than the radius of the orifice (Table 4.1).

If orifice plate can be biased negatively up to the sheath potential, a majority of the electrons will be repelled and hence prevented from entering the probe. The fraction

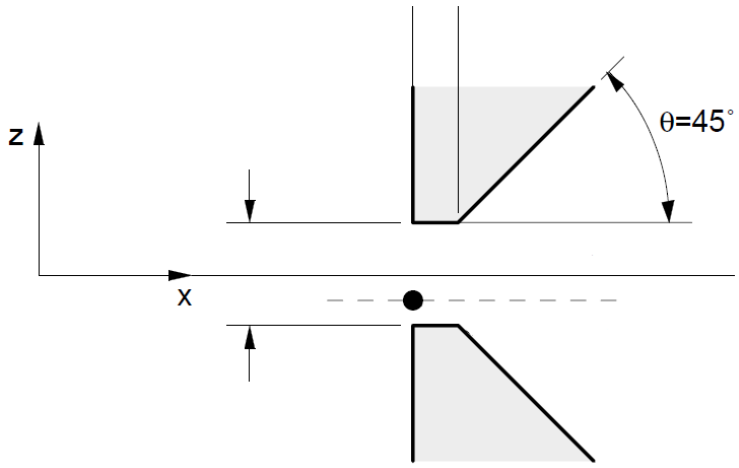

Figure 4.3: Schematic of cross section of the knife-edge slit geometry [42].

of electrons that enter probe chamber and will be repelled by the first grid is

$$\% \text{ transmitted} = \text{erfc}\left(\sqrt{\frac{e|V_{sh}|}{kT_e}}\right) \tag{4.1}$$

where V_{sh} is the sheath potential and $\text{erfc}(x)$ is the complementary error function

$$\text{erfc}(x) = \frac{2}{\sqrt{\pi}} \int_x^\infty \exp(-y^2) dy. \tag{4.2}$$

Taking into account the value of the classical sheath potential ($\sim 3T_e/e$) less then 1% of all electrons will reach the first grid [66].

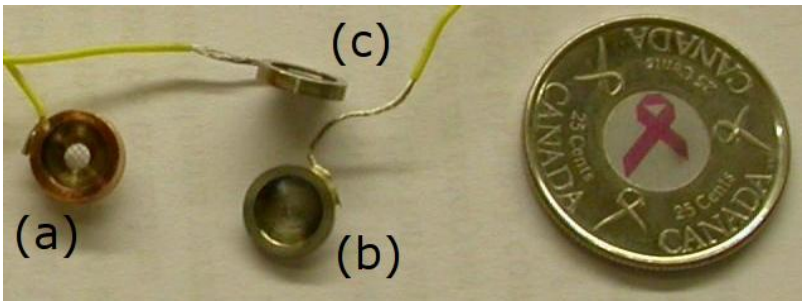

Figure 4.4: Photo of the RFEA components: grid mounted on the (a) copper washer, (b) orifice plate and (c) collector each is made of stainless steel.

4.2.2 Grids

Grids used in the STOR-M's RFEA are commercially available VECO grids used for Transmission Electron Microscopy (Ted Pella, Inc.), which are very rigid and offer superior strength while handling [85]. These 3.05 mm OD grids (Fig. 4.5) are manufactured using a precision electroplating process and have a thickness of 20 μm with a hole width of 450 μm and bar width of 50 μm. Nickel was chosen as a grid material for its low price (100 grids for about $20), hardness of thin grids, low secondary-electron emission and high melting point. Nickel is magnetic, but no significant influence on the performance of RFEA was observed during preliminary tests. Additionally several tokamaks: Alcator C [66], ISTTOK [64] and Tore Supra [71] used nickel as a grid and/or orifice plate material.

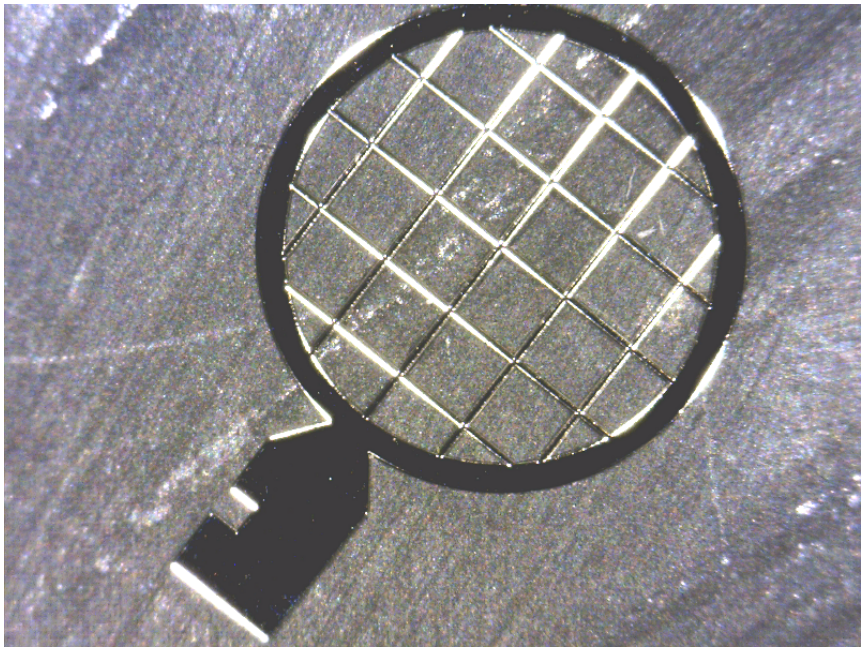

Figure 4.5: Magnified image of the nickel grid used on RFEA. Grid wires are 50 μm wide with 450 μm in between.

Due to small sizes, the grids are supported with a copper washer (OFE) of 0.4 mm thickness and 2.2 mm diameter holes. The grid must be aligned parallelly to the orifice plate. When a slit is used instead of a round orifice, all meshes must be carefully arranged to be diagonal to the vertical entrance in order to prevent blocking

of the path of ions by a single grid wire. Transmission of an individual ion through the grids depends on the ion kinetic energy, both perpendicular and parallel to the magnetic field as well as a grid geometry. It is possible to estimate which ions pass through the grids. Okubo *et al.* [86] and later Nachtrieb [42] reported that the most of the ions have the same probability of transmission (geometrical) and that to the first order of approximation, the grid transmission is independent of the ion energy and is equal to the geometrical transmission.

Grid wires in RFEA are 50 μm thick ($2r_{\mathrm{gr}}$) with wire separation (D) of 450 μm, which gives a geometrical transmission coefficient of

$$\xi = \frac{(D - 2r_{\mathrm{gr}})^2}{D^2} = 0.79 \tag{4.3}$$

which agrees with the geometrical transmission obtained from counting pixels in a magnified image of the grid.

For the negative biased grid, the transmission will be modified due to perturbations of ions whose trajectories pass close to the grid. In this case, the effective grid radius will be

$$r_{\mathrm{gr,eff}} = r_{\mathrm{gr}}\sqrt{1 + \frac{V}{V_0}} \tag{4.4}$$

where V is the grid potential and V_0 is the initial ion energy [87], and the effective transmission will be $\Xi_{\mathrm{eff}} \sim 0.5 - 0.75$. The overall transmission coefficient, Ξ, is the multiple of all the individual components' transmission coefficients:

$$\Xi = \prod_{i=1}^{3} \xi_i \tag{4.5}$$

where ξ_i is the transmission coefficient of a grid.

4.2.3 Collector

The final element of RFEA is a collector made of stainless steel (SAE grade 316), which was chosen mainly for very low secondary-electron emission.

4.2.4 Space-Charge Limitations

Brillouin flow

In 1945 Brillouin indicated that a non-neutral beam of charged particles will remain confined by a magnetic field up to a certain space-charge limits [88,89]. Brillouin flow occurs when the outward electrostatic force due to the space charge effect is balanced by the centripetal force imposed by the magnetic field and the beam confinement depends on the strength of magnetic field B and the charge density n. The particles in the beam stay confined up to the critical density

$$n_B = \frac{\varepsilon_0 B^2}{m_i}. \tag{4.6}$$

This condition is equivalent to:

$$\omega_{\mathrm{p,i}} = \omega_{\mathrm{c,i}}, \tag{4.7}$$

where $\omega_{\mathrm{p,i}} = \sqrt{n_B e^2/\varepsilon_0 m_i}$ is the ion plasma frequency and $\omega_{\mathrm{c,i}} = \sqrt{e^2 B^2/m_i^2}$ is the ion cyclotron frequency. That critical density n_B is called the Brillouin density and in STOR-M SOL $n_B \sim 10^{15}$ m^{-3}. It means that if the density of ions in the beam is higher than the Brillouin density, the non-neutral plasma beam will no longer be in equilibrium and the beam will start broadening. The current carried by the beam of ions moving with the thermal velocity $\mathrm{v_{th}}$ along magnetic field B through the orifice of the RFEA with a cross sectional area A_{slit} is given by

$$i = qn\mathrm{v_{th}}A_{\mathrm{slit}} \tag{4.8}$$

where q is the ion charge and n is the ion density in the beam. For the STOR-M tokamak the critical case (i.e. $n = n_B$) is when $i = i_B \sim 0.2$ μA.

The collected current is about one magnitude larger ($i_{\mathrm{RFEA}} \sim 3$ μA) than the critical current i_B and calculated current through the orifice is about two orders of magnitude larger ($i_{\mathrm{orifice}} \gtrsim 17$ μA), so the ion beam that will enter the RFEA will start expanding. The difference between i_{RFEA} and i_{orifice} is due to transmission losses on the grids and orifice.

Space-charge accumulation

One of the problems in designing a Retarding Field Energy Analyzer is space charge limitations which determine the grid separation. The estimation of the maximum permissible current density between the grids is extremely difficult, even though some analytic expressions have been offered [90]

$$j_{\mathrm{sc,crit}} \approx 3.85 \cdot 10^{-8} \frac{\left(qV_{rp} + E_{||}\right)^{\frac{3}{2}}}{\left(z - z_m\right)^2} \left(1 + 0.024 \sqrt{\frac{T_i}{qV_{rp} + E_{||}}}\right), \tag{4.9}$$

where $j_{\mathrm{sc,crit}}$ is in A/cm^2, V_{rp} is the potential applied to the electron repelling grid, $E_{||}$ (in eV) is the initial average ion energy, $z - z_m$ (in cm) is the distance between electron and ion repelling grids and T_i is the ion temperature (in eV). Estimations of the critical ion current for the STOR-M's RFEA before space charge is likely to become important is about $i_{\mathrm{sc,crit}} \sim 250\ \mu$A. Nachtrieb [42] observed and later Nedzelskiy *et al.* [64] confirmed, that a sharp knee on the $I(V)$ characteristic may be considered as an indication that the space-charge effect influence is insignificant which is also the case in STOR-M RFEA. In addition, before encountering the first repelling grid, both ions and electrons are still present in the plasma beam that enters RFEA chamber providing a neutralizing effect in reducing the diverging action of a single species beam. Electrons will be mainly present in the central part of the beam, due to different Larmor radii.

Analytic methods can only provide rough estimates of the RFEA limitations. Numerical simulation might be useful in determining limits of the RFEA, however during experimental testing of the energy analyzer, it is possible to determine its limits as well. One such test is to study the pattern of the collected current as a function of the biased voltage when one of the grids is being triangularly swept. If the space charge limits are violated, the collected current exhibits a sort of hysteresis pattern, and if space charge limits are not violated, the collected current retraces the same pattern and can be overlapped during plasma plateau of the discharge [42,64,66,67]. Detailed discussion of normal and abnormal behavior of RFEA in the STOR-M tokamak will be discussed in Chapter 5.

Perturbation to the Parallel Energy Distribution Function

The nonuniformity of the potential in the RFEA can alter the parallel component of the ion distribution function. To minimize and localize perturbations, a fine, thin grids, mounted and aligned on a supporting washer, were used. The relative change in ion energy, determined by the nonuniformity of the potential across the grid window, is given by [62]

$$\frac{\triangle E}{E} \approx \frac{D^2}{16s^2} \sim 0.15\%, \tag{4.10}$$

where D is the wire separation and s is the grid separation, 0.45 mm and 2.9 mm, respectively.

4.2.5 Probe Installation

The internal components of RFEA are assembled inside a protective housing. The housing which forms the probe head is made from Boron Nitride and has three components: the insulating housing which forms the basic structure of the probe, the insulating cap and two insulating ceramic rods that connect the probe with a feedthrough while protecting the signal wires from plasma (Fig. 4.1 and Fig. 4.2). A schematic of the internal parts of the probe head is shown in Fig. 4.7 and a photographs are shown in Fig. 4.1 and Fig. 4.2. The Boron Nitride (Grade AX05 Combat® Boron Nitride) was chosen due to its high thermal resistance, excellent electrical insulation properties, extremely low or negligible outgassing in ultra-high vacuum environments, and machinability. Ceramic rods (OD = 4.6 mm) are made from alumina (Al_2O_3), which is also a very good insulator with a high operating temperature ($\sim 1750°C$). In the Boron Nitride housing a small aperture ($\varnothing = 2$ mm) was drilled to provide an access for the plasma to the orifice plate. The probe was mounted on Huntington® Mechanical Laboratories linear feedthrough, which allows for measurements between minor radii of 16 cm and 11 cm. The axis of the probe is aligned along the local magnetic field, which is predominantly in the toroidal direction, facing against the toroidal ion drift. The probe head (h,w,l: $21 \times 15 \times$

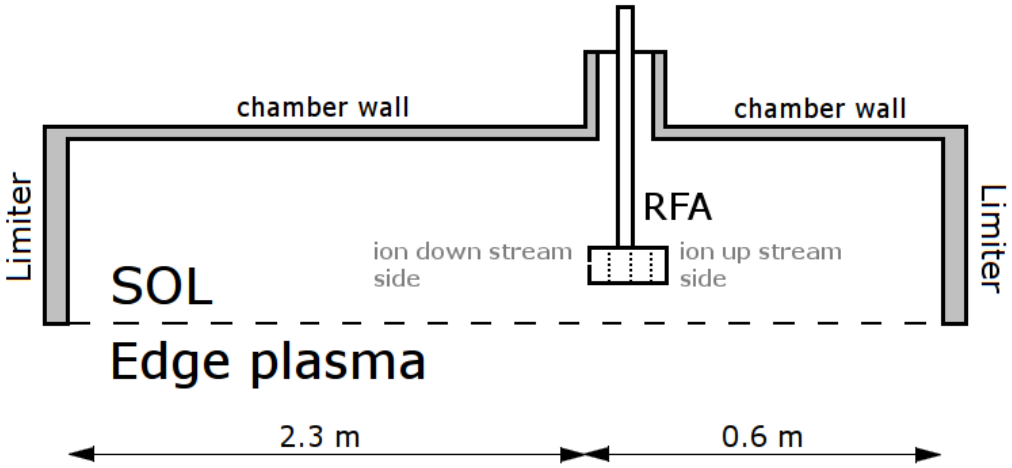

Figure 4.6: Side view of the experimental installation on STOR-M (not drawn to scale) showing the relative position of the probe with respect to limiters and the orientation of the probe with respect to the plasma current and toroidal field.

20 mm^3) is designed to fit inside the horizontal diagnostic port of STOR-M of inner radius 4.8 cm. An array of Langmuir probes and a Gundestrup probe are installed horizontally in ports separated toroidally from the RFEA. The Langmuir probe array is separated by 10 cm and located in front of the orifice plate of RFEA. The Gundestrup probe is separated by 20 cm and shifted even more than the Langmuir probe in the counter current direction.

The main internal components of the probe are the orifice plate, grids attached to supporting washers and the collector. Each have an independent bias control and from each current may be collected and measured. The first component in the assembly is the orifice plate. Behind the orifice plate there are three copper washers which form a support for the grids. The final component of this setup is the collector. All electrodes are isolated electrically from each other by MACOR ceramic washers, with approximately 2.9 mm spacing between grids. MACOR was chosen due to its excellent thermal characteristic (up to 1000°C), very good electrical insulation, and very low thermal expansion and outgassing [91]. Additionally all electrodes were packed together in the MACOR cup, which provided additional support (mechanically compresses together the orifice plate, washers with grids, collector and MACOR spacers) and electrical isolation from the 0.2 mm thick copper foil screen,

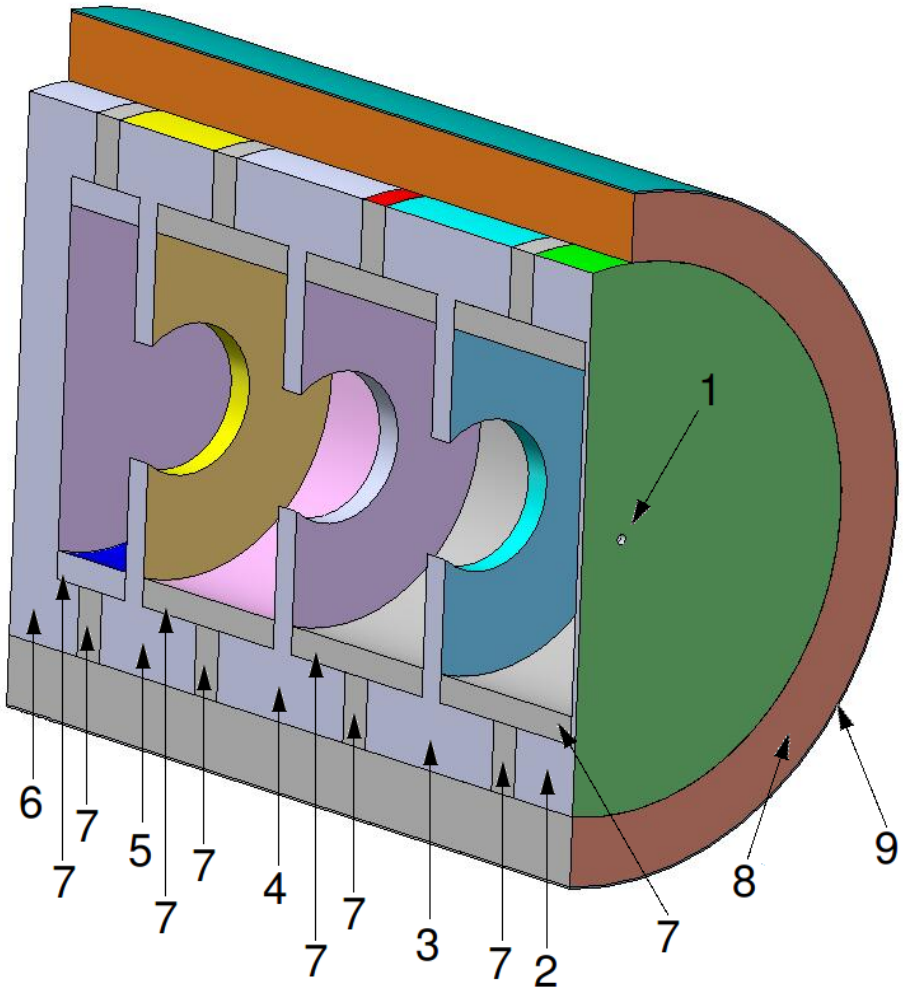

Figure 4.7: View of internal components of RFEA, showing: 1. orifice, 2. orifice plate, 3. electron repelling grid, 4. ion retarding grid, 5. secondary electron repelling grid, 6. collector, 7. MACOR insulators, 8. MACOR cup, 9. copper foil (electrostatic shield). Grids and wires to the grids omitted for clarity.

that electrostatically shields the whole assembly.

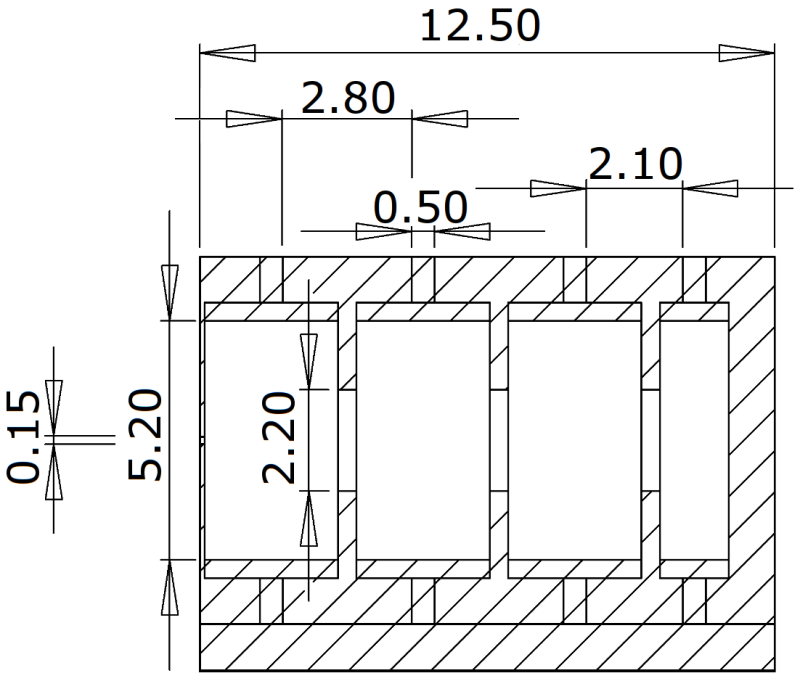

Figure 4.8: Dimensions of the RFEA internal components.

The electrical connections between electrodes and feedthrough are provided via coaxial and twisted pair cables. Inside the alumina rods coaxial cables were used for connecting the orifice plate, ion repelling grid, and collector. From the alumina rods to the feedthrough connections twisted pair was used. For electron repelling grids twisted pair was used all the way. The electrostatic screen was connected to tokamak ground.

Preliminary experiments showed the importance of electrostatic shielding in RFEA measurements. When coaxial and twisted pair replaced unshielded cables and copper foil screen was added, the noise level was significantly lowered.

4.2.6 Comparison of the RFEA devices in the STOR-M, JET and ISTTOK Tokamaks

Following the description of JET [67] and ISTTOK [64] RFEAs, this section summarizes and compares their critical parameters with the critical parameters of STOR-M

RFEA (Table 4.2). The critical space-charge limited current was estimated using Eq. 4.9 and the critical Brillouin flow current density was calculated using Eq. 4.8. The transmission coefficients were discussed and calculated in Section 4.2.2.

Comparison of the natural ambipolar collection length, $L_{\rm col}^{\rm amb}$, with the magnetic connection length, $L_{\rm col}^{\rm amb}$, indicated that RFEA can be considered as a nonperturbed probe. Such analysis was done in Section 3.1.1.

Parameter	**STOR-M**	**JET**	**ISTTOK**
Larmor radius [mm]	1.5	0.5	1.3
Critical current $I_{\rm sc,crit}$ in ion mode [μA]	250	250-360	230*
Brillouin current $I_{\rm B,crit}$ [μA]	0.2	20	4
Geometrical transmission	0.79	0.81	0.8
Entrance slit area [mm^2]	0.018	0.12	0.28
Measured ion side ion current [μA]	3	80	15
Measured current density [μA/mm^2]	170	670	54
Natural ambipolar collection length $L_{\rm col}$ [m]	1	14	0.6
Magnetic connection length $L_{\rm con}$ [m]	2.89	40	1.41
Internal diameter of the RFEA [mm]	5.2	10	4

* 30 μA in [64]. $I_{\rm sc,crit} = 230$ μA by our estimations using data from [64].

Table 4.2: Comparison of the RFEA devices in the STOR-M, JET [67] and ISTTOK [64] tokamaks.

According to Table 4.2, in STOR-M as well as in ISTTOK and JET measured RFEA current is higher then the Brillouin current, thus the ion beam radius is increasing inside the RFEA in all devices. The maximal shift of ion trajectories from the axis is equal two Larmor radii plus additional shift due to this increasing. In such conditions usage of the average Larmor radius, not the entrance slit radius, as a beam radius in the rough current density estimations is looking reasonably, as it has been done in JET and ISTTOK. The measured RFEA current is significantly lower than the current density limit estimation by Eq. 4.9, and consequently the space charge limitation may not be responsible for the abnormal RFEA behavior in all devices

(Section 5.5).

4.3 Electronics

For measurement with the RFEA, two types of power supplies are required: DC and sweeping. A block diagram of the probe biasing is shown in Fig. 4.9. Constant negative bias (-110 V and -9 V) is applied to the electron repelling grids in order to repel primary and secondary electrons. Generally current drawn by the grids was not measured, except for one campaign, where current from (primary) electron repelling grid was measured to study abnormal RFEA behavior.

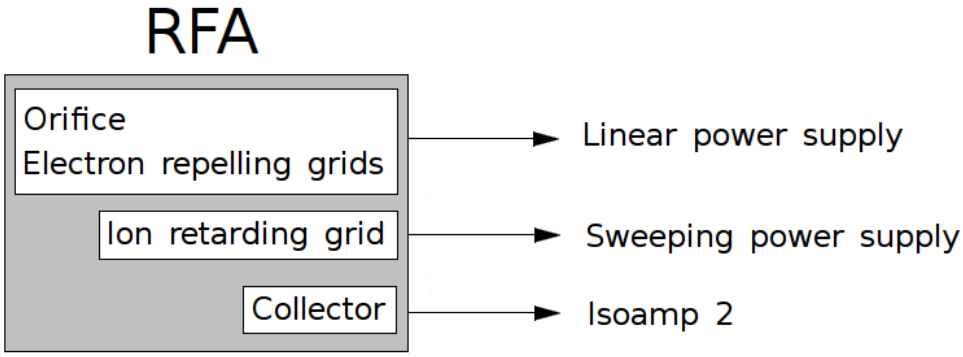

Figure 4.9: Block diagram of orifice, grid and collector electronics. Orifice and electron repelling grids each have a separate power supply.

To determine the ion temperature from the current-voltage characteristic, voltage on the ion retarding grid and the current collected by the collector needs to be measured. This was done using a custom manufactured sweeping power supply and isoamplifiers. For the purpose of the RFEA measurements the ion retarding grid is usually ramped using a $0.5 - 2$ kHz triangular wave and the biasing voltage can be up to 100 V. The power supply consists of 4 independent channels of which 3 are DC and one is sweeping. Additionally the power supply was redesigned to easily switch from ion mode to electron mode, without changing connections between the probe and power supply.

The voltage from the sweeping power supply is monitored by a voltage monitor and the output is send to the data acquisition system. The signal from the collector

is amplified by the isoamplifier (Isoamp2). Additionally the design of the Isoamp2 allows the removal of injected common-mode noise from the signals. In the DAQ two channels are used. One is used to measure the voltage on the ion repelling grid and the second measures ion current collected by the collector. Figure 4.10 shows a block diagram of the RFEA connections. The detailed electrical schematics of the

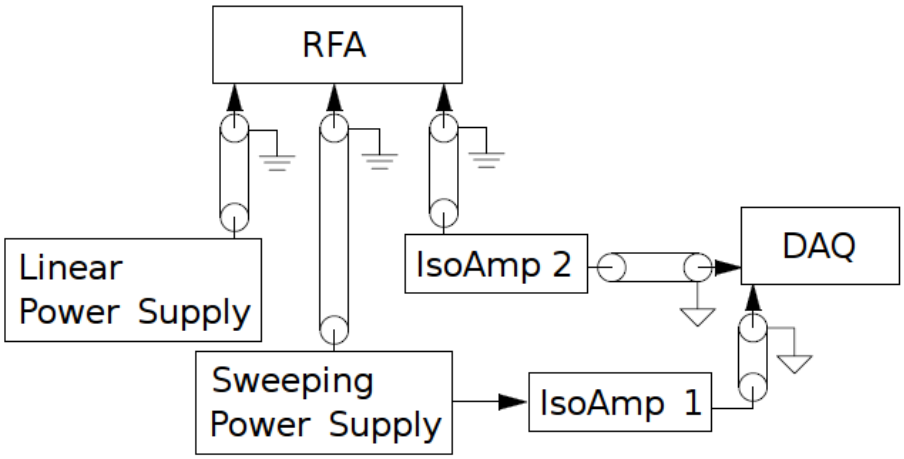

Figure 4.10: Block diagram of the RFEA power supply and isoamplifiers system.

RFEA electronics are described in Sections 4.3.1 and 4.3.2.

The two signals from the RFEA are sent across the room by a coaxial cable to a National Instruments ADC board NI-6133 with 2 MS sampling rate that has been used for data collection [92]. NI-6133 is a 8 channel 14-bit ADC with full-scale input range of ± 10 V. While capable of simultaneous sampling of up to 2.5 MS per channel, during measurements a sampling rate of 2 MS was used. The data is stored on a Windows PC, where it can be accessed and processed. Custom software for data analysis was developed.

4.3.1 Isoamplifiers

Isolation amplifiers are generally in use when low current is measured in the presence of high voltage [93, 94]. Iso-amps provide high electrical isolation (up to a few kV) and are very useful in amplification of low-level signals, what is the case for RFEA operation in the STOR-M tokamak. The Fig. 4.11 and Fig. 4.13 represents

the schematic and the final form of iso-amp used in RFEA measurements, which additionally includes differential amplifier.

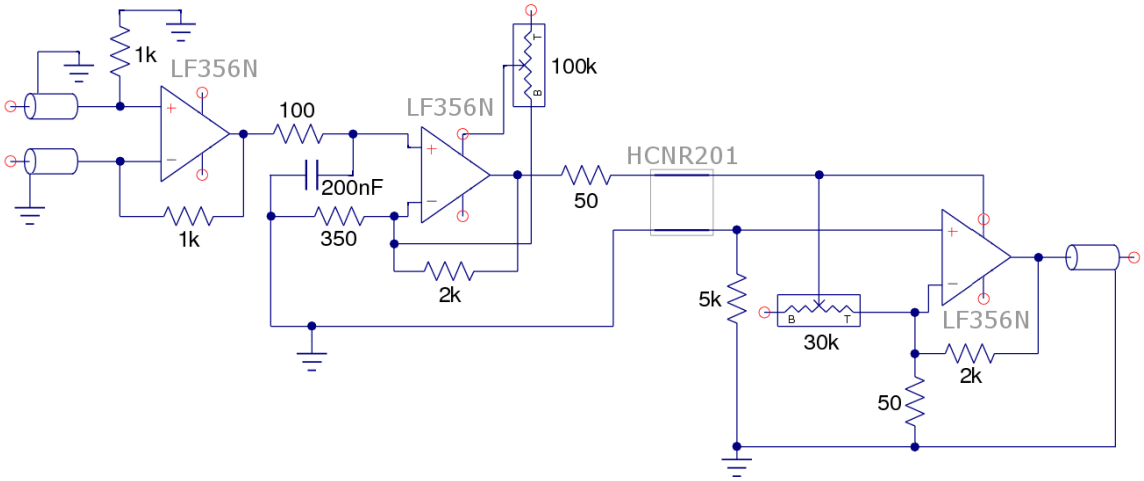

Figure 4.11: Isoamplifier circuit.

The base design of isoamp used in experiments is as follows. The input and output of the isoamp are LF356 JFET input operational amplifiers [95], which are electrically isolated by an optocoupler HCNR200 [96]. LF356 JFET op-amps were chosen, because they feature low offset currents/voltage and voltage drift and are low cost. They are designed for applications where wide bandwidth, low voltage and current noise, high common-mode rejection and large dc voltage gain is required. Operational amplifiers were powered with ±12 V power supplies built in the lab. The iso-amp design allows the selection of gains from 1 to 10^6, by adjusting the resistance of input resistors of the operational amplifiers. Miniature potentiometers (100 kΩ and 30 kΩ) are installed on the circuit board for calibration (ex. offset and frequency).

Optocoupler HCNR200 [96] provides good electrical insulation (tested for up to 1 kV), good stability, flexibility, linearity, bandwidth, high speed and low cost. Analog isolations circuits can be designed for amplification that have either unipolar or bipolar, with positive or negative input or output voltages.

Connections between the probe and feedthrough are coaxial and twisted pair cables, yet significant noise due to capacitive and inductive coupling of the cables has been observed. This induced voltage introduces hysteresis in RFEA I(V) characteristics,

which is similar to the one described in ISTTOK tokamak [64]. To remove the hysteresis and to suppress noise by two orders, an additional dummy wire twisted with the RFEA collector was used with the redesigned isoamplifier (isoamp2) shown in Fig. 4.11. In RFEA isoamp2 in an input circuit differential amplifier of induced noise voltage was added [97]. The dummy wire was connected to the input of the differential amplifiers, which amplifies only the differential portion of the input signal and rejects the common mode portion of the input signal, so the electromagnetic noise picked up by the "dummy wire" was removed from the total signal. In other words, differential amplifier strips injected common-mode noise off the signal.

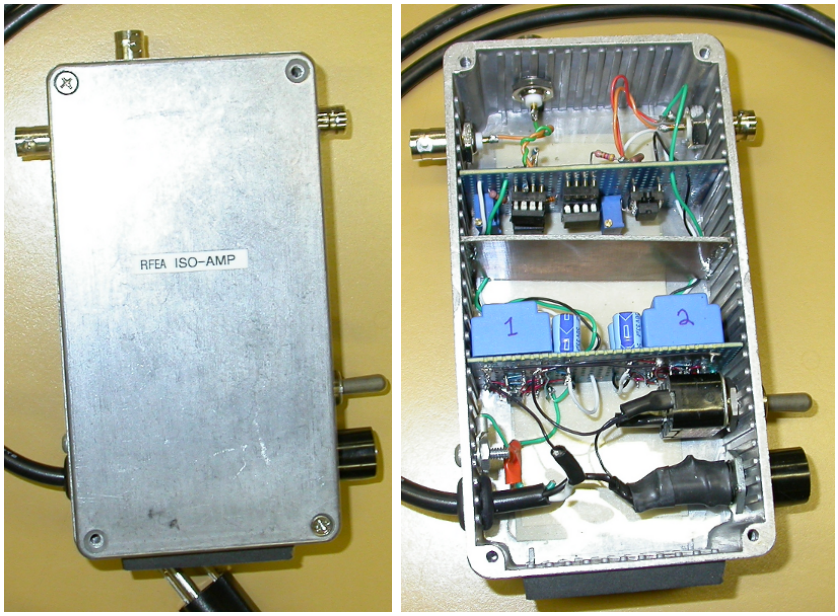

Figure 4.12: Isoamplifier Isoamp 2 (with common mode rejection) connecting RFEA (collector) and DAQ.

4.3.2 Power Supply

The power supply built for RFEA consists of two types of power supplies: DC and sweeping. The sweeping one consists of constant DC, triangular wave generator with transistor and isoamplifier that was used as a voltage monitor.

The circuit of DC power supply is presented in Fig. 4.14. This design at reasonable cost is very good for low current loads (very smooth voltage with a negligible ripple)

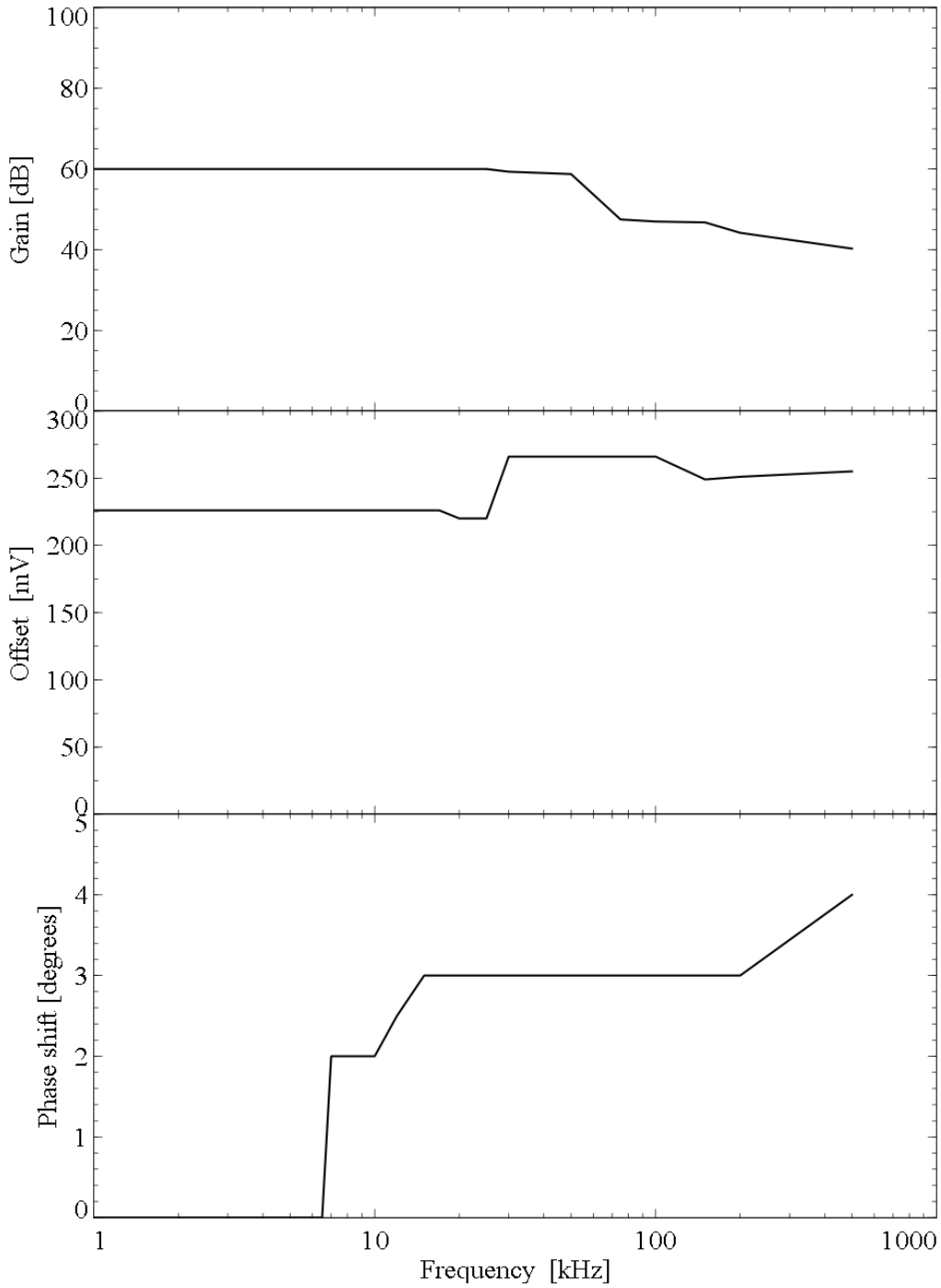

Figure 4.13: Gain, Offset and Phase shift vs. Frequency of the base design of isoamp used in experiments (isoamp1 and isoamp2).

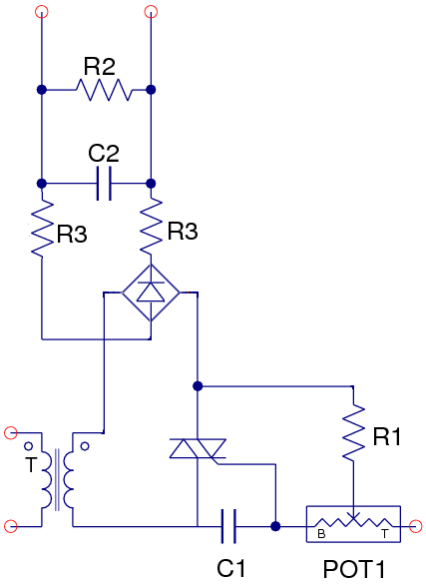

Figure 4.14: Power supply.

which are presents in RFEA. It consists of an isolation transformer N-67A, which is a power transformer designed especially for isolating equipment from direct connection to the power line (115 V to 115 V with full secondary load equal 1.3 A RMS). The primary and secondary windings are wound on separate arbors which are assembled on a laminate core separated by insulation, which provide 1500 V isolation between them [98]. Since N-67A is not a center-tapped transformer, for each polarity one transformer was used.

In the power supply a bridge rectifier KBPC1 was used, which is a 3 A single phase fullwave bridge rectifier [99].

The capacitors used in the power supply have two purposes: first is to smooth the rectified voltage (ripple filtering) and second is to act as a storage for additional charges so that power supply will be able to provide constant voltage level during operation (during load demands capacitor $C_2 \sim 680 - 1360\ \mu$F).

The purpose of resistors $R3 \sim 0.5 - 1$ kΩ is to limit current. The time between tokamak discharges and thereby time between operations of the power supply is about 3 minutes. Those resistors limit current to capacitor C_2 so the load on the transformer is lower (spreaded over the time). Resistor $R2 \sim 50$ kΩ acts as a permanent load, which is very helpful in the adjusting power supply (especially

under light loads).

The power supply presented in Fig. 4.14 is regulated, which means, that the output voltage can be adjusted up to about ±110 V and, with some adjustments to the circuit, even more. It provides good accuracy and precision within a few volts. The subcircuit of potentiometer $POT_1 \sim 50$ kΩ, triac Q2015R [100] and a capacitor $C_1 \sim 1$ μF is responsible for regulation of power supply. The subcircuit is used on the AC side and the regulation mechanism is as follows. When capacitor C_1 is charged up, it is discharges into the gate of triac which triggers the triac into conduction. For the remaining of the main half cycle the triac conducts. It turns off when the main voltage passes through zero. After certain time when C_1 is charged and discharged it provides new trigger for the triac. To control the rate of charging of the capacitor (and thus time when the triac fires), potentiometer POT_1 is used. By using potentiometer, the amount of power delivered to the load can be varied. Resistor $R1 \sim 3$ kΩ (2 W) is used to prevent short circuits.

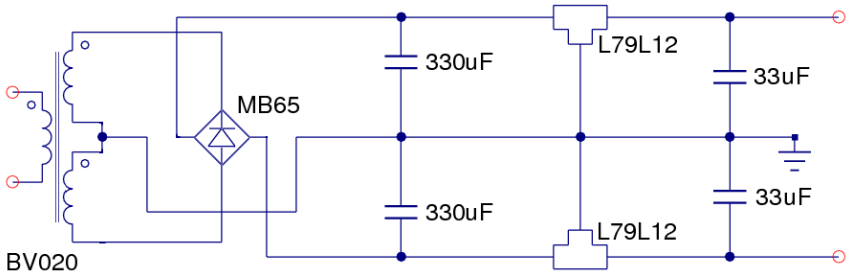

Figure 4.15: Power supply for isolation amplifier.

To power the isoamplifiers bipolar power supplies (±12 V) were built (Fig. 4.15). Transformer BV020 is a centertapped transformer [101] with secondary winding providing ±12 V and 29 mA (0.35 VA). MB6S, a full wave rectifier is a surface mount bridge rectifier. The power supply uses two types of capacitors (330 μF and 33 μF). The purpose of the first pair of capacitors is ripple filtering and the purpose of the second capacitors is further smoothing of the signal. In the power supply fixed regulators were used: MC78L06A for positive and L79L12 for negative polarities [102].

Sweeping Power Supply

The sweeping power supply (Fig. 4.16) is composed of two operational amplifiers, a transistor, a linear power supply and an isoamplifier that was used as a voltage monitor.

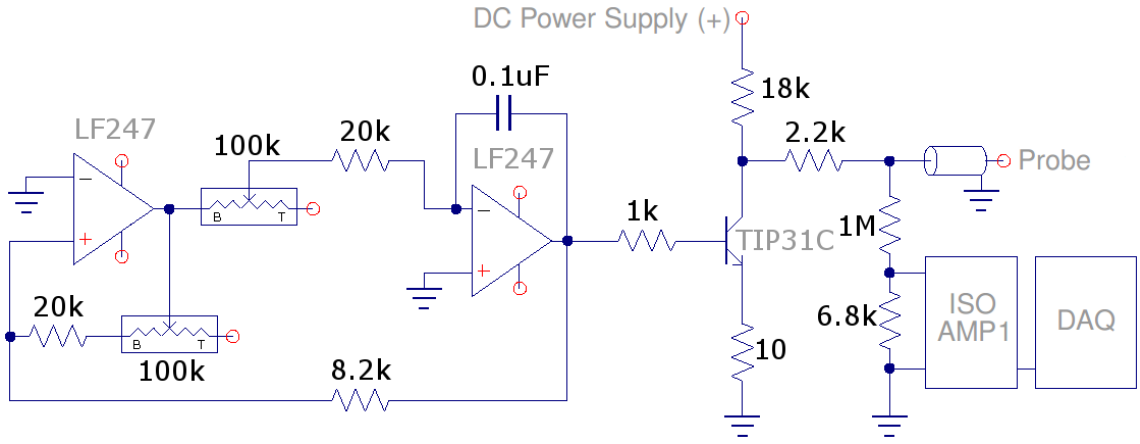

Figure 4.16: Base design for the sweeping power supply.

The set of two op-amps generates a triangular waveforms. The output of the first operational amplifier, which is a square wave, is integrated by the second op-amp. The output of the integration op-amp is a triangular wave [97]. The circuit allows modification of frequency (potentiometer R3), and amplitude (potentiometer R2) independently. Additionally, for the circuit to work, condition R2 > R3 is necessary. Operational amplifiers are powered with ±12 V linear power supply described above. The output of the triangular wave generator is connected with the base of transistor TIP31C, which is a silicon plastic power transistor designed for the use in general purpose amplifiers and switching applications [103]. The base current controls the collector current, which is connected to the output of the linear power supply presented in Fig. 4.14, which is further connected to the ion retarding grid in RFEA. To dissipate heat during transistor operation, a heat sink was installed.

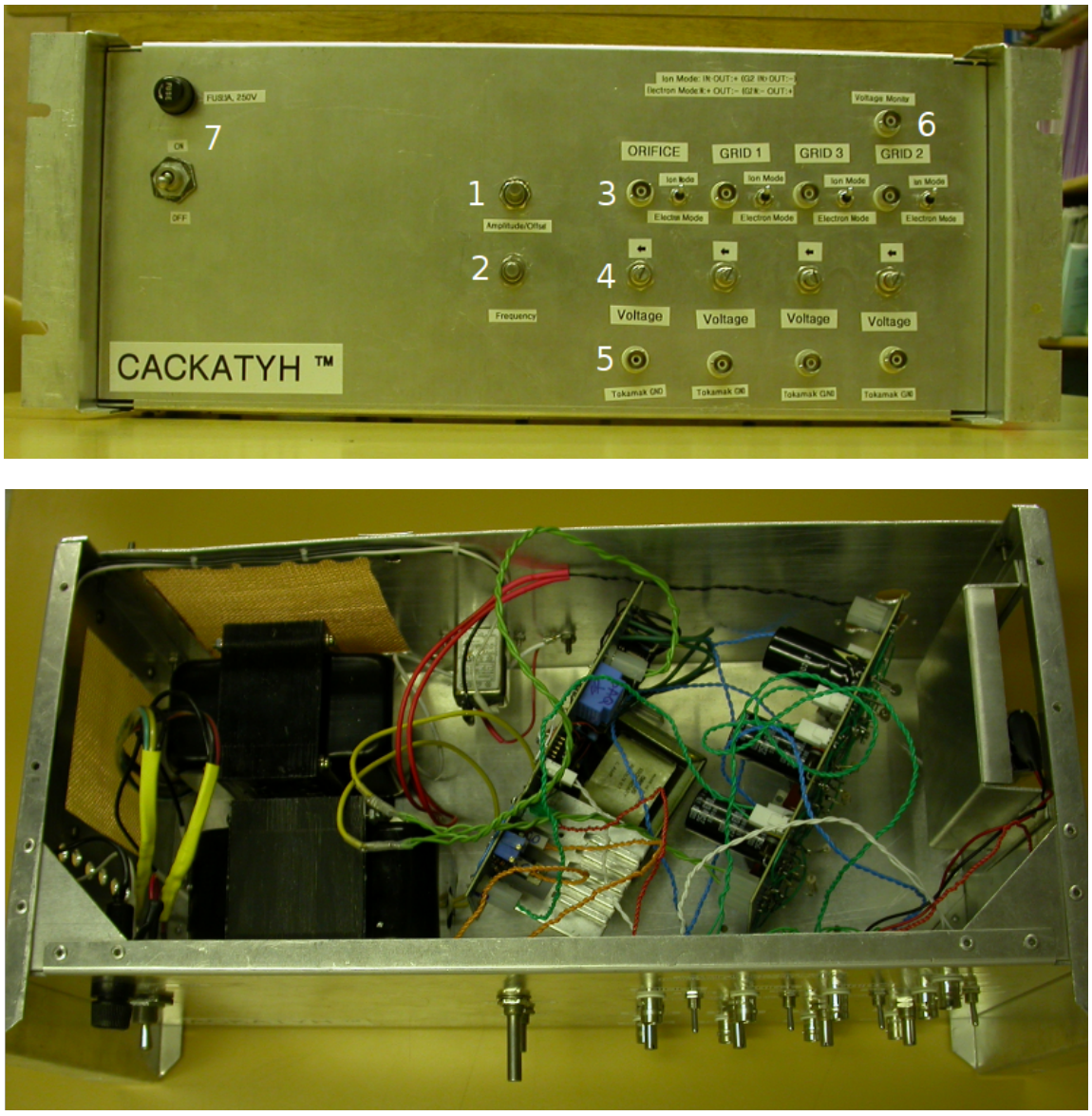

Figure 4.17: RFEA power supply: (1) amplitude regulator, (2) frequency regulator, (3) BNC outputs for RFEA with switch to operate in ion/electron mode, (4) voltage regulator, (5) BNC outputs grounded to tokamak ground, (6) voltage monitor, (7) switch ON/OFF and fuse.

Chapter 5

Experimental results

In this chapter the experimental results of operation of retarding field energy analyzer (RFEA, RFA) on STOR-M are described. The first section presents the general RFEA setup used in experiments during normal Ohmic discharge in STOR-M. The next section describes the method of obtaining the ion temperature using single directional RFEA and Gundestrup probe. Sections 5.3 and 5.4 discuss and present the results obtained during normal behavior of RFEA. The final section describes abnormal behavior observed during retarding field energy analyzer operation.

5.1 Introduction

In STOR-M, four phases of the plasma discharge can be distinguished. The discharge starts with an initial breakdown during which pre-ionization happens. This process is performed by the hot filament and the RF field. The purpose of this stage is to produce seed electrons, which are accelerated by the toroidal field. The collisions with neutral hydrogen produce more electrons. The next stage, current ramp up phase, lasts up to 10 ms. Those two phases are powered by a fast ohmic capacitor bank. After 10 ms the slow ohmic capacitor bank maintains the quasisteady current state (plateau) for up to about 40-50 ms, when the discharge is terminated by a strong gas puff in order to prevent runaway electrons production.

To obtain a high quality discharge, many factors must be considered. During every discharge plasma position is controlled by an active feedback system. To supply additional hydrogen, proper setting of the gas puffing is required (up to 5 puffs). Another important feature that affects the quality of the discharge is the presence

of impurities that contaminate hydrogen plasma. Everytime the chamber is opened and exposed to atmosphere (during installation of new probes, repairs, etc.), it is necessary to run a glow discharge which should be followed with about 24 hours of pumping and a few hundred discharges to obtain a good vacuum, with base pressure 1.2×10^{-7} Torr.

During RFEA experiments configuration presented in Figure 5.1 was used. The sign

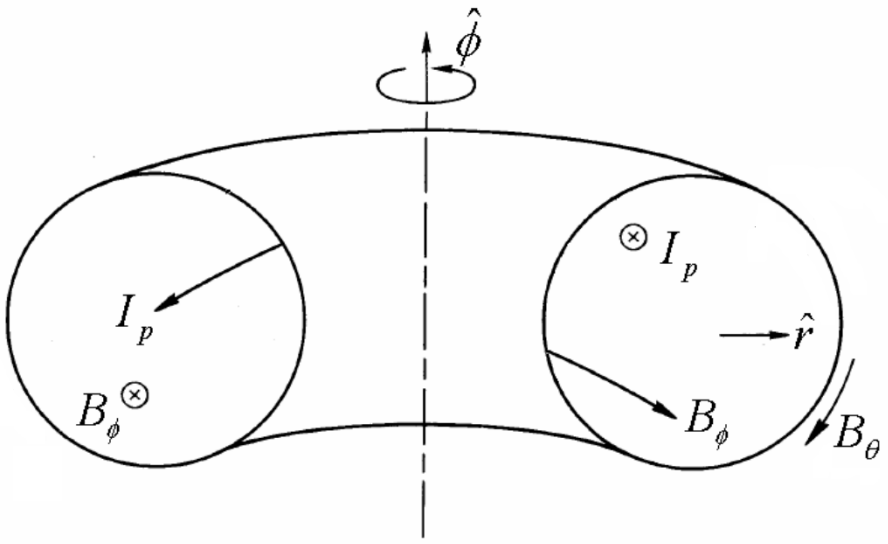

Figure 5.1: Orientation of parameters during normal operation of STOR-M (adapted from [28]).

convention under the right hand (r, ϕ, θ) coordinate system is as follows: the toroidal field B_ϕ is clockwise and plasma current I_p is counterclockwise when seen from the top of the tokamak. The poloidal field B_θ is downward at the outboard midplane. The plasma current was about $I_{\rm pl} \sim 20 - 25$ kA and the loop voltage was about $V_{\rm lp} \sim 2 - 4$ V. The plasma position was very stable during the experiments with RFEA, so it should not contributed to the total fluctuations of the collected signal. The main purpose of the RFEA was to obtain ion temperature in the SOL. The probe was also considered as a proof of principle in the further process of developing RFEA for STOR-M (Sec. 6.2). The RFEA was mounted in horizontal port of STOR-M, facing the ion down stream. RFEA was mounted on linear feedthrough in order to perform radial scans and additionally it was possible to rotate RFEA with respect to the toroidal field B_T in order to find the best alignment, since the RFEA measures

parallel energy of ions. As expected, when the probe was aligned with the magnetic field, the signal was the strongest, since the flux that entered the probes' orifice was maximal. When the probe was rotated away from the parallel position, the signal weakened until it disappeared completely. Additionally, when the RFEA was misaligned, the abnormal behavior appeared at radial positions, where with proper alignment, such phenomenon was not observed. The abnormal behavior of RFEA, described in Section 5.5, manifests in the generation of a negative current in the collector plate at $3 - 20$ ms.

Different combinations of grid connections and grid numbers have been used in the RFEA operation [67]. Two ion mode RFEA configurations that were used in STOR-M, are shown in Fig. 5.2. Reversing the grid potentials allows the analysis of electron

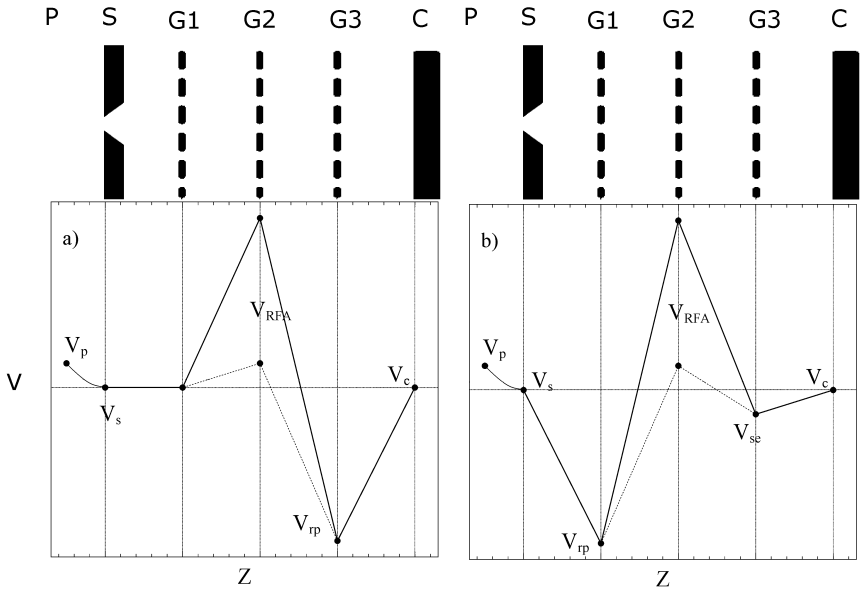

Figure 5.2: RFEA schematic and potential distribution in the ion mode, where P is plasma, S is entrance slit, G1-G3 are grids, C-collector, V_{p}, V_{s}, V_{rp}, V_{RFEA}, V_{SE}, V_{c} are plasma, entrance slit, electron repelling, sweeping ion retarding, secondary electron emission suppression and collector potentials. a) two grids configuration; b) configuration with e^- suppression in the third grid.

temperature in the electron mode of RFEA operation.

To illustrate RFEA results, the general configuration of the probe is presented here. Generally the ion retarding grid was swept between 0 V and +70 V, which was

sufficient to repel all ions except when the probe was in the vicinity of the limiter, where sweeping amplitude was increased to +100 V. Plotting the current collector as a function of the ion retarding grid voltage gives the $I-V$ characteristic. As mentioned earlier, by taking the derivative of the $I-V$ characteristic (Eq. 2.4), the ion (or electron) distribution function can be obtained. Yet a more practical approach used widely relies on fitting an exponential to the $I-V$ characteristic. From fitting, the ion temperature can be obtained.

During the experiments, the probe was moved between r=16 cm and 11.5 cm over a number of discharges so the radial profile can be obtained.

In other tokamaks, where bidirectional RFEA was used, the asymmetry of measurements between ion down and upstream was observed [58, 59, 66, 67]. It is proposed that many different parameters might affect that, such as direction and the varying magnitude of the B_T, unstable plasma position, different ambipolar collection lengths or the presence of high toroidal flow [63,66,67,70]. High toroidal flow might be a substantial source of momentum transferred to ions, which would produce asymmetric ion temperatures measurements.

5.2 Method of Ion Temperature Determination by One-Side RFEA and Gundestrup Probe

Theoretical and numerical models used to study plasma-RFEA interaction, show that plasma rotation significantly affects the measured RFEA distribution function. The shift in the parallel ion velocity distribution function, determined by ion drift velocity, introduces additional V_{shift} offset in $I-V$ characteristics. In the JET tokamak it has been observed that RFEA measurements show lower ion temperature on the ion upstream than on the ion downstream side, an effect which has been predicted theoretically due to the plasma rotation [63, 67].

In STOR-M tokamak, high parallel flow velocities ($M_{||} = 0.4$) has been measured by a Gundestrup probe [38, 76]. To account for the plasma rotation in the T_i measurements, design of the bidirectional RFEA has been proposed (Sec. 6.2.2). An

accurate estimation of the ion temperature can be obtained by taking the average of the temperatures measured on each side of the bidirectional RFEA

$$T_i = \frac{T_+ + T_-}{2}, \tag{5.1}$$

where T_+ and T_- are ion temperatures from ion downstream and upstream sides respectively. For ion temperatures relevant to tokamak SOL plasmas (i.e., $T_i > T_e$), this averaging procedure yields unperturbed ion temperature within an accuracy of a few percent [63]. Comparison of the Gundestrup probe data and RFEA measurements from the plasma rotation side can only be used for rather accurate determination of T_i with one side measured only. According to analytical estimation, verified by numerical simulations, ion temperature normalized to the electron temperature measured by the RFEA is [63]:

$$T_\pm(\varphi_s) = \tau \pm U_0\sqrt{\frac{\pi\tau}{2}}\left[\mathrm{erf}\left(\frac{\pm U_0}{\sqrt{2\tau}} - \sqrt{\frac{\varphi_s}{\tau}}\right) + 1\right]\exp\left(\frac{\left(\sqrt{2\varphi_s} \mp U_0\right)^2}{2\tau}\right) \tag{5.2}$$

where $\tau = T_{i,0}/T_i$ is the unperturbed ion temperature normalized to the electron temperature, $U_0 = M_{||}\sqrt{1+\tau}$ is the mean ion velocity (also called plasma drift velocity), $M_{||}$ is the parallel Mach number, $\varphi_s = e(V_{\mathrm{RFEA}} - V_{\mathrm{shift}})/kT_e$ is the retarding potential normalized to electron temperature and k is the Boltzmann constant. The sign in the Equation 5.2 corresponds to measurements with RFEA facing ion downstream ("+") and upstream ("−") side. According to the experimental setup used in JET [67] and ISTTOK [64], the retarding voltage interval used for T_i determination is about

$$e(V_{\mathrm{RFEA}} - V_{\mathrm{shift}}) = (0-4)kT_i. \tag{5.3}$$

In the SOL region of a tokamak, the assumption $\tau = T_{i0}/T_e = 1.5-2$ is reasonable. [58, 59, 64, 66, 67]. The interval of the normalized retarding potential

$$\varphi_s = \frac{2e(V_{\mathrm{RFEA}} - V_{\mathrm{shift}})}{kT_{i0}} \sim 0-8 \tag{5.4}$$

is used for RFEA measurements. In the STOR-M tokamak, the parallel Mach number is determined by the Gundestrup probe. The experimental Mach number can be

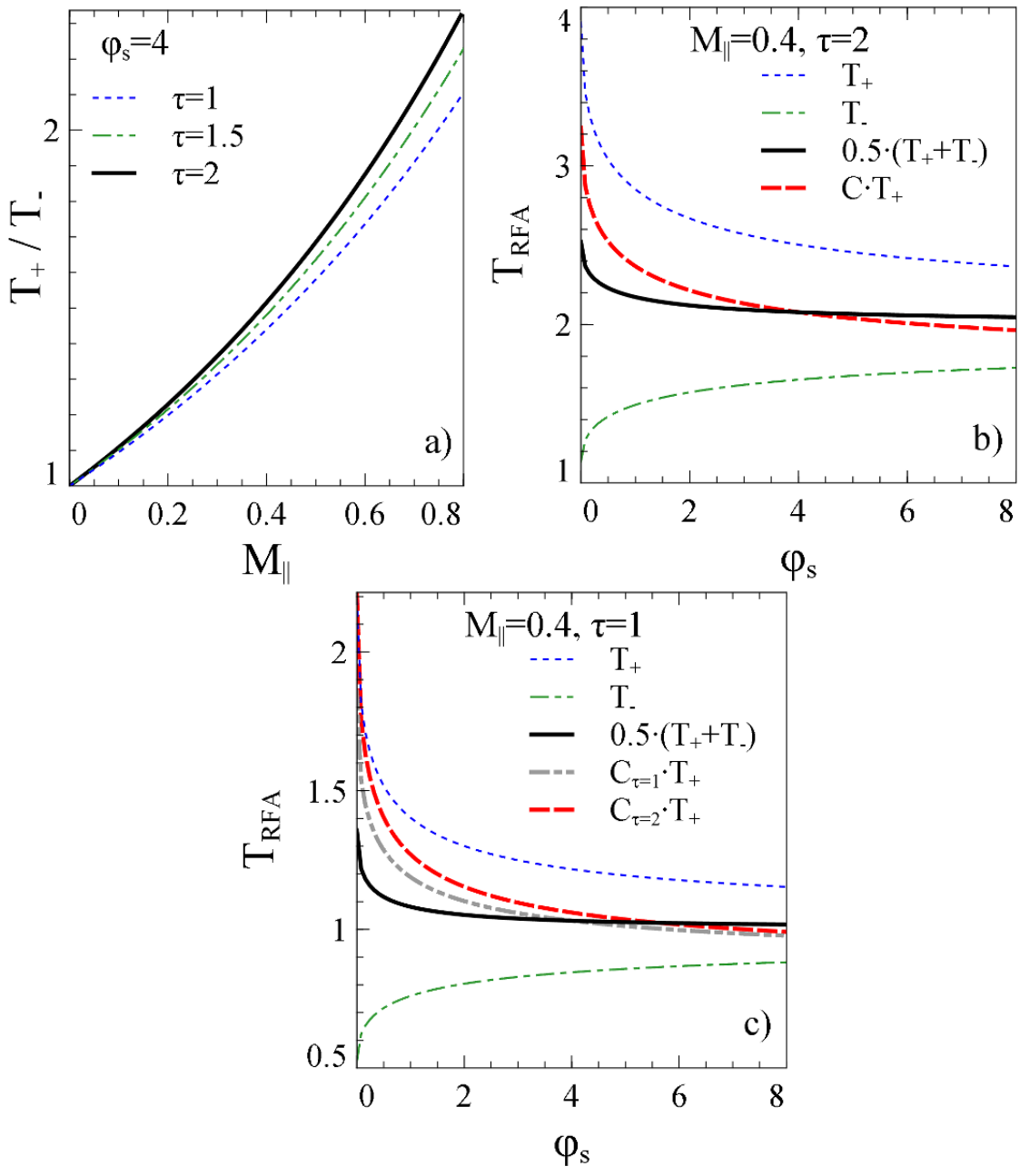

Figure 5.3: (a) The dependence of upstream and downstream temperature ratio on the Mach number for different τ. (b,c) Calculations of T_{RFEA} from downstream side T_+, upstream side T_-, its average (solid line) and corrected (dashed line) ion temperatures. For comparison, the corrected ion temperature (dash-dot-dot line) based on $\tau = 1$ is replotted in c).

used to determine the ratio of upstream to downstream side temperatures

$$\alpha = \frac{T_- (\varphi_s = 4)}{T_+ (\varphi_s = 4)} \tag{5.5}$$

and the ion temperature can be determined by single-sided RFEA data and the parameter α:

$$T_{i0} \sim < T_i > = 0.5(T_+ + T_-) \sim 0.5(1 + \alpha)T_+ = cT_+ \tag{5.6}$$

Resonable assumptions for τ and ϕ_s are used due to the absence of simultaneous electron temperature measurements. The dependence of the two-side ion temperature ratio on the Mach number is shown in Fig. 5.2a. The dependence of α on the Mach number is not sensitive to τ values. Results of two-side ion temperature calculations, average ion temperature and ion temperature obtained by plasma rotation side data normalization are shown in Fig. 5.2a for a case of $M_{||} = 0.4$, $\tau = 1$ and in Fig. 5.2b for $M_{||} = 0.4$, $\tau = 2$.

The upstream and downstream temperature ratio represents accuracy of the proposed technique. The dependence of the temperature ratio on τ is not significant, as seen in Fig. 5.2. The τ dependence in the region $\tau = 1 - 2$ is an order of magnitude smaller than the $M_{||}$ dependence in the range $0 < M_{||} < 0.8$. The difference between the averaged temperature based on two-sided RFEA and the corrected temperature based on single-side RFEA and Mach number is less than 10% in the region $\varphi_s \sim 2 - 8$ as seen in Fig. 5.3. The error of the proposed technique is expected to be similar to that in the two sided average technique claimed in [63] for the $\tau = 1 - 2$ range.

5.3 Experimental Results in Normal RFEA Operation

Different combinations of RFEA grids connection have been tested in the STOR-M tokamak in the ion and electron modes of RFEA measurements. The configuration with the first grid connected to the grounded orifice, sweeping ion retarding voltage

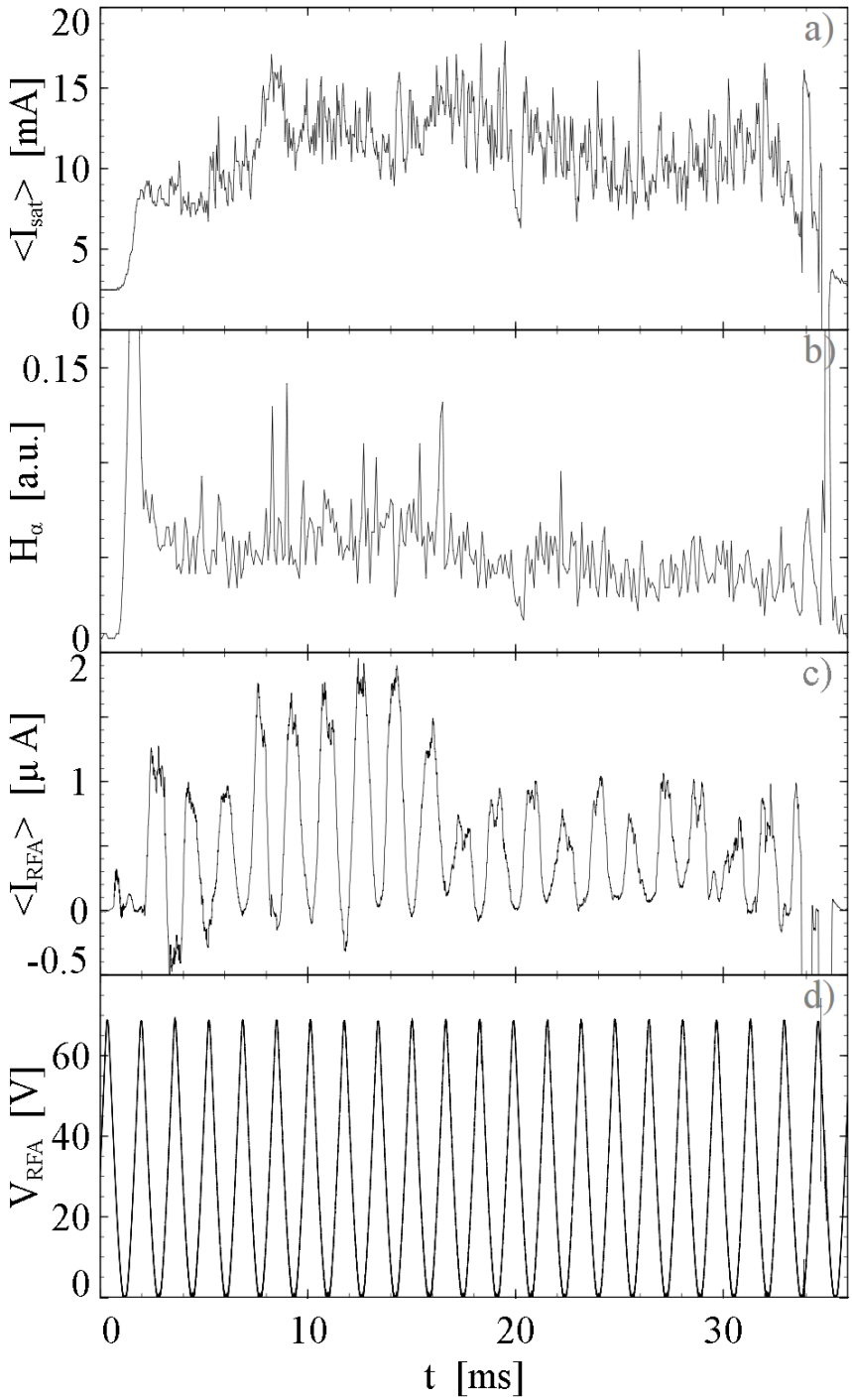

Figure 5.4: (a) Ion saturation current collected by a collector plate of the Gundestrup probe parallel to plasma current using 10 kHz low pass filter (r=13 cm), (b) H_α emission, (c) filtered RFEA collector current using 10 kHz low pass filter and (d) RFEA sweeping voltage of unaveraged RFEA collector current. The radial position of the probe $r = 15$ cm ($\triangle$r=2 cm). RFEA orifice is grounded.

applied to second grid and electron repelling voltage applied to the third grid, shown in Fig. 5.2, has been proved as a best ion mode configuration for STOR-M. In this configuration the appearance of abnormal RFEA behavior is minimal. This configuration is similar to the main JET RFEA configuration [67]. Fig. 5.4 presents typical ion mode signals in this configuration.

According to previous measurements [38,75], the plasma potential in the SOL region of STOR-M is positive. In this case, a grounded orifice is more negative than the plasma and will not repel any ions. Such a RFEA measurement scheme has been used in all ion mode experiments. Fig. 5.5 shows unaveraged RFEA collector current and the floating potential signal measured by the Langmuir probe from the same discharge shown in the Fig. 5.4.

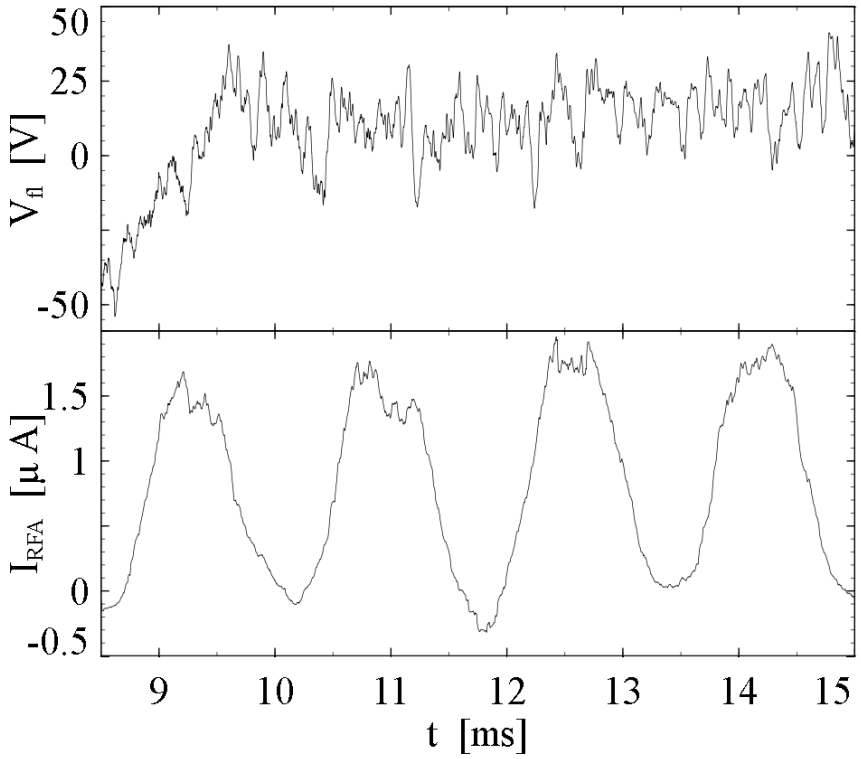

Figure 5.5: RFEA collector current I_{RFA} and the floating potential V_{fl} measured by the Langmuir probe.

The decrease in the current fluctuations at the highest retarding voltage indicates that influence of electrostatic noise induced by plasma potential fluctuations on measured signals is not dominant. According to conventional RFEA principles

[40, 64, 67, 90, 104], fluctuations of the electron density and temperature should not affect the measurement of T_i due to complete electron current retarding. Observed RFEA signal fluctuations can be explained by the ion density and temperature fluctuations in the SOL region of STOR-M. As well, plasma potential fluctuations modify the I(V) characteristic through V_shift variations. This potential shift is equal to the difference between the plasma potential V_pl and the probe ground [105].

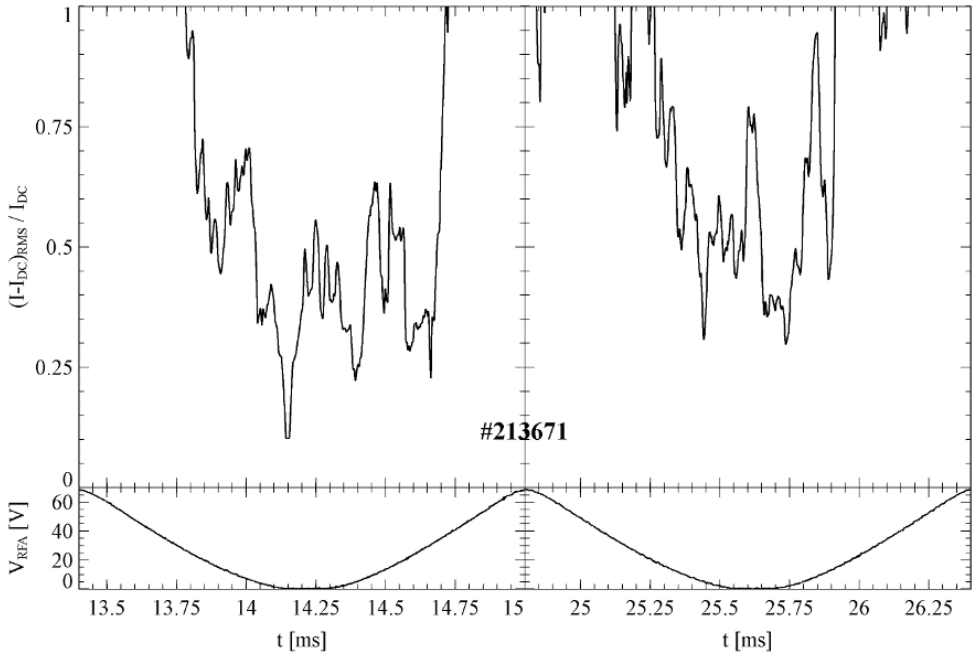

Figure 5.6: Ratio of the fluctuating part of the RFEA collector current to averaged the RFEA collector current and RFEA retarding voltage in two different time windows.

The RFEA measurements strongly depend on plasma conditions like plasma position, plasma-wall interaction, edge density and potential fluctuations. The fluctuation of those parameters will significantly contribute to fluctuations of the measured values. Plasma parameter fluctuations in the SOL region of tokamaks are usually very high and the STOR-M tokamak is no exception [38, 75]. By using simultaneously RFEA to measure T_i and the Rake probe to measure T_e, the variation of the ion and electron energies can be expressed as a function of the STOR-M plasma conditions. Simple comparison of ion density fluctuation measured in JET and RFEA collector current fluctuations using Fig. 5.7 data from [67] shows that expected RFEA signal

fluctuations are averaged by low bandwidth electronics. In STOR-M discharges during RFEA testing non harmonic bursty fluctuations with maximum statistical appearance in $15-20$ kHz are observed both in RFEA collector current and in floating potential measured by the Langmuir probe. In such conditions, about 10 bursts appeared during 0.5 ms of rising time of the retarding potential, or about half of burst during sweep time where the retarding voltage is considered as a constant in the I(V) characteristic. Thus, fluctuations significantly disturb the I(V) characteristic and affect ion temperature measurements. The retarding voltage sweeping rate should be around 5 ms for applicability of the simple time averaging filter technique. Such a slow rise time is significantly slower than the ions Maxwellization time in the STOR-M tokamak and ion temperature may change significantly during the RFEA voltage scan. Simple electrical or numerical filtering does not help in such a situation and numerical averaging of the data set, if the scans are fast enough, is more accurate. This technique introduces time averaging of the ion velocity distribution function as well as average of the collector current fluctuations versus retarding potential. Averaging of the distribution function, in contrast to its shape distortion in the case of slow retarding voltage scan, allows evaluation of a more accurate average ion temperature.

In addition to the clear dependence of collector current fluctuations to retarding voltage, characterized by the signal to noise ratio, clear signal fluctuation time evolution has been observed. At the beginning of the discharge ($6 - 15$ ms), the fluctuating part of the collector signal is less significant and appears in the wide retarding voltages range in comparison with the later phase of the discharge ($15 - 30$ ms). Fig. 5.6 shows the ratio of fluctuating component to the time averaged current at the beginning and during the later phase of the discharge.

5.4 Evaluation of the Ion Temperature in STOR-M Tokamak

5.4.1 Ion Mode

As mentioned already, a high level of ion density and temperature fluctuations introduces difficulties in ion temperature function determination and averaging of many

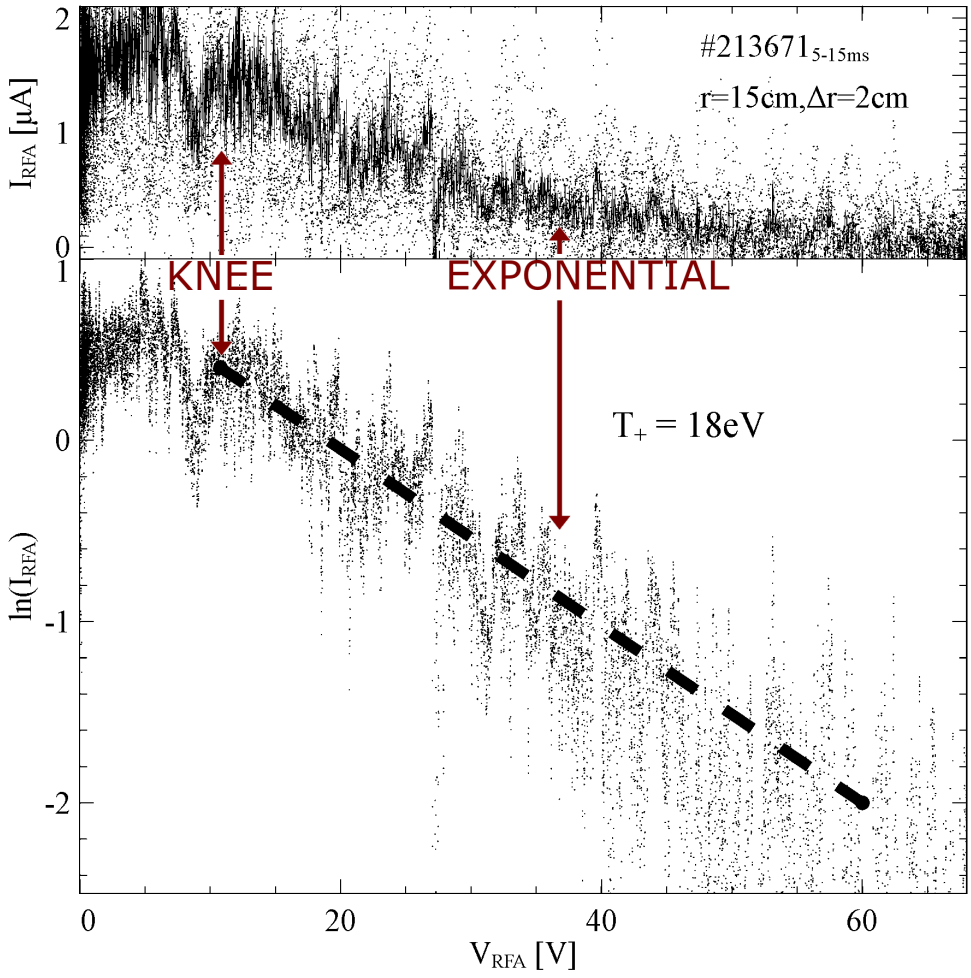

Figure 5.7: RFEA $I(V)$ characteristic in ion mode and fitting line in logarithmic scale corresponding to the RFEA ion temperature $T_+ =$ 18 eV.

slopes is required for data analysis. Fig. 5.7 shows the $I(V)$ characteristic of the RFEA in ion mode operation, based on slope averaging from 5 to 15 ms of the dis-

charge. The plasma potential around $10 - 15$ V has been determined from the knee of the $I(V)$ characteristic in Fig. 5.7. In the present discharge V_{shift} is equal to the plasma potential (orifice and collector are grounded) and the knee voltage is equal to the plasma potential.

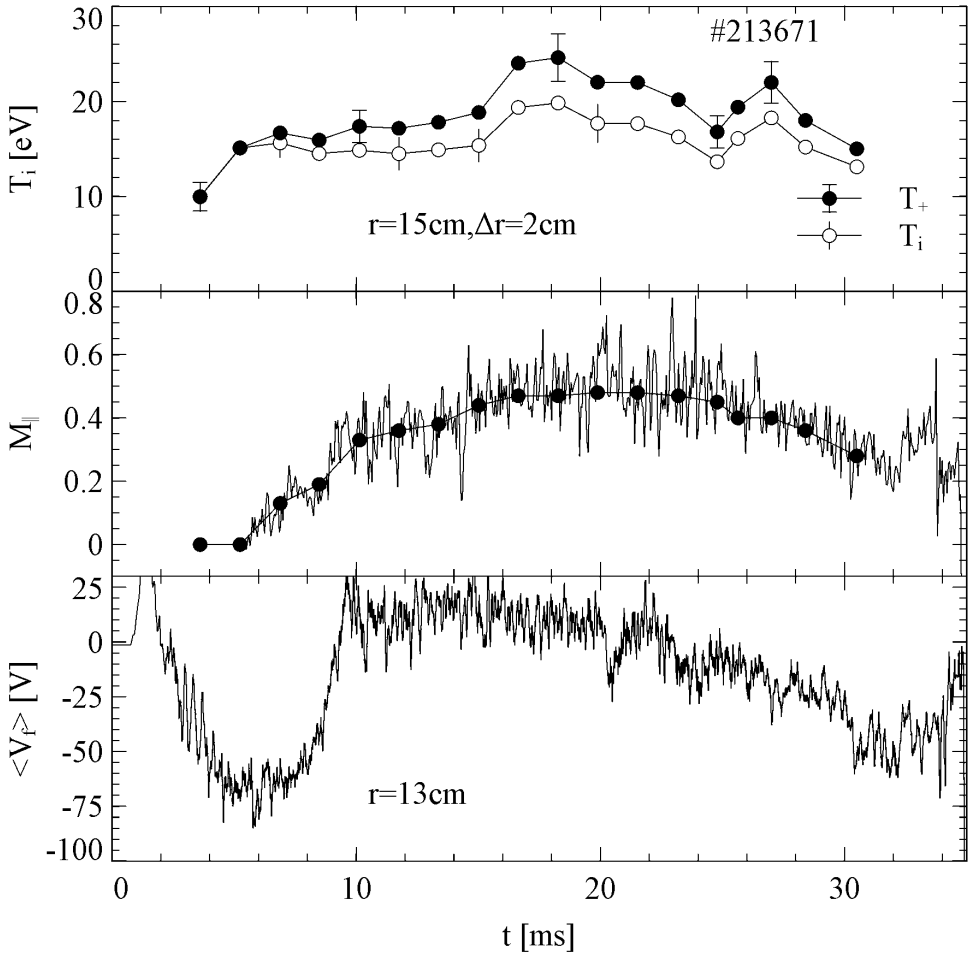

Figure 5.8: From top: time trace of T_+ and ion temperature at $r = 15$ cm obtained using four RFEA slopes (3 ms) averaging, averaged parallel mach number measured by Gundestrup probe at $r = 13$ cm, time averaged floating potential from Langmuir probe at $r = 13$ cm, and time averaged ion density measured by ion saturation current from collector plate of the Gundestrup probe the in ion down stream direction.

Ion temperature determination shows variation of ion temperature during STOR-M discharges. Time evolution of the measured temperature T_+ in the ion down stream side RFEA and ion temperature reconstructed using Gundestrup probe data

T_i is shown in Fig. 5.8. The quick rise of the ion temperature can be clearly seen at the beginning of the discharge, during plasma current ramp up. Increase in T_+ during initial discharge stage up to $12 - 15$ ms is correlated with the plasma current increase and toroidal spin up in the direction of the plasma current. The

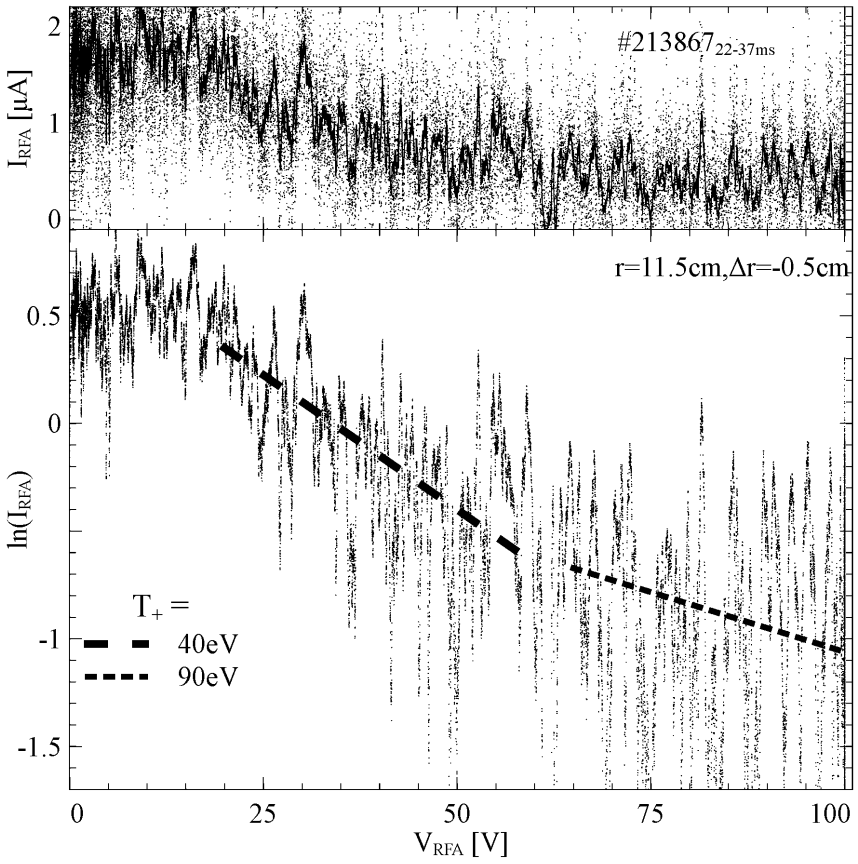

Figure 5.9: RFEA I(V) characteristic in ion mode and fitting line in logarithmic scale corresponding to the ion temperature 40 eV. Probe was at position 0.5 cm deeper than the Separatrix (LCFS). Additionally the $I(V)$ characteristic indicates a high energy tail in the ion distribution function, but due to the fluctuating nature of the signal, it is impossible to determine unique ion temperature of this tail. Estimates of 90 eV seem to be resonable.

Mach number increases from 0 to 0.55 during the early phase of the discharge. The floating potential drop usually observed at the beginning of the STOR-M discharge is characterized by negative SOL plasma potential [38]. Absence of a clear correlation between ion temperature and floating potential indicates that at the radial location of RFEA, plasma potential is still positive at $r = 15$ cm. This information, in

addition to plasma potential measurement by RFEA, shows that grounding of the orifice does not introduce the repelling of ions.

According to experimental results in the SOL region, ion temperature is significantly higher than the electron temperature. Similar observations have been made in different tokamaks particularly in the Tore Supra tokamak [106]. The electron temperature profile is consistent with Langmuir probe measurements [38, 75] and is in the range of $20-40$ eV. The ion temperature profile is very similar to JET results from the ion down stream side [67] and TORE SUPRA results [106].

In contrast to the SOL region, the $I(V)$ characteristic in the plasma edge region indicates a high energy tail in the ion distribution function. An example of the RFEA I(V) characteristic measured at position 0.5 cm deeper than the last close magnetic surface (at r=11.5 cm) is shown in Fig. 5.9.

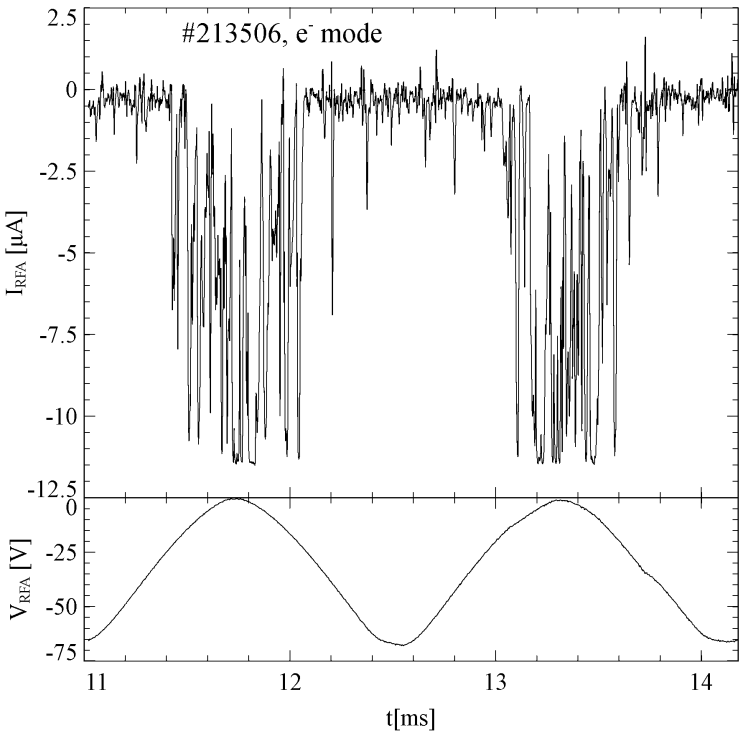

Figure 5.10: RFEA in electron mode of operation. Radial position of RFEA r=14 cm with orifice biased to +40 V. It is clearly seen, that the level of signal fluctuation in electron mode is significantly higher than in ion mode.

In the SINP tokamak [107] a high energy tail has been observed. It has been at-

tributed to sawtooth activity. The fluctuating nature of the RFEA signal observed in the STOR-M tokamak does not allow us to determine unique high energy ion temperature. The 90 eV line in Fig. 5.9 is shown as a reasonable estimate. Ion energy up to $150 - 200$ eV has been registered in STOR-M by RFEA at that position in sweeping mode as well as in constant retarding voltage mode of RFEA measurements.

5.4.2 Electron Mode

The RFEA has been successfully tested in the electron mode as well. Figure 5.10 shows an example of the RFEA collector current and the retarding voltage time traces in this mode. The level of fluctuations when the absolute value of retarding voltage is maximal is significantly less than when it is minimal. This is an indication that electron temperature and density fluctuation influences on the measured current is significantly higher than electrostatic noise. The level of signal fluctuation in electron mode is significantly higher than averaged collector current, in contrast to RFEA ion mode. The fluctuating nature of the collector current signal in the electron mode can introduce higher than in the ion mode asymmetry (in the slope voltage) of collector current during different slopes of retarding voltage. This asymmetry is determined by plasma temporal evolution only and is not related with RFEA features. For example, in Fig. 5.10, for the central rising and falling slopes the current fluctuation levels are lower than in outer slopes. In such conditions, only statistical analysis of many RFEA slopes can give reliable electron temperature. In the electron mode, RFEA current disappears if the absolute value of the retarding voltage is significantly lower than that in the ion mode. This is a clear indication that the electron temperature is lower than ion temperature in the SOL region of the STOR-M tokamak.

5.4.3 Radial Profile of the Ion Temperature

In order to study the radial force balance equation in the SOL region, it is necessary to determine the spatial profile of the ion temperature, from which the ion pressure gradient can be estimated. STOR-M RFEA can measure ion (and electron) temper-

ature from ion down stream side in radial direction between radii 16 cm and 11 cm, but additionally there are limitations on operation, like abnormal behavior. Figure 5.11 present the radial profile of the ion temperature. By reversing the polarity of the grids, electron temperature was obtained and was compared with results from the Rake probe from previous experimental campaigns. The results, not presented here, agree to within a few eV [38].

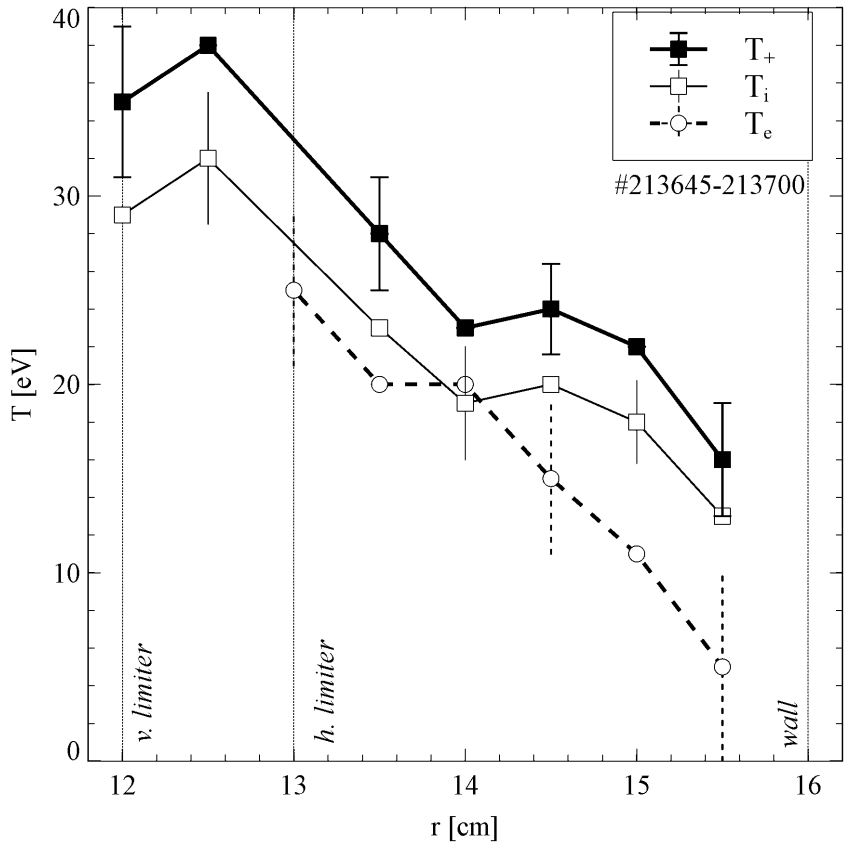

Figure 5.11: Radial profiles of T_+, ion and electron temperatures measured by RFEA using a set of STOR-M discharges by mechanical movement between discharges.

Temperatures in the radial profile (Fig. 5.11) have been reconstructed from averaging about $10 - 18$ RFEA slopes in the flat top stage of STOR-M discharges. Variation of RFEA radial position has been performed between discharges and data from a set of similar STOR-M discharges has been used.

It is clearly seen in Fig. 5.11 that the ratio T_+/T_e is the highest near the wall and it steeply reduces as it approaches radial position 14 cm. Between 14 cm and 13 cm

the ratio remains constant.

From the radial profile of ion temperature, the ion pressure gradient can be obtained. During the RFEA experimental campaign, the Rake probe, due to technical problems, was out of operation for the most of the time, and it was impossible to obtain the radial profile of the floating potential and consequently estimate the radial electric field from the formula $E_r = -\nabla V_f - 3T_e/e$ [38]. Without the E_r, the radial force balance equation (1.14) cannot be verified.

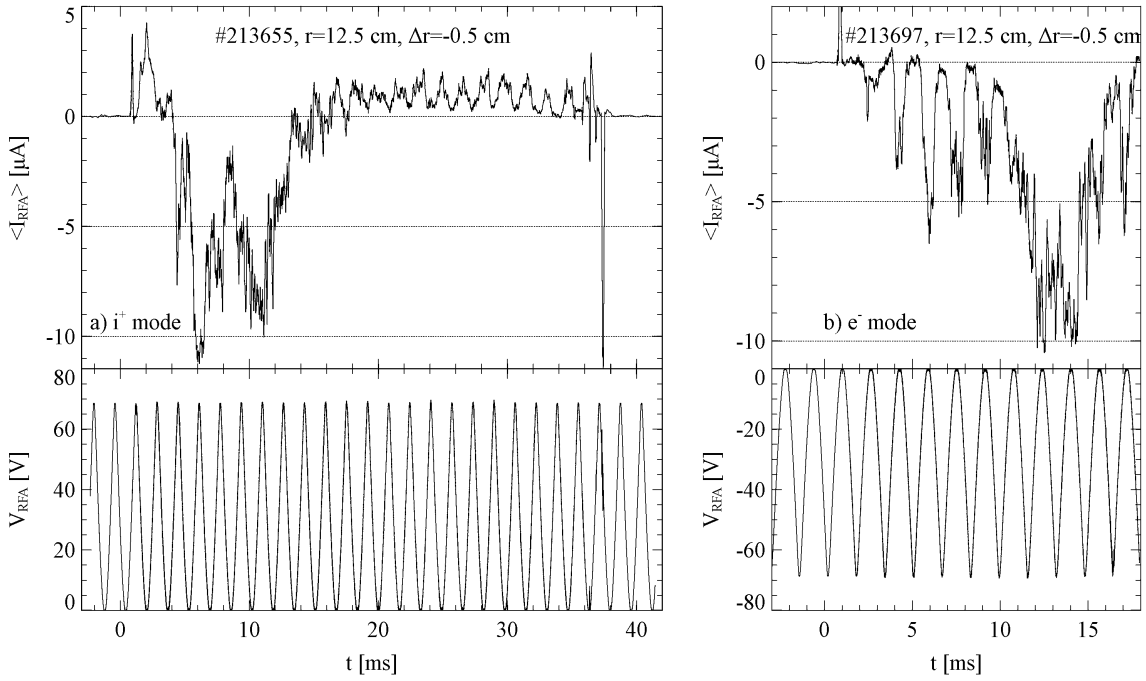

Figure 5.12: Abnormal RFEA behaviour in the ion mode and electron mode. Waveforms of RFEA collector current, ion retarding grid triangular shape retarding voltage. RFEA position r=12.5 cm. Orifice, first grid and collector are grounded.

5.5 Abnormal RFEA Behavior

RFEA principles and design features are rather simple, however, RFEA physics in practical applications is rather complicated. For example, the abnormal behaviour observed in JET [67] and ISTTOK [64] tokamaks has not yet been explained. It has been observed in the STOR-M tokamak as well. An example of STOR-M discharge

with abnormal RFEA behavior in the ion mode is shown in Fig. 5.12.
Generation of negative current in the RFEA collector plate at $3 - 20$ ms indicates that the RFEA is in the abnormal mode of behavior. Abnormal RFEA behavior has been observed in normal STOR-M discharges only when RFEA radial position is deeper than r = 14 cm, while in JET and ISTTOK, abnormal behavior appears when RFEA location is sufficiently deep in the plasma [64, 67]. RFEA collector current measured in the STOR-M tokamak is always at least one order of magnitude smaller than the space-charge limited current (250 μA), as shown in Table 4.2.
Abnormal RFEA behavior has been observed in the electron mode as well. It appears when the RFEA is deep enough into the plasma, as in the ion mode. An example of abnormal behavior in electron mode is shown in Fig. 5.12.

5.6 Summary

In this chapter experimental results of RFEA measurements on STOR-M tokamak are presented. Several figures present typical data: collected signal in the normal mode of operation, $I - V$ characteristic and logarithmic fitting in SOL and edge plasma, ion and electron radial profile and an example of RFEA abnormal behavior. In this chapter several things have been pointed out:

- High level of fluctuations present in the raw current signal. Proper techniques to lower the signal noise, discussed in Chapter 4, were applied such as an additional electrostatic screen, coaxial and twisted pair cables or the redesign of the isoamps.

- Presence of a sharp knee, which indicates the plasma potential voltage ($10 - 15$ V). This observation agrees with previous measurements of plasma potential in STOR-M. A sharp knee may also indicate that the space-charge effect influence on RFEA operation is insignificant.

- $I - V$ characteristic presents exponential decrease in ion current as the ion retarding bias increases above the knee voltage.

- Ion and electron temperatures have been successfully measured by RFEA. Experimentally observed ion temperature is about $12 - 35$ eV. In SOL the ion temperature is higher than the electron temperature ($T_\mathrm{i}/T_\mathrm{e} \sim 2$). The electron temperature ($5 - 25$ eV) is consistent with previous Langmuir probe measurements [38, 76].

- A technique of single side RFEA data correction using experimental Mach number has been proposed. This technique compensates the influence of plasma rotation on the ion temperature determination for a single sided RFEA design.

- In contrast to the SOL region, the plasma edge region indicates a high energy tail in the ion distribution function.

- Abnormal behavior of the RFEA has been observed in ion and electron modes of RFEA operation when it is inserted deep into plasma. Registered RFEA abnormal current of about 5 μA is two orders of magnitudes lower than the critical current threshold estimated using Larmor radius as a beam radius; However role of the critical current threshold in the abnormal RFEA behavior requires more accurate estimations.

- Different combinations of RFEA grids connection have been tested in the STOR-M tokamak in the ion and electron modes of RFEA measurements. The configuration with the first grid connected to the grounded orifice, sweeping ion retarding voltage applied to second grid and electron repelling voltage applied to the third grid, shown in Fig. 5.2, has been proved as a best ion mode configuration for STOR-M. In this configuration the appearance of abnormal RFEA behavior is minimal. This configuration is similar to the main JET RFEA configuration.

- The results and discussion of using Retarding Field Energy Analyzer in STOR-M tokamak, will be published in Review of Scientific Instruments [110].

Chapter 6

Conclusions and Future Work

6.1 Conclusions

The focus of this thesis is to experimentally investigate ion temperature in the plasma boundary of the STOR-M tokamak. This thesis addresses issues related to the development and application of a probe capable of measuring the ion temperature. The instrument used to study the ion and electron temperatures in the SOL and edge plasma of STOR-M is a single directional plasma diagnostic, called the Retarding Field Energy Analyzer (RFEA). The main purpose of designing a RFEA is ion temperature measurements, however the diagnostic also allows electron temperature measurements. The probe is mounted via the horizontal port of STOR-M tokamak on a linear feedthrough. The RFEA orientation is in parallel with the magnetic field so that the orifice of the probe faces into ion upstream side. All components of the energy analyzer components are designed to withstand high heat fluxes.

STOR-M's RFEA can be treated as a non-perturbing probe, which means, that the natural ambipolar collection length $L_{\mathrm{col}}^{\mathrm{amb}}$ is smaller than the magnetic connection length L_{con}. Therefore, the boundary plasma parameters measured by the probe are unperturbed.

The RFEA is used to measure ion and electron parallel energy distributions. A typical energy analyzer consists of an orifice plate with a small orifice (or a slit), two or more biasable grids and a collector. To maximize transmission, the orifice should be shaped like a knife-edge and the orifice plate should be as thin as possible. During the design process several factors must be considered, such as the radius of the orifice, which should be comparable to Debye length or the space charge accumulation inside

the probe.

Distribution functions obtained from the RFEA measurements follow closely the expected Maxwellian form, both for ions and electrons. This provides experimental evidence of the negligible effect of the space charge accumulation inside the RFEA. From such distributions, the ion temperature (and the electron temperature) are readily obtained. Electron temperature measurements obtained from a Langmuir probe measurements agrees well with the results from the RFEA. In STOR-M, and other tokamaks, measured ion temperature is about twice as high as the electron temperature, and the ratio decreases with the (minor) radius.

6.2 Suggestions for Future Work

The use of a RFEA provides additional possibilities for the study of the SOL and edge plasma in STOR-M. The RFEA and the required hardware was completely designed and constructed in the Plasma Physics Laboratory at the University of Saskatchewan and operated in STOR-M for the first time. During the probe operation critical issues, such as alignment with respect to the magnetic field and noise reduction, were identified then resolved and ideas for further probe development were obtained.

6.2.1 Diagnostic Improvements

- Bidirectional measurements. The current design allows for measurement from one side only. By having two energy analyzers in the Mach probe configuration, the ion temperature from both the ion downstream and upstream sides could be measured simultaneously. Additionally, the technique proposed in Sec. 5.2 where single sided RFEA data is corrected using the experimentally determined Mach number, can be verified. This technique compensates the influence of the plasma rotation on the ion temperature determination for a single sided RFEA design.

- Ion density. In the Radial Force Balance Equation (Eq. 1.14) one of the vari-

ables is the ion density n. A single Langmuir probe installed near the orifice would provide information about the ion density in the vicinity of RFEA.

- Increase of the grid and chamber dimensions. By increasing the size of the grids and chamber, the RFEA would be able to operate deeper inside the plasma, where ions are more energetic and where abnormal behavior appears. To verify the hypothesis that charging of the internal ceramics might be one of the reasons for abnormal behavior, a tiny conductor plate in the middle of ceramic isolator could be installed and the current from this collector measured. Collected signals from normal and abnormal behavior could be analyzed.

- Shield box. Improve the quality of electrostatic shielding by replacing the thin copper screen with a stainless steel shield box. This should significantly reduce the noise.

- Transmission coefficients. Perform further studies of transmission coefficients of the grids and the entrance orifice.

- Probe upgrades. The probe could be redesigned for easier reconstruction or future repairs. Additionally experiments have shown, that it is sufficient to use two grids in the configuration described in [67]. This would reduce the size of the probe and since the collector would be closer to the orifice plate, the problem with misalignment would be smaller.

- Redesign of the electronics. When the RFEA has passed the Separatrix, the high energy tail of the ions was observed. To perform more measurements in that region, the DC power supply should be redesigned, so that it may be biased up to ± 150 V and remain stable for higher current loads. Additional isoamplifiers would allow a current measurement from the electron repelling grid.

- Different confinement scenarios. By employing a RFEA in STOR-M, ion temperature can be measured during various confinement scenarios.

- Numerical simulations. In further research on RFEAs it would be desirable to employ numerical simulations such as Particle in Cell [61] or SIMION® [111] in order to study such phenomena as abnormal behaviour, slit/grid transmission coefficients or RFEA operational limits.

6.2.2 Future Bidirectional Design of the RFEA for the STOR-M Tokamak

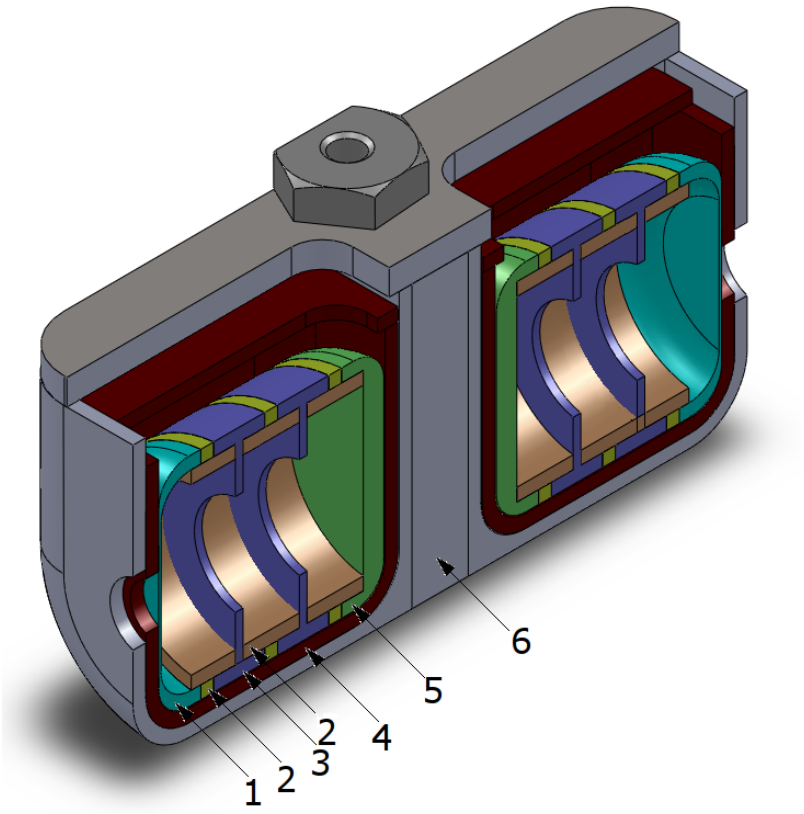

Figure 6.1: View of internal components of the new bidirectional RFEA, showing: 1. orifice plate, 2. MACOR insulators, 3. grid supporting washer, 4. MACOR cup, 5. collector, 6. stainless steel shield box. Grids and wires to the grids omitted for clarity.

6.2.3 Enhancement of RFEA

The main function of the Retarding Field Energy Analyzer is to measure the ion (and electron) temperature, however the measured temperature is of all ion species,

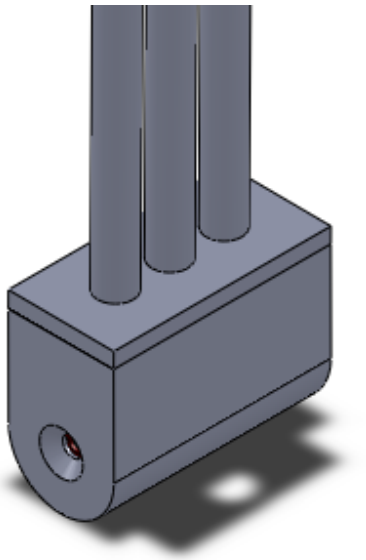

Figure 6.2: View of the new bidirectional design of RFEA.

including impurities (from the wall, probes, etc.). RFEA, in the configuration used in STOR-M, JET or ISTTOK tokamaks, is not sensitive to single ion species. It would be useful to measure the temperature of the impurities in the boundary plasma, as it would provide additional knowledge about the behavior and contribution of the impurities to the overall boundary plasma (the contribution toward the ion and electron energy balances). Knowledge of impurities would be beneficial in understanding mechanisms of plasma-surface interactions.

In the Alcator C-Mod tokamak, the energy analyzer was combined with an ion mass spectrometer (omegatron probe), which enabled a measurement of the temperature of impurities in the boundary plasma of Alcator C-Mod [42]. Such modification would be highly desirable in further studies of the SOL and edge plasma in STOR-M or STOR-U.

Bibliography

[1] J. Ongena and G. Van Oost: *Energy For Future Centuries. Will Fusion Be An Inxehaustible, Safe And Clean Energy Source?*. 2001.

[2] International Energy Agency (IEA): World Energy Outlook, Key World Energy Statistics.

[3] European Environment Agency (EEA).

[4] F. Joos: *The Armospheric Carbon Dioxide Perturbation*. Europhysics News, **27**, 6, 1996.

[5] M. Kleemann: *Potentials and limits of renewable sources of energy*. Fus. Tech., 33, 1998.

[6] I.E. Tamm and A.D. Sakharov: *Teoriya magnitnogo termoyadernogo reaktora*. Fizika Plazmy i Problema Ypravlaemykh Termoyadernykh Reaktsij (Ed. M.A. Leontovich), Tom 1, 1958.

[7] M. N. Rosenbluth: *New ideas in Tokamak confinement*. AIP, Institute for Advanced Physics Studies. La Jolla International School of Physics, 1992.

[8] M.S. Rabinovich: *Stellarator Program*. Sov. Phys. Usp., 14, 1971.

[9] P.E. Moroz: *Spherical stellarator configuration*. Phys. Rev. Lett., 77, 1996.

[10] JET Press Release, 1997.

[11] International Fusion Research Council, Nucl. Fusion, 45, 2005.

[12] ITER: International Thermonuclear Experimental Reactor website.

[13] G. Van Oost: Duplicate lecture notes *Plasmafysica 1* (2005-2006). Department of Applied Physics, Ghent University.

[14] P. Peleman: *Development of an Advanced Probe and Study of Edge Plasma Flows and Transport in Tokamaks*. PhD Thesis, Ghent University, 2006.

[15] S. Eliezer, Z. Henis, J.M. Martinez-Val and M. Piera: *Deuterium-tritium fusion reactors without external tritium breeding*. Physics Letters A, 243, 1998.

[16] T.G. Spiro and W.M. Stigliani: *Environmental Science in Perspective*. Suny Press, 1985.

[17] Georgia State University, HyperPhysics website.

[18] J.D. Lawson: *Some criteria for a useful thermonuclear reactor*. Proc. Phys. Soc., 70, 1957.
(http://www.jet.efda.org/pages/multimedia/yop/dec05-aere-gpr1807.pdf)

[19] T. J. Dolan: *Fusion Research*. Pergamon Press, 1982.

[20] W.M. Stacey: *Fusion: An Introduction to the Physics and Technology of Magnetic Confinement Fusion*. Wiley-Interscience, 1984.

[21] M. Trautmann, K.W. Rothe, J. Wanner and H. Walther: *Determination of the deuterium abundance in water using a cw chemical df laser*. Appl. Phys., 24:49, 1981.

[22] S. Kaufman and W.F. Libby: *The natural distribution of tritium*. Phys. Rev., 93:1337, 1954.

[23] IEER Tritium Report: The environmental, health, budgetary, and strategic effects of the Department of Energy's decision to produce tritium.

[24] G. L. Rogoff: Ed., IEEE Transactions on Plasma Science, 19, 1991.

[25] L. Tonks *The birth of plasma*. Amer. J. Phys., 35, 1967.

[26] NASA: THEMIS.

[27] M. N. Saha: *On a Physical Theory of Stellar Spectra*. Proc. of the Royal Society of London, A (99), 1921.

[28] F.F. Chen: *Plasma Physics and Controlled Fusion. Vol. 1: Plasma Physics*. 2nd Edition, Springer, 1984.

[29] R. Fitzpatrick: Lecture notes *Introduction to Plasma Physics: A Graduate Course*.

[30] Max-Planck-Institut für Plasmaphysik website.

[31] Website of Laboratory for Plasma Physics of the Ecole Royale Militaire: ITER and Fusion Energy.

[32] J. Wesson: *Tokamaks*. 3rd Ed., Clarendon Press, 2004.

[33] EFDA-JET website.

[34] J. Stockel, M. Spolaore, P. Peleman, *et al.*,: *Dynamics of the edge transport barrier at plasma biasing on the CASTOR tokamak*. Journal of Physics: Conference Series, 63, 2007.

[35] J. Stockel, J. Adamek, P. Balan, *et al.*,: *Advanced probes for edge plasma diagnostics on the CASTOR tokamak*. Journal of Physics: Conference Series, 63, 2007.

[36] S.I. Krasheninnikov: *On scrape off layer plasma transport*. Phys. Lett. A, 283, 2001.

[37] A. Hirose, C. Xiao, O. Mitarai, J. Morelli, H. M. Skarsgard: *STOR-M Tokamak design and instrumentation*. Physics in Canada, Hiro1, March/April 2006.

[38] M. Dreval, C. Xiao, D. Trembach, *et al.*: *Simultaneous evolution of plasma rotation, radial electric field, MHD activity and plasma confinement in the STOR-M tokamak*. Plasma Phys. Control. Fusion 50, 2008.

[39] G. Federici, C.H. Skinner, J.N. Brooks, *et al.*: *Plasma-material interactions in current tokamaks and their implications for next step fusion reactors*. Nucl. Fusion, 41, 2001.

[40] G.F. Matthews, J.M. Pedgley, R.A. Pitts, P.C. Stangeby *Edge impurity ion analysis using plasma ion mass spectrometry*. J. of Nucl. Materials, 176-177, 1990.

[41] G.F. Matthews: *Tokamak plasma diagnosis by electrical probes*. Plasma Phys. Control. Fusion, 36, 1994.

[42] R.T. Nachtrieb: *Ion Mass Spectrometry on the Alcator C–Mod Tokamak*. PhD Thesis, MIT, 2000.

[43] I. Langmuir, H.M. Mott-Smith: *Langmuir probe technique*. General Electric Rev, 1924.

[44] H.M. Mott-Smith, I. Langmuir: *The theory of collectors in gaseous discharges*. Phys. Rev. 28, 1926.

[45] L. Tonks, I. Langmuir: *Oscillations in Ionized Gases*. Phys. Rev. 33, 1929.

[46] V.I. Demidov, S.V. Ratynskaia, K. Rypdal: *Electric probes for plasmas: The link between theory and instrument*. Rev. of Sci. Inst., 73, 2003.

[47] J.P. Gunn, C. Boucher, P. Devynck: *Edge flow measurements with Gundestrup probes*. Phys. Plasmas, 8, 2001.

[48] C.S. MacLatchy, C. Boucher, D.A. Poirier, J. Gunn: *Gundestrup: A Langmuir/Mach probe array for measuring flows in the scrape-off layer of TdeV*. Rev. Sci. Instrum., 63, 1992.

[49] I. Katsumata, M. Okazaki: *Ion Sensitive Probe – A New Diagnostic Method for Plasma in Magnetic Fields*. Jpn. J. Appl. Phys., 6, 1967.

[50] N. Ezumi: *PIC Simulation of the Motion of Plasma around Ion Sensitive Probes*. Contrib. to Plas. Phys., 41, 2001.

[51] R. Schrittwieser, J. Adamek, C. Ionita, *et al.*: *Direct Measurements of the Plasma Potential by Katsumata-type Probes*. 33rd EPS Conference on Plasma Phys. Rome, ECA 30I, P-4.196. 2006.

[52] H. Amemiya: *Measuring Method for Ion Temperature by Asymmetric Probes in Magnetic Fields*. Japanese Journal of Applied Physics, 28, 1989.

[53] K. Uehara, T. Kawakami, H. Amemiya, K. Höthker, A. Cosler, W. Bieger: *Measurements of ion temperature and flow velocity using symmetric and asymmetrc double probes in the boundary plasma of the JFT-2M tokamak*. Nuc. Fusion, 38, 1998.

[54] K. Höthker, H.-J. Belitz, W. Bieger and H. Amemiya: *A new method to determine ion temperatures in magnetized plasmas by means of an electrical probe*. Rev. Sci. Instrum., 61, 1990.

[55] R.P. Schorn, E. Wolfrum, F. Aumayr, *et al.*: *Radial temperature distributions of* C^{6+} *ions in the TEXTOR edge plasma measured with lithium beam activated charge exchange spectroscopy*. Nucl. Fusion., 32, 1992.

[56] J.P. Gunn: *Magnetized plasma flow through a small orifice*. Phys. of Plasmas, 8, 2001.

[57] J.P. Gunn, J. Adamek, O. Barina, *et al.*,: *A DC Probe Diagnostic for Fast Electron Temperature Measurements in Tokamak Edge Plasmas*. 29th EPS Conference on Plasma Phys. and Contr. Fusion Montreux 2002, ECA, 26B, 2002.

[58] M. Kocan, R. Panek, J. Stockel, *et al.*: *Ion temperature measurements in the tokamak scrape–off layer*. J. of Nuclear Materials, 363, 2007.

[59] P. Balan, R. Schrittwieser, J. Adamek, *et al.*: *Measurements of the Parallel and Perpendicular Ion Temperatures by Means of an Ion-sensitive Segmented Tunnel Probe*. Contrib. Plasma Phys., 44, 2004.

[60] L. Tonks, H.M. Mott-Smith, I. Langmuir: *Flow of Ions Through a Small Orifice in a Charged Plate*. Phys. Rev., 28, 1926.

[61] J.P. Verboncoeur, A.B. Langdon, N.T. Gladd: *An object-oriented electromagnetic PIC code*. Computer Physics Communications, 1995.

[62] J.A. Simpson: *Design of Retarding Field Energy Analyzers*. Rev. of Sci. Instr., 32, 1961.

[63] F. Valsaque, G. Manfredi, J.P. Gunn, E. Gauthier: *Kinetic simulations of ion temperature measurements from retarding field analyzers*. Phys. Plasmas, 9, 2002.

[64] I.S. Nedzelskiy, C. Silva, H. Figueiredo, H. Fernandes and C.A.F. Varandas: *Compact retarding field energy analyzer for the tokamak ISTTOK boundary plasma*. Rev. of Sci. Instr., 77, 2006.

[65] R.A. Pitts: *Ion Energy, Sheath Potential and Secondary Electron Emission in the Tokamak Edge*. PhD Thesis, UKAEA Culham Laboratory/AEA Fusion and University of London, 1990.

[66] A.S-H. Wan: *Ion and Electron Parameters in the Alcator C Tokamak Scrape–Off Region*. PhD Thesis, MIT, 1986.

[67] R.A. Pitts, R. Chavan, S.J. Davies, *et al.*: *Retarding field analyzer for the JET plasma boundary*. Rev. of Scien. Instrum, 74, 2003.

[68] R.A. Pitts: *Ion velocity distributions at the tokamak edge*. Phys. Fluids, B 3, 1991.

[69] P.C. Stangeby: *Large probes in Tokamak scrape-off plasmas. The collisionless scrape-off layer: operation in the shadow of limiters or divertor plates*. J. Phys. D: Appl. Phys., 18, 1985.

[70] A.J. Hayzen, D.O. Overskei and J. Moreno *Probe Measurements of the Boundary Plasma in Alcator C*. MIT Plasma Fusion Center Report, PFC/JA-81-10, 1981

[71] M. Kocan, J.P. Gunn, M. Komm, J.-Y. Pascal, *et al.*: *On the reliability of scrape-off layer ion temperature measurements by retarding field analyzers*. Rev. Sci. Instrum., 79, 2008.

[72] D. Van Houtte and Equipe TORE SUPRA: *One Minute Pulse Operation In The Tore Supra Tokamak*. Nuc. Fusion, 33, 1993.

[73] M. Kocan, J.P. Gunn, J.-Y. Pascal, *et al.*: *Measurements of scrape-off layer ion-to-electron temperature ration in Tore Supra ohmic plasmas*. J. Nucl. Mater., 2009.

[74] J.D. Ramboz: *Machinable Rogowski Coil, Design, and Calibration*. IEEE: Transactions on Intrumentation and Measurement, 45(2), 1996.

[75] W. Zhang: *Improved Ohmic Confinement Induced by Turbulent Heating and Electrode Biasing in the STOR-M Tokamak*. PhD Thesis, University of Saskatchewan, 1993.

[76] G. St.Germaine: *Plasma Flow Velocity Measurements with a Gundestrup Probe in the STOR-M Tokamak*. MSc Thesis, University of Saskatchewan, 2006.

[77] R.L. Merlino: *Understanding Langmuir probe current-voltage characteristics*. Am. J. Phys., 75, 2007.

[78] C.S. MacLatchy, C. Boucher, D.A. Poirier, and J. Gunn: *Gundestrup: A Langmuir/Mach probe array for measuring flows in the scrape-off layer of TdeV*. Rev. Sci. Instrum., 63, 1992. Q2015R

[79] I.H. Hutchinson: *Principles of Plasma Diagnostics*. Cambridge University Press, 2nd edition, 2002.

[80] C. Xiao, T. Niu, *et al.*: *Design and initial operation of multichord soft x-ray detection arrays on the STOR-M tokamak*. Rev. Sci. Instr., 79, 2008

[81] G. Fuchs, Y. Miura and M. Mori: *Soft x-ray tomography on tokamaks using flux coordinates*. Plasma Phys. Control. Fusion, 36, 1994.

[82] Y.H. Ding, G. Zhuang, *et al.*: *Soft X-ray imaging diagnostic system on the J-TEXT tokamak*. Nucl. Instr. and Meth., A, 2009.

[83] J.R. Davis: *Stainless steels*. ASM International, 1994.

[84] P.J. Gierszewski: *Plasma/Neutral Gas Transport in Divertors and Limiters*. ScD Thesis, MIT, 1983.

[85] *Data Sheet:* TedPella.com: Veco Handle Grids 12584-NI, 50 mesh, Pitch 500 μm; Hole Width 450μm; Bar Width 50μm.

[86] M. Okubo, N. Mizugachi, S. Okuga and S.Goto: *Characteristic of a novel ion energy spectrum $f(E_{||}, E_{\perp})$ analyzer in measurements of plasma flow in a magnetic mirror throat*. Rev. Sci. Instrum., 70, 1999.

[87] G.F. Matthews: *Ion and Electron Parameters in the Alcator C Tokamak Scrape–Off Region*. PhD Thesis, University of Oxford, 1985.

[88] L. Brillouin: *A Theorem of Larmor and Its Importance for Electrons in Magnetic Fields*. Phys. Rev., 67, 1945.

[89] J.R. Pierce and L.R. Walker: *"Brillouin Flow" with Thermal Velocities*. J. Appl. Phys., 24, 1953.

[90] A.W. Molvik: *Large acceptance angle retarding-potential analyzers*. Rev. Sci. Instrum., 52, 1981.

[91] *Data Sheet:* MACOR.

[92] *Specifications:* NI PCI-6133 Simultaneous Sampling Multifunction DAQ.

[93] H. Zumbahlen: *Linear Circuit Design Handbook*. Newnes, 2008.

[94] R.F. Graf, W. Sheets: *The encyclopedia of electronic circuits*. McGraw-Hill Professional, 1996.

[95] *Data Sheet:* LF356 JFET input operational amplifiers.

[96] *Data Sheet:* HCNR200 high-linearity analog optocoupler.

[97] Op Amp Circuit Collection, National Semiconductor, Application Note 31, Sept. 2002.

[98] *Data Sheet:* power transformer N-67A.

[99] *Data Sheet:* single phase rectifier bridge KBPC1.

[100] *Data Sheet:* triac Q2015R.

[101] *Data Sheet:* transformer BV020.

[102] *Data Sheet:* ±12 V fixed voltage regulators: MC78L06A and L79L12.

[103] *Data Sheet:* Complementary Silicon Plastic Power Transistor TIP31C.

[104] C. Böhm and J. Perrin: *Retarding-field analyzer for measurements of ion energy distributions and secondary electron emission coefficients in low-pressure radio frequency discharges*. Rev. Sci. Instrum. 64, 1993.

[105] G.A. Emmert, R.M. Wieland, T.A. Mense and J.N. Davidson: *Electric Sheath and Presheath in a Collisionless, Finite Ion Temperature Plasma*. Phys. Fluids., **24**, 803 (1980).

[106] M. Kocan, J.P. Gunn, J.-Y. Pascal, G. Bonhomme, C. Fenzi, E. Gauthier and J.-L. Segui: *Edge ion-to-electron temperature ratio in the Tore Supra tokamak*. Plasma Phys. Control. Fusion, 50, 2008.

[107] S. Raychaudhuri, S.K. Saha, S. Chowdhury, D. Banik, and A.K. Hui *Observation of high energy ion tail in the SINP tokamak plasma*. Phys. Plasmas, 13, 2006.

[108] M.E. Rudd, Y.-K. Kim, D.H. Madison and J. W. Gallagher *Electron production in proton collisions: total cross sections*. Rev. Mod. Phys. 57, 1985.

[109] J.E. Miraglia and M.S. Gravielle: *Ionization of the He, Ne, Ar, Kr, and Xe isoelectronic series by proton impact*. Phys. Rev., A 78, 2008.

[110] M. Dreval, D. Rohraff, C. Xiao and A. Hirose: *Retarding field energy analyzer for the STOR-M plasma boundary*. Submitted for publication to Review of Scientific Instruments.

[111] SIMION - electron and ion/electron optics simulation.